HECATE factors control cell fate transitions and organ patterning in *Arabidopsis thaliana*

Dissertation
submitted to the
Combined Faculties for the Natural Sciences and for Mathematics
of the Ruperto-Carola University of Heidelberg, Germany
for the degree of
Doctor of Natural Sciences

Presented by

Msc. Christophe Gaillochet
Born in: Paris, France
Oral examination: 04/12/2017

Dissertation
submitted to the
Combined Faculties for the Natural Sciences and for Mathematics
of the Ruperto-Carola University of Heidelberg, Germany
for the degree of
Doctor of Natural Sciences

Presented by

Msc. Christophe Gaillochet
Born in: Paris, France
Oral examination: 04/12/2017

HECATE factors control cell fate transitions and organ patterning in *Arabidopsis thaliana*

Referees: Prof. Dr. Jan Lohmann
Prof. Dr. Karin Schumacher

Table of contents

Abbreviations

A	Adenine
aa	Amino acid
Ac	Acetate
ARE	Auxin response element
BA	6-Benzylaminopurine
bp	Base pair
BZ	Boundary zone
CDS	Coding sequence
ChIP	Chromatin immunoprecipitation
CK	Cytokinin
CMM	Carpel margin meristem
CSM	Complete supplement mixture
Cyc	Cycloheximide
CZ	Central zone
DAPI	4', 6-Diamidino-2-phenylindole
dex	Dexamethasone
DMSO	Dimethylsulfoxyde
DNA	Deoxyribonucleic Acid
dNTP	Deoxynucleoside triphosphate
EDTA	Ethylenediaminetetraacetic acid
EtOH	Ethanol
FRET	Fluorescence resonance energy transfer
FLIM	Fluorescence-lifetime imaging microscopy
GFP	Green fluorescent protein
GA	Giberrellic acid
GO	Gene ontology
H	Histidine
IP	Immunoprecipitation
kb	Kilobasepair (=1000bp)
K-Ferri	Potassium Ferricyanide
K-Ferro	Potassium Ferrocyanide
L	Leucine
M	Molar

MAPK	Mitogen-activated protein kinases
NLS	Nuclear localisation signal
OC	Organising centre
PCR	Polymerase chain reaction
PMSF	Phenylmethane sulfonyl fluoride
PMT	Photomultiplier
PZ	Peripheral zone
qRT-PCR	Quantitative reverse transcription polymerase chain reaction
RAM	Root apical meristem
RNA	Ribonucleic acid
rpm	Revolutions per minute
RZ	Rib zone
SAM	Shoot apical meristem
SEM	Scanning electron microscopy
SC	Stem cells
T	Tryptophan
TAIR	The Arabidopsis Information Resource
T-DNA	Transfer DNA, transferred by *A. tumefaciens*
WT	Wild type
w/o	without
w/v	Weight / Volume
X-Gluc	ß-Glucoronidase
Y2H	Yeast-two-hybrid

Zusammenfassung

Pflanzen sind über ihre gesamte Lebensspanne hinweg in der Lage neue Gewebe und Organe auszubilden. Diese bemerkenswerte Eigenschaft verdanken sie der kontinuierlichen Aktivität pluripotenter Stammzellen die in meristematischem Gewebe vorliegen und spezifische Zelllinien hervorbringen können. Die Steuerungsprozesse die der Reifung von Stammzelllinien und deren schlussendlicher Differenzierung zugrunde liegen, sind daher essenziell für die Ausgestaltung des Pflanzenkörpers und bedingen letztlich den Fortpflanzungserfolg. Innerhalb des Meristems ist die Integration phytohormoneller Signalwege, wie etwa von Auxin und Cytokinin, mittels transkriptioneller Regulatoren von zentraler Bedeutung um Stammzellaktivität und Differenzierung in Einklang zu bringen. Unser derzeitiges Wissen um die regulatorischen Interaktionen die für den korrekten Ablauf dieser molekularen Kommunikationsmechanismen verantwortlich sind, ist jedoch äußerst begrenzt.

In der vorliegenden Arbeit untersuchen wir die Funktion von HECATE (HEC) bHLH Transkriptionsfaktoren bei der Stammzellhomöostase und der Bildung von Organen, dabei verfolgen wir einen integrativen Ansatz und vereinen live-cell imaging, Computer basierte Modellierung, Genomanalyse und funktionale genetische Charakterisierung. Wir zeigen, dass *HEC* Gene im Spross Apikal Meristem Funktionen bei der zeitlichen Steuerung der Stammzelldifferenzierung übernehmen, indem sie lokal Cytokinin Signale im Zentrum des Meristems verstärken und Auxin Signale in der Peripherie unterdrücken. Im Gegensatz dazu scheinen *HEC* Gene die Differenzierung des Griffels im Gynözeum zu beeinflussen indem sie den Auxin Fluss regulieren und die Effekte von Cytokinin puffern. Durch die Rekonstruktion von Gennetzwerken beginnen wir die regulatorischen Interaktionen, die für die vielfältigen Funktionen von HEC verantwortlich sind, aufzudecken und konnten NGATHA Transkriptionsfaktoren als, für die Kontrolle der Stammzellaktivität relevante, direkte Interaktionspartner identifizieren. Zusammen tragen unsere Ergebnisse zum tieferen Verständnis der Funktionsweise molekularer Netzwerke bei, die die Stammzellaktivität und die Gynözeum Differenzierung bei der Pflanzenentwicklung steuern.

Abstract

Throughout their life span, plants keep the ability to generate new tissues and organs. This remarkable developmental property relies on the continuous activity of pluripotent stem cells localized in meristems, which generate cell progenies acquiring specific cellular identities. Thus, the regulatory processes controlling the progression of stem cell lineages and their final differentiation are essential to establish the whole body plan and to ultimately define plant reproductive success. The integration of phytohormonal signals like auxin or cytokinin with key transcriptional regulators is central for balancing stem cell activity and differentiation (reviewed in Gaillochet and Lohmann, 2015), however our current understanding of the regulatory interactions mediating this molecular communication remains elusive.

In this study, we used an integrated approach–including live-cell imaging, computational modeling, genome-wide profiling and genetic functional characterization–to investigate the function of the bHLH transcription factors HECATE (HEC) in controlling stem cell homeostasis and organ patterning. We found that HEC regulatory function is highly versatile and tightly interacts with cytokinin and auxin signalling pathways under multiple developmental contexts. We show in the shoot apical meristem that HEC function regulates the timing of stem cell differentiation by locally promoting cytokinin at the centre of the meristem and repressing auxin signals at the periphery. In contrast, we found that *HEC* genes pattern style differentiation at the gynoecium by regulating auxin flow and by buffering cytokinin responses. Using a gene network reconstruction approach, we started to unravel the regulatory interactions mediating HEC functional versatility and identified NGATHA transcription factors as relevant direct targets controlling shoot meristem activity. Together, our findings refine the molecular and developmental framework for shoot meristem activity and gynoecium differentiation.

I. Introduction

I.1 Plants as information systems

Plants are sessile organisms that can live up to thousands of years in the most remarkable cases, and are thus exposed to multiple stresses and important variations in their growth conditions throughout their life cycle. In order to develop and thrive in these changing environments, plants need to dynamically integrate internal and external signals and translate them into robust yet plastic developmental programs. By analogy to machine learning systems, authors suggested that plants could be described as multi-layered perceptrons, as they receive environmental and developmental inputs and further process this information by complex multi-layered molecular circuits. The output of this network in turn defines their developmental responses and eventually their ecological success (Scheres and van der Putten, 2017). From this concept, it emerges that the wiring of regulatory networks and their spatio-temporal deployment contribute to plant developmental plasticity and robustness. Importantly, these networks integrate the activity of multiple regulatory players including transcription factors, signalling peptides, microRNAs and phytohormones (Scheres and van der Putten, 2017).

I.1.1 Phytohormone signalling pathways

Phytohormones are key regulatory molecules triggering molecular and cellular responses at minute concentrations. Conceptually, phytohormonal signalling cascades follow a stereotypic plan: Hormones are perceived at the level of receptors to initiate a signal that is transduced through several factors and in turn modulates the activity of transcription factors, leading to changes in gene expression and cellular responses (Figure 1) (reviewed in Shan et al., 2012). Thus, the concentration of active phytohormones within tissues is crucial to determine downstream cellular responses, and is actively controlled by biosynthetic and conjugating enzymes, enhancing or reducing the phytohormone levels respectively (reviewed in Hwang et al., 2012; Zhao, 2010). In addition, hormones are transported by trans-membrane carrier proteins, which facilitate their movement across large cellular domains and control their spatial distribution (Benjamins and Scheres, 2008; Tal et al., 2016; Zürcher et al., 2016). In line with the crucial role of these families of molecules throughout development, plants extensively diversified and refined their hormonal network across evolution (Vriet et al., 2015; Weijers and Wagner, 2016).

In *Arabidopsis*, the main phytohormones include cytokinins, auxin, gibberellic acid, brassinosteroids, abscisic acid and the gas ethylene.

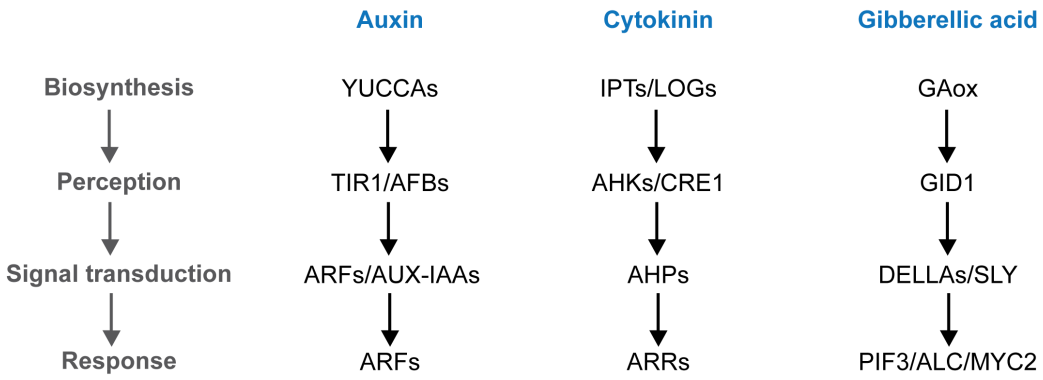

Figure 1: Signal transduction in plant hormone signalling
Information flow in hormonal signalling pathways from biosynthesis to perception, signal transduction and response. Arrows depict the direction of the signal transduction

Cytokinins are a class of N6-substituted adenine derivatives involved in the regulation of multiple processes during plant development, including tissue patterning, nutrition or senescence (reviewed in (Hwang et al., 2012). Active cytokinins are produced in a multi-step process that requires the activity of ISOPENTENYL-TRANSFERASEs (IPT) (Miyawaki et al., 2004; Miyawaki et al., 2006) and LONELY GUY (LOG) enzymes (Kuroha et al., 2009), whereas CYTOKININ OXYDASE (CKX) enzymes catalyze their degradation (Werner et al., 2003). Cytokinins are transported across cells by PURINE PERMASE 14 (PUP14), localized at the plasma membrane (Zürcher et al., 2016). The signalling cascade is mediated by a two-component phosphorelay system; cytokinins are perceived by ARABIOPSIS HISTIDINE KINASE (AHK) localized at the plasma membrane, which trigger the autophosphorylation of a conserved histidine residue for further relay to an aspartate located at the C-terminus of the receiver domain (Hwang and Sheen, 2001; Riefler et al., 2006). The signal is next transfered by phosphorylation of ARABIDOPSIS HISTIDINE PHOSPHOTRANSFER PROTEINS (AHPs), which shuttle from the cytoplasm to the nucleus and activate Type-B ARABIDOPSIS RESPONSE REGULATORS (ARRs) transcription factors. In turn, B-type ARRs promote the expression of cytokinin response genes including the negative cytokinin regulators A-type ARRs (Hwang and Sheen, 2001).

Similarly to cytokinin, the auxin signalling pathway displays a plethora of functions during development, including root stem cell maintenance, organ patterning but also stress responses (reviewed in (Weijers and Wagner, 2016). The most abundant

active auxin is the indole-3-acetic acid and derives from tryptophan. Multiple biosynthesis pathways act in parallel, involving TRYPTOPHAN AMINO-TRANSFERASE of ARABIDOPSIS (TAA1) or the YUCCA (YUC) family genes (Cheng et al., 2006; Stepanova et al., 2008). Interestingly, although auxin signalling function is extraordinary versatile, it is perceived and signals through only few key components in the nucleus: the AUXIN RESPONSE FACTORs (ARFs), the AUXIN/INDOLE-3-ACETIC ACID (Aux-IAAs), and the TRANSPORT INHIBITOR RESISTANT 1/ AUXIN SIGNALLING F-BOX (TIR/AFB) F-box proteins (Dharmasiri et al., 2005; Gray et al., 2001). Under low auxin concentration, ARF activity is repressed by their physical association with AUX/IAA proteins. Upon auxin perception, TIR1/AFB proteins, which are a subunit of the SCF ubiquitin ligase complex, associate and target AUX/IAAs for degradation, thereby releasing ARF transcriptional activity (Calderon-Villalobos et al., 2012; Gray et al., 2001). At the cellular level, auxin distribution is controlled by a set of transmembrane carrier proteins including PINs, PIN-LIKEs (PILS), AUXIN 1/LIKE AUX1 (AUX1/LAX) and ATP-BINDING CASSETTE SUBFAMILY B (ABCB) proteins (Barbez et al., 2012; Friml et al., 2002a; Friml et al., 2002b; Geisler et al., 2005; Péret et al., 2012; Yang et al., 2006). At the sub-cellular level, PINOID, D6PK and PP2A control PIN polar localisation and auxin flow directionality by regulating PINs phosphorylation status (Michniewicz et al., 2007; Weller et al., 2017) .

Interestingly, the logic governing hormonal perception is shared among multiple hormonal pathways. Similarly to auxin, gibberellic acid (GA) perception releases the transcriptional activity of downstream transcription factors by promoting the degradation of DELLA proteins, negative regulators of the hormonal pathway (reviewed in Oliva et al., 2013). Upon GA perception, the receptor GA INSENSITIVE DWARF1 (GID1) promotes the association between the F-box protein SLEEPY1 (SLY1)/GID2 and DELLA proteins, leading to their ubiquitination and their degradation, consequently releasing GA response genes from transcriptional repression (Murase et al., 2008; Shimada et al., 2008). Importantly, DELLA proteins physically interact with a myriad of transcription factors including PHYTOCHROME INTERACTING FACTOR3 (PIF3), PIF4, ALCATRAZ (ALC), MYC2 and thus connect GA homeostasis to a range of cellular processes including light response, fruit development or defence mechanisms (reviewed in Sun, 2010).

I.1.2 Computational modelling to study dynamical systems

Although many hormonal circuitry components have been identified and the core logic of the signal transduction has been resolved, hormonal regulatory networks are non-linear as a result of their intertwinement with other signalling pathways and their regulation at multiple scales (Depuydt and Hardtke, 2011), thereby hindering our understanding of how an initial hormonal input is translated into cellular responses. To bridge this gap, computational modelling has been increasingly used to formalize and simplify the structure of hormonal regulatory networks to simulate their dynamics in space and predict their developmental role (reviewed in Voß et al., 2014).

Studies have utilized cellular-based models and defined local rule on the spatial distribution of PIN proteins and their cellular polarity within the root or in the shoot apical meristem to further understand the dynamics of auxin transport (de Reuille et al., 2006; Grieneisen et al., 2007; Jönsson et al., 2006; Smith et al., 2006). These models revealed that the patterns of PIN proteins instructed the patterns of auxin accumulation observed at the tissue scale, suggesting that local PIN localisations pattern auxin distribution at the organ scale (de Reuille et al., 2006; Grieneisen et al., 2007; Jönsson et al., 2006; Smith et al., 2006).

In contrast to these models, Vernoux & al reconstructed an auxin regulatory network at the shoot apical meristem, and used ordinary differential equations to predict the regulatory output of this gene network. Their work revealed that the wiring of the auxin network buffered fluctuating hormonal levels to produce stable transcriptional outputs (Vernoux et al., 2011).

By bridging these two type of models, multi-scale models integrate information at the organ and cellular level together with the structure of gene regulatory networks underlying cellular behaviour (reviewed in Voß et al., 2014). Brand et al built such a model to describe the role of GA during root meristem cell elongation and revealed that the dilution of GA concentration in the cells of the elongation zone led to a stabilization of the DELLA proteins and local growth arrest (Band et al., 2012).

Collectively, these studies on hormonal networks showed that the use of an iterative approach combining quantitative experimental data together with multiscale computational models has the potential to infer and predict new biological mechanisms that may not be testable experimentally due to technical limitations (Voß et al., 2014)

I.2 A stem cell journey in the shoot meristem: from birth to differentiation

In contrast to animals, plants build the bulk of their body plan post-embryonically. This extraordinary property relies on the activity of localized pools of pluripotent stem cells, which are the source of most plant cells and eventually give rise to roots, leaves, flowers and seeds. Throughout the whole plant life span, stem cells are maintained in organs called meristems. The primary shoot and the root apical meristem are located at the very tip of the stem and the root respectively and are responsible for longitudinal growth, giving rise to above- and underground tissues, whereas plant lateral growth is generated from cambial activity at the inner tissues of the stem (reviewed in Gaillochet and Lohmann, 2015).

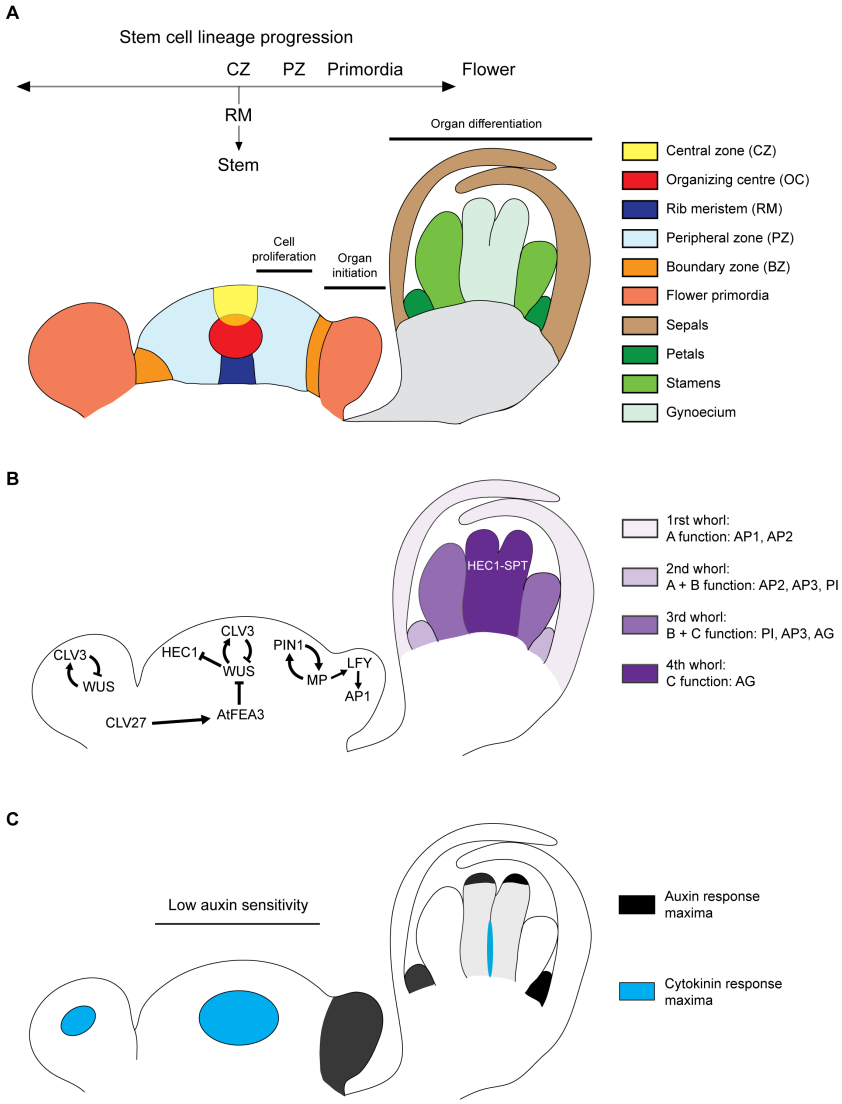

Figure 2: Schematic representation of *Arabidopsis* inflorescence.
(A) Cellular fates and organs established along the progression of stem cell lineages. **(B)** Core transcriptional regulatory network patterning sub-domains of the inflorescence. **(C)** Patterns of auxin and cytokinin response

I.2.1 SAM dynamics

At the core of meristematic activity, pluripotent stem cells self-renew and can enter individual cellular lineage before they adopt differentiated identities. Importantly, this system is built on multiple regulatory layers including cell fate specification, cell proliferation and morphogenesis, which are continuously adjusted and coordinated. In line with these properties, the inflorescence shoot apical meristem (SAM) is composed of multiple functional domains displaying different cellular behaviour. The organising centre (OC) acts as a stem cell niche by instructing and maintaining stem cell fate in the overlying domain, the central zone (CZ). As plant cells are embedded in rigid cell walls, anticlinal stem cell divisions occurring at the CZ passively displace daughter cells laterally towards the peripheral zone (PZ) and towards the outer edge of the SAM, where they generate flower primordia. In turn, primordia initiate floral meristems, which contribute to floral bud outgrowth, before they differentiate into four floral whorls: sepal, petal, stamen or carpel (Figure 2A). On the vertical growth axis, periclinal stem cells divisions in the CZ, displace cells to the OC, the rib meristem and towards the stem, where they fully differentiate (Figure 2A; reviewed in (Gaillochet et al., 2015). The observation of the shoot meristem dynamics from the birth of a stem cell to its differentiation raises the question of how the successive cellular identities are acquired and coordinated during this process.

I.2.2 Molecular control of shoot meristem activity

Past molecular studies have extensively characterized the molecular network underpinning SAM activity and revealed that the integration of phytohormonal signals and transcriptional networks are essential to establish spatial patterns and control cellular behaviour within this structure (Figure 2B). At the centre, stem cell maintenance is regulated by the activity of two parallel pathways. First, the homeodomain transcription factor WUSCHEL (WUS) instructs stem cell fate non-cell autonomously from its region of expression, the organising centre (OC) to the CZ, where it promotes *CLAVATA3* (*CLV3)* expression (Laux et al., 1995; Mayer et al., 1998). This intercellular communication requires WUS protein movement from the OC to the CZ through plasmodesmata (Daum et al., 2014; Yadav et al., 2011). Interestingly, WUS amino acid sequence defines its migratory behaviour, sub-cellular partitioning but also its stability (Daum et al., 2014; Rodriguez et al., 2016). In addition, the formation of WUS homodimers may also influence its movement and ability to directly activate or repress *CLV3* expression (Daum et al., 2014; Perales et

al., 2016). *CLV3* encodes for a small peptide that is arabinosylated and secreted into the CZ intercellular space and signals to the OC (Brand et al., 2000; Rojo et al., 2002; Schoof et al., 2000). At the plasma membrane, CLV3 directly binds the Leucine-rich-repeat (LRR) receptor like kinases (RLK) CLV1 and BARELY ANY MERISTEMS (BAM) receptors, which associate with CLV2 and RPK2 co-receptors (Bleckmann et al., 2009; Clark et al., 1997; Nimchuk et al., 2015; Ogawa et al., 2008; Shinohara and Matsubayashi, 2015). In turn, the signal is transmitted by G-proteins and mitogen-activated protein kinase (MAPK) to transcriptionally repress *WUS* expression (Betsuyaku et al., 2011; Bommert et al., 2013; Ishida et al., 2014). As a consequence, the WUS-CLV3 regulatory interaction defines a negative feedback loop that stabilizes the number of stem cells within the shoot meristem (Brand et al., 2000; Schoof et al., 2000). In addition to its role in instructing stem cell fate, WUS activity prevents stem cell differentiation by directly repressing differentiation genes including KANADI1 (KAN1), KAN2, YABBY3 and ASYMETRIC LEAVES 2 (AS2) (Yadav et al., 2013). Importantly, WUS tightly interacts with phytohormonal signalling pathways. Cytokinin promotes WUS expression, which in turn sensitizes the OC to cytokinin signals by repressing the transcriptional repressors *ARABIDOPSIS RESPONSE REGULATORS* (*ARR*) *ARR7* and *ARR15*. Consequently, cytokinin and WUS form a positive auto-regulatory loop that stabilizes the position of the OC domain (Chickarmane et al., 2012; Gordon et al., 2009; Leibfried et al., 2005).

In parallel to the *WUS* signalling system, the KNOTTED-like homeobox (KNOX) transcription factor SHOOTMERISTEMLESS (STM) maintains stem cell fate by downregulating the expression of the differentiation genes *ASYMETRIC LEAVES 1* (*AS1*) and *AS2.* In addition, STM negatively regulates giberrellic acid accumulation and directly promotes the expression of the cytokinin biosynthetic enzyme *ISOPENTENYL TRANSFERASE 7* (IPT7) (Byrne et al., 2000; Byrne et al., 2002; Jasinski et al., 2005; Yanai et al., 2005). Taken together, WUS and STM function promote stem cell identity and maintain the spatial organization at the centre of the SAM by promoting cytokinin response and by preventing the expression of differentiation genes (Byrne et al., 2000; Jasinski et al., 2005; Leibfried et al., 2005; Yadav et al., 2013).

In contrast to the centre of the meristem, where the relative positions of OC, CZ and PZ are fixed, lateral organs at the periphery are continuously established in localized domains, following a regular geometrical pattern, termed phyllotaxis (reviewed in Kuhlemeier, 2007). The autocatalytic auxin dynamics controls this process by

integrating transport, signalling and biosynthesis (Bhatia et al., 2016; Cheng et al., 2006; Hardtke and Berleth, 1998; Reinhardt et al., 2003b).

Importantly, the ARF transcription factor MONOPTEROS (MP) orchestrates auxin signalling dynamics at multiple levels. First, MP expression pattern follows the pattern of auxin signalling and in turn promotes auxin responses, forming a positive feedback loop (Bhatia et al., 2016; Lau et al., 2011). In addition, MP locally re-directs the polar localization of the auxin-efflux transporter PIN FORMED 1 (PIN1) towards its sites of expression and thereby enhances local auxin accumulation (Bhatia et al., 2016). As a result, this positive feedback system dynamically creates auxin sinks, which later fade when auxin flow is redirected towards the vascular system (Jönsson et al., 2006; Reinhardt et al., 2003b). Second, MP positively regulates *AHP6* expression, which stabilizes phyllotactic patterns by modulating cytokinin responses at the PZ (Besnard et al., 2014). Third, by associating with SWI-SNF chromatin remodelling ATPases BRAHMA (BRM) and SPLAYED (SYD), MP triggers cell fate switch by modifying the chromatin landscape, allowing the expression of the floral meristem genes *LEAFY* (*LFY*), *AINTEGUMENTA* (*ANT*), *AINTEGUMENTA-LIKE 6* (*AIL6*) and *FILAMENTOUS FLOWER* (*FIL*) (Wu et al., 2015). In addition, MP modulates cytokinin signalling across the SAM by directly repressing *ARR7* and *ARR15* expression (Zhao et al., 2010), and thus participate in relaying a signal from the primordia to the centre of the SAM.

In parallel to MP function, primordia modulate SAM activity by repressing *WUS* expression through the CLV27/ LRR RLK ARABIDOPSIS THALIANA FASCIATED EAR 3 (AtFEA3) signalling (Je et al., 2016). Together, these communication feedbacks contribute to coordinate cell production at the centre with the formation of lateral organs at the periphery of the SAM and consequently couple meristem size with the rate of lateral organ initiation (Landrein et al., 2015).

I.2.3 Molecular control of floral meristem activity

After their birth in the CZ and their transition through the PZ and flower primordia, cell lineages acquire floral fates. Upon initiation, the floral meristem acquires meristematic activity through the re-establishment of cytokinin responses and WUS-CLV3 signalling (reviewed in (Denay et al., 2017). In parallel, the two transcription factors LFY and APETALA 1 (AP1) orchestrate the acquisition of floral meristem fate and exclude expression of inflorescence meristem genes from the floral meristem such as *TERMINAL FLOWER 1* (*TFL1*) (Kaufmann et al., 2010; Weigel et al., 1992;

Winter et al., 2011). In addition, AP1 and LFY trigger the specification of floral organs by promoting the expression of 4 classes of floral homeotic genes: A, B, C and E function genes (Kaufmann et al., 2010; Winter et al., 2011). Mechanistically, the combinatorial expression of these homeotic genes defines four spatial domains organized in concentric rings that later differentiate in sepals, petals, stamens and carpel (Figure 2A, B; Coen and Meyerowitz, 1991).

Upon flower differentiation, the number of floral organ produced is defined by the floral meristem activity, which is under the control of a negative regulatory loop: *WUS* promotes *AGAMOUS* expression at the inner 2 whorls of the developing flower, which in turn represses *WUS* expression through the expression of KNUCKLES (KNU). As a result, this negative feedback loop times floral meristem termination (Lohmann et al., 2001; Sun et al., 2014; Sun et al., 2009). In addition to its function in terminating the floral meristem, AGAMOUS orchestrates the differentiation of two carpels, which later fuse to form the female reproductive organ: the gynoecium or fruit (reviewed in Roeder and Yanofsky, 2006).

I.2.4 Molecular control of gynoecium patterning

The gynoecium is essential for plant reproductive capacity as it is the site where fertilization, seed maturation and seed dispersal take place. During fertilization, pollen grains are received and germinate at the apical part of the gynoecium called the stigma, which is composed of epidermal cells associated with the style. Pollen tubes are then guided through the transmitting tract at the centre of the ovary, and deliver sperm cells to the female gametophyte located within the ovules. Gynoecium development is initiated at the centre of the flower from two carpels primordia that grow and later fuse. During this process, the developing fruit is patterned around three axes of symmetry: apical-basal, medio-lateral and abaxial-adaxial (reviewed in Østergaard, 2009).

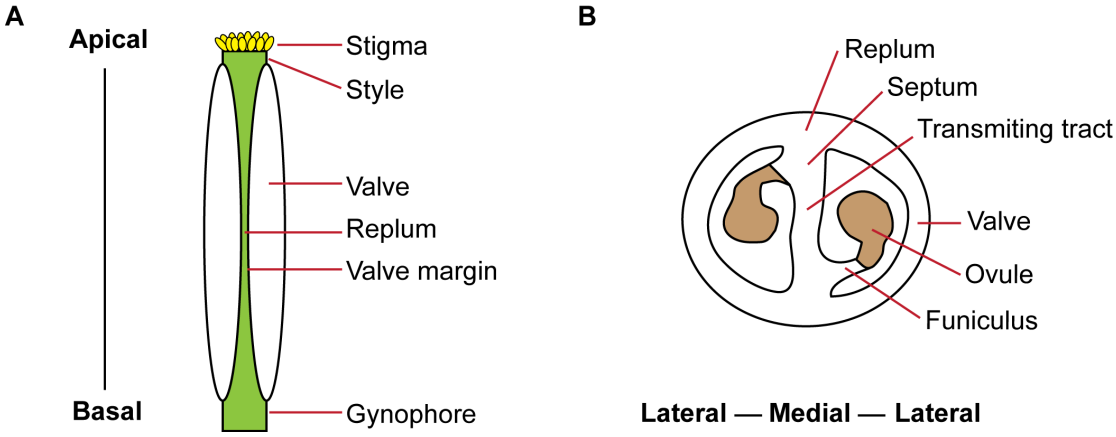

Figure 3: Gynoecium patterning
(A-B) Schematic representation of lateral (A) and transversal (B) views of *Arabidopsis* gynoecium at stage 12-13

Apical-basal patterning specifies the style and stigma apically, the ovary at the centre and the gynophore at the base of the gynoecium (Figure 3A). Auxin plays a critical role during this process as inhibiting polar auxin transport or interfering with ARF3/ETTIN function leads to strong patterning defects (Nemhauser et al., 2000). PIN1 and PIN3 polar localization guides auxin transport apically and participates in building apical auxin signalling maxima (Larsson et al., 2014; Moubayidin and Østergaard, 2014). This apical domain coincides with the expression of STYLISH (STY) and SPATULA (SPT) transcription factors, which specify style and stigma identity (Heisler et al., 2001; Kuusk et al., 2002; Trigueros et al., 2009). In addition, NGATHA factors (NGA1-4) form a small clade of B3-domain transcription factors that redundantly control style fusion (Alvarez et al., 2006). Importantly, the activity of these factors is tightly intertwined with auxin signalling as STY and NGA factors promote the expression of auxin biosynthesis genes including *YUC4*, thereby concentrating auxin at the apical part of the gynoecium (Eklund et al., 2010; Martínez-Fernández et al., 2014).

On the other hand, medio-lateral patterning defines the replum externally and a meristematic ridge internally, from which arises the reproductive organs including the septum, transmitting tract and ovules but also part of the style and stigma. Laterally, the valves are formed. By allowing efficient seed dispersal, theses structures are crucial for post-fertization processes (reviewed in Østergaard, 2009).

Finally, abaxial-adaxial patterning is regulated by the transcription factor KAN1 (Pires et al., 2014), which instructs abaxial polarity in the gynoecium and ultimately define different cell identities between the inner and the outer part of the valves

I.3 *HECATE* genes control shoot meristem and gynoecium development

From the progression of a shoot stem cell to a differentiated gynoecium cell, multiple organs are built from the activity of meristematic regions, such as the SAM, the floral meristem (FM) or the carpel margin meristem (CMM). Interestingly, the regulatory network controlling meristematic activity displays similarities between the gynoecium and the floral or shoot meristem, suggesting that a conserved core regulatory network has been co-opted in multiple developmental contexts (Girin et al., 2009). In line with this idea, HECATE (HEC) bHLH transcription factors regulate shoot meristem activity and gynoecium development (Gremski et al., 2007; Schuster et al., 2014).

In the shoot apical meristem, WUS directly represses *HEC1* expression. In line with this regulation, HEC1 is expressed at the CZ, PZ and primordia but is absent from the OC (Schuster et al., 2014). HEC1 exclusion from the OC by WUS is crucial to maintain stem cell fate as HEC1 misexpression in the OC leads to stem cell exhaustion and subsequently to SAM arrest. Consistently, WUS and HEC1 regulatory signatures present opposite trends.

HEC1 acts redundantly with its two closest homologous genes–HEC2 and HEC3–and HEC loss-of-function plants (*hec1,2,3* triple mutant) display a smaller meristem together with changes in *WUS* and *CLV3* expression compared to wild type plants. In contrast, HEC gain-of-function in the CZ expands the stem cell system and represses *WUS* and *CLV3* expression, suggesting that HEC function can promote meristematic activity independently of the WUS/CLV3 feedback system. Mechanistically, HEC interacts with cytokinin signalling by positively regulating the expression of the A-type ARRs ARR7 and ARR15. This in turn creates a negative regulatory loop on the WUS/CLV3 signalling system by lowering cytokinin responses after prolonged HEC activity in the CZ (Schuster et al., 2014).

At the gynoecium, HEC genes are expressed at the transmitting tract and at the style, whose development is impaired in *hec1,2,3* mutants, leading to plant sterility (Gremski et al., 2007). HEC proteins form heterodimers with another bHLH transcription factor SPT suggesting that they could functionally interact during gynoecium medio-lateral patterning. Interestingly, HEC ectopic expression in the fruit gives rise to flower phenotypes reminiscent of plants impaired in auxin transport or signalling, indicating that HEC function may also control auxin signalling pathways during gynoecium development (Gremski et al., 2007).

I.4 Aims

My PhD project was built around three central goals:

1) Characterizing HEC function in the shoot apical meristem

2) Characterizing HEC function in the gynoecium

3) Building a HEC1 regulatory network to identify molecular players mediating its function

1) In the shoot apical meristem, the observation that HEC activity in the stem cells could enlarge the SAM and completely repress the expression of the core regulatory players, was surprising and suggested that it could act independently of WUS and CLV3 signalling to directly control cell proliferation (Schuster et al., 2014). In addition, the strong expression of HEC1 at the SAM periphery and the formation of pin-like inflorescences in *HEC* gain-of function plants, suggested that *HEC* genes might also regulate lateral organ initiation. However, the developmental and molecular processes mediating HEC activity in the SAM still remained elusive (Schuster et al., 2014). To tackle these questions, we specifically aimed at:

- Characterizing the SAM cellular dynamics after modulation of HEC activity
- Analysing the role of HEC genes during lateral organ initiation
- Unravelling the molecular mechanisms mediating HEC function in distinct domains of the SAM

2) The analysis of *hec1,2,3* mutant plants showed that the style and transmitting tract at the fruit were defective, leading to plant sterility. Mechanistically, since HEC factors could physically interact with the bHLH transcription factor SPT, this suggested that they could form a functional protein complex. Furthermore, the defects observed in gynoecia after overexpressing HEC1 were reminiscent of mutants impaired in auxin homeostasis (Gremski et al., 2007; Nemhauser et al., 2000). Although these data started to unveil the molecular interactions mediating HEC function at the gynoecium, our knowledge of the regulatory mechanisms underpinning remained elusive. To bridge this gap, we specifically aimed at:

- Testing the functional interaction between HEC and SPT
- Further dissecting the interaction between HEC, auxin and cytokinin during gynoecium development

3) Under different developmental or cellular contexts, HEC factors can exhibit various regulatory functions. Surprisingly in the SAM, although HEC function in the CZ promoted SAM expansion, HEC1 misexpression in the OC terminated the SAM activity, whereas HEC overexpression at the SAM periphery interfered with lateral organ initiation (Gremski et al., 2007; Schuster et al., 2014). In addition to these contrasting functions in the SAM, HEC factors have also been shown to regulate gynoecium development and seedling photomorphogenesis (Gremski et al., 2007; Zhu et al., 2016).

Although HEC functional versatility has been described, our molecular understanding of this property remained elusive. To further investigate this question, we specifically aimed at:

- Reconstructing HEC1 regulatory networks using protein-protein interaction screenings and genome-wide profiling approaches
- Identifying HEC1 regulatory modules and functionally relevant candidate genes
- Testing newly identified regulatory interactions in the SAM and in the gynoecium

II. Material

II.1 Organisms

II.1.1 Plants

pWUS:3xYFP-NLS_pCLV3:mCherry-NLS (Pfeiffer et al., 2016)*; pTCSn:erGFP* (Zürcher et al., 2013)*; pPIN1:PIN1-GFP* (Heisler et al., 2005)*; hec1,2,3* (Schuster et al., 2014); *pDR5v2:3xYFP-NLS* (*Col-Utrecht*); R2D2 (*Col-Utrecht*) (Liao et al., 2015); *wus-1_pWUS:WUS-GFP* (Daum et al., 2014)*; pSPT:GUS* (Groszmann et al., 2010)*; pHEC1:GUS* (Schuster et al., 2015)*, p16:GUS* (Schuster et al., 2014)*; nga1; nga1,2; nga1,3; nga1,3,4* (Trigueros et al., 2009); *spt-1*2 (Ichihashi et al., 2010); *pALC:ALC-GUS (Ler)* (Rajani and Sundaresan, 2001), *pRGA:GFP-RGA (Ler)* (Silverstone et al., 2001) were previously described. *alcatraz* mutant line corresponds to SALK_103763. When not specifically mentioned, all plants used in this study are in the Col-0 background.

II.1.2 Bacterial strains

Escherichia coli:

DH5α: (Life technologies; Carlsbad, USA); F– Φ80*lac*ZΔM15 Δ(*lac*ZYA-*arg*F) U169 *rec*A1 *end*A1 *hsd*R17 (rK–, mK+) *pho*A *sup*E44 λ– *thi*-1 *gyr*A96 *rel*A1

DB3.1: (Life technologies; Carlsbad, USA); F– *gyr*A462 *end*A1 Δ(sr1-*rec*A) *mcr*B *mrr hsd*S20(rB–, mB–) *sup*E44 *ara*-14 *gal*K2 *lac*Y1 *pro*A2 *rps*L20(SmR) *xyl*-5 λ– *leu mtl*1

XL1MR: (Stratagene; La Jolla, USA) Δ(mcrA)183Δ(mcrCB-hsdSMR-mrr)173 endA1 supE44 thi-1 recA1 gyrA96 relA1 lac

Agrobacterium tumefaciens:

ASE: KanR, CamR, pSoup+ (TetR)

Saccharomyces cerevisiae:

Ah109: *MATa, trp1-901, leu2-3, 112, ura3-52, his3-200, gal4Δ, gal80Δ, LYS2:: GAL1UAS-GAL1TATA-HIS3, GAL2UAS-GAL2-TATA-ADE2, URA3::MEL1UAS-MEL1 TATA-lacZ* (James *et al.,* 1996)

pJ69-4a: MATa, trp1-, Δ901, leu2-3, 112, ura3-52, his3-,Δ200, gal4Δ, gal8Δ, GAL2-ADE2, LYS2::GAL1-HIS3, met2::GAL7-lacZ (James *et al.,* 1996)

pJ69-4alpha: MATalpha, trp1-, Δ901, leu2-3, 112, ura3-52, his3-200, gal4Δ, gal80Δ, GAL2-ADE2, LYS2::GAL1-HIS3, met2::GAL7-lacZ (James *et al.,* 1996)

Y187: MATα, ura3-52, his3-200, ade2-101, trp1-901, leu2-3, 112, gal4Δ, met, gal80Δ, MEL1, URA3::$GAL1_{UAS}$-$GAL1_{TATA}$-lacZ (Harper *et al.*, 1993)

II.2 Vectors and Constructs

II.2.1 Vectors

pDONR221 (Life technologies; Carlsbad, USA)

pDEST22 (Thermo Fischer Scientific; Waltham, USA)

pDEST32 (Thermo Fischer Scientific; Waltham, USA)

pGADT7 (Clontech; Mountain View, USA)

pGBKT7 (Clontech; Mountain View, USA)

pGGC (Lampropoulos et al., 2013)

pGREENIIS vector series (Markus Schmid, Jan Lohmann, Detlef Weigel)

pENTR1A (Life technologies; Carlsbad, USA)

pGGZ003 (Lampropoulos et al., 2013)

II.2.2 Constructs

All constructs generated for this study were recorded on the FileMakerPro database from Prof. Jan Lohmann´s laboratory, Centre for Organismal Studies, Heidelberg University.

II.3 Chemicals

II.3.1 Dyes

Working stocks:

1 mg/ml DAPI (4', 6-diamidin-2-phenylindole)	(Roth; Karlsruhe, Germany)
20 μM FM4-64; 1 mM stock in DMSO	(Life technologies; Carlsbad, USA)
10 μg/mL Propidium iodide	(Sigma-Aldrich; St. Louis, USA)

II.3.2 Antibiotics

1000x stocks:

100 mg/ml Ampicilin	(Sigma-Aldrich; St. Louis, USA)
25 mg/ml Chloramphenicol in EtOH	(Roth; Karlsruhe, Germany)
50 mg/ml Gentamycin	(Sigma-Aldrich; St. Louis, USA)
50 mg/ml Hygromycin B (2000x stock)	(Roche; Basel, Switzerland)
50 mg/ml Kanamycin	(Roth; Karlsruhe, Germany)

100 mg/ml Spectinomycin	(Sigma-Aldrich; St. Louis, USA)
10 mg/ml Tetracyclin in EtOH	(Sigma-Aldrich; St. Louis, USA)

II.3.3 Herbicides

10 *µ*g/mL Glufosinate: Basta®	(Bayer; Leverkusen,Germany)
3 *µ*l/l Butafenacil: Inspire ®	(Syngenta; Basel, Switzerland)

II.3.4 Antibodies

Primary antibody

Anti-GFP: GFP-trap®	(Chromotek; Planegg, Germany)

Secondary antibody

Anti-digoxigenenin-AP (FAB fragments)	(Roche; Basel, Switzerland)

II.3.5 Plant treatments

6-Benzylaminopurine	(Sigma-Aldrich; St. Louis, USA)
Gibberellic acid	(Sigma-Aldrich; St. Louis, USA)
Dexamethasone	(Sigma-Aldrich; St. Louis, USA)
Cycloheximide	(Sigma-Aldrich; St. Louis, USA)

II.3.6 Histology

Blocking reagent	(Roche; Basel, Switzerland)
Ethanol	(Sigma-Aldrich; St. Louis, USA)
Formaldehyde	(Sigma-Aldrich; St. Louis, USA)
Formamide	(Sigma-Aldrich; St. Louis, USA)
Glycogen	(Fermentas; Waltham, USA)
Paraplast	(Leica; Wetzlar, Germany)
NBT-BCIP stock solution	(Roche; Basel, Switzerland)
Roti ®-Histol	(Merck; Darmstadt, Germany)
Roti ®-Clear	(Merck; Darmstadt, Germany)
t-RNA from yeast	(Roche; Basel, Switzerland)
Xylol	(Merck; Darmstadt, Germany)

II.3.7 Yeast-two-hybrid assay

3-Amino-1,2,4-triazole (3-AT)	(Sigma-Aldrich; St. Louis, USA)
Lithium Acetate (LiAC)	(Sigma-Aldrich; St. Louis, USA)
PEG 3350	(Merck; Darmstadt, Germany)
UltraPure herring sperm DNA solution	(ThermoScientific; Waltham, USA)
Bacto-agar	(Roth; Karlsruhe, Germany)
Bacto yeast extract	(Roth; Karlsruhe, Germany)
Bacto-tryptone	(Roth; Karlsruhe, Germany)
Adenine	(Sigma-Aldrich; St. Louis, USA)
Complete supplement mixture (CSM)	(MP biomedicals; Santa Ana, USA)
Yeast neutral base w/o aa	(MP biomedicals; Santa Ana, USA)
Glass Beads (0.17; 0.18 mm)	(Sartorius, Göttingen, Germany)
Phenol/Chloroform/Isoamyl Alcohol	(Roth; Karlsruhe, Germany)

II.3.8 Chromatin immunoprecipitation

Protease inhibitor cocktail	(Sigma-Aldrich; St. Louis, USA)
Phenylmethane sulfonyl fluoride (PMSF)	(ThermoScientific; Waltham, USA)
Igepal CA-630	(Sigma-Aldrich; St. Louis, USA)
Protein-A Agarose	(Santa Cruz Biotechnology; Santa Cruz, USA)

II.3.9 GUS staining

Potassium Ferrocyanide (K-Ferro)	(Merck; Darmstadt, Germany)
Potassium Ferricyanide (K-Ferri)	(Merck; Darmstadt, Germany)
X-Gluc	(Roth; Karlsruhe, Germany)

II.3.10 Plant growth

Phyto-agar	(Duchefa; Harlem, Netherlands)
Silwet L-77	(Lehle Seeds; Round Rock, USA)

II.4 Enzymes

II.4.1 Restriction endonucleases

All restriction enzymes used in this study were obtained from Fermentas (Waltham, USA) or from NEB (Ipswich, USA).

II.4.2 DNA- / RNA- modifying enzymes

DNAse I (RNAse free)	(Fermentas; Waltham, USA)
RNAse (DNAse free)	(Fermentas; Waltham, USA)
T4 DNA ligase	(Fermentas; Waltham, USA)

II.4.3 PCR

Phusion DNA polymerase	(Finnzymes; Espoo, Finland)

II.4.4 Cloning

BP clonase	(Thermo Fisher Scientific; Waltham, USA)
LR clonase	(Thermo Fisher Scientific; Waltham, USA)

II.4.5 *In situ hybridization*

Proteinase K (recombinant PCR grade)	(Roche; Basel, Switzerland)

II.5 Nucleic acids and nucleotides

Oligonucleotides	(Eurofins genomics; Luxembourg)
GeneRuler DNA ladder mix	(ThermoScientific; Waltham, USA)
dNTPs	(ThermoScientific; Waltham, USA)

II.6 Kits

II.6.1 DNA extraction and purification

innuPREP DOUBLE pure kit	(Analytikjena; Jena, Germany)
innuPREP plasmid mini kit	(Analytikjena; Jena, Germany)
MiniElute Reaction Cleanup kit	(Qiagen; Hilden, Germany)

II.6.2 RNA extraction, cDNA synthesis

RNAeasy plant mini kit	(Qiagen; Hilden, Germany)
RevertAid First Strand cDNA synthesis kit	(ThermoScientific; Waltham, USA)

II.6.3 Genotyping PCR

JumpStart™ REDTaq® ReadyMix™	(Sigma-Aldrich; St. Louis, USA)

II.6.4 Quantitative real time PCR

ABsolute qPCR SYBR Green mix	(ThermoScientific; Waltham, USA)

II.6.5 *In situ hybridization* probe synthesis

DIG RNA labelling kit	(Roche; Basel, Switzerland).

II.6.6 Construction of next-generation sequencing libraries

Rubicon Thru-Plex DNA-seq kit	(Rubicon genomics; Ann harbor, USA)
NEB Poly (A) Magnetic isolation module	(NEB; Ipswich, USA)
NEBnext Ultra Direction RNA Prep Kit	(NEB; Ipswich, USA)
NEBnext Multiplex Oligo's for Illumina	(NEB; Ipswich, USA)

II.7 Media

II.7.1 Plant culture media

½ MS Agar plates	2.15 g/l MS salts
	0.75% Phyto-agar (w/v)
	Adjusted to pH 5.7 with KOH

Antibiotics were mixed to liquid media (55°C) at concentration indicated in section II.3.3.

II.7.2 Bacterial culture media

LB medium	5 g/l Yeast extract
	10 g/l Trypton
	5 g/l NaCl

1ml/l antibiotic stock added after autoclaving (55°C)

II.7.3 Yeast culture media

II.7.3.1 Yeast growth

YPAD	20 g/l Glucose
	10 g/l Bacto yeast extract
	20 g/l Bacto Tryptone
	80 mg/l Adenine
	pH adjusted to 6.5
	w/ or w/o 20 g/l Bacto agar

II.7.3.2 Transformation

1M LiAC	
PEG 3350 (50% (w/v))	
2 mg/ml Salmon sperm DNA	
2xYPAD	40 g/l Glucose
	20 g/l Bacto yeast extract
	40 g/l Bacto Tryptone
	80 mg/l Adenine
	pH adjusted to 6.5

II.7.3.3 Selection

Single drop out medium (-T or -L)	6.7 g/l Yeast nitrogen base w/o aa
	20 g/l Bacto-agar
	20 g/l Glucose
	0.94 g/l CSM -L or -T
	pH adjusted to 5.8
Double drop out medium (-L,T)	6.7 g/l Yeast nitrogen base w/o aa
	20 g/l Bacto-agar
	20 g/l Glucose
	0.64 g/l CSM -L,T
	pH adjusted to 5.8
Triple drop out medium (-H,L,T)	6.7 g/l Yeast nitrogen base w/o aa
	20 g/l Bacto-agar
	20 g/l Glucose
	0.61 g/l CSM -H,A,L,T
	200 mg/l Adenine-hemisulfate
	pH adjusted to 5.8
	Supplemented or not with 3-AT

II.8 Buffers and solutions

II.8.1 *A. thaliana* transformation

Infiltration medium	2.15 g/l MS salts
	5% sucrose
	0.015% Silwet L-77
	pH adjusted to 5.7

II.8.2 Extraction of plasmid DNA from yeast

Breaking buffer	2% Triton X-100
	1% SDS
	100 mM NaCl
	100 mM Tris-Cl, pH 8.0
	1 mM EDTA

II.8.3 Extraction of genomic DNA from *A. thaliana*

Extraction buffer	200 mM Tris-HCl pH 7.5
	250 mM NaCl
	25 mM EDTA
	0.5% SDS (w/v)
TE Buffer	10 mM Tris-HCl pH 8.0
	1 mM EDTA

II.8.4 Tobacco leaf transfection

Transfection buffer	10 mM $MgCl_2$
	10 mM MES, pH 5.7
	150 μM Acetosyringone

II.8.5 Chromatin immuno-precipitation

Cross-linking buffer	1% Formaldehyde
Extraction buffer 1	0.4 M Sucrose 10 mM Tris-HCl (pH 8.0) 10 mM $MgCl_2$ 5 mM ß-Mercaptoethanol 1 mM PMSF 1x Protease inhibitor
Extraction buffer 2	0.25 M Sucrose 10 mM Tris-HCl (pH 8.0) 10 mM $MgCl_2$ 1% Triton X-100 5 mM ß-Mercaptoethanol 1 mM PMSF 1x Protease inhibitor
Extraction buffer 3	1.7 M Sucrose 10 mM Tris-HCl (pH 8.0) 2 mM $MgCl_2$ 0.15% Triton X-100 5 mM ß-Mercaptoethanol 1 mM PMSF 1x Protease inhibitor
Nuclei lysis buffer	50 mM Tris-HCl (pH 8.0) 10 mM EDTA (pH 8.0) 1% SDS 1 mM PMSF 1x Protease inhibitor

ChIP dilution buffer	1.1% Triton X-100 1.2 mM EDTA (pH 8.0) 16.7 mM Tris-HCl (pH 8.0) 167 mM NaCl
Low salt wash buffer	150 mM NaCl 0.1% SDS 1% Triton X-100 2 mM EDTA (pH 8.0) 20 mM Tris-HCl (pH 8.0)
High salt wash buffer	500 mM NaCl 0.1% SDS 1% Triton X-100 2 mM EDTA (pH 8.0) 20 mM Tris-HCl (pH 8.0)
LiCl wash buffer	0.25 M LiCl 1% Igepal CA630 1% Na-deoxycholate 1 mM EDTA (pH 8.0) 10 mM Tris-HCl (pH 8.0)
TE buffer	10 mM Tris-HCl (pH 8.0) 1 mM EDTA (pH 8.0)
Elution buffer	1% SDS 0.1 M $NaHCO_3$

II.8.6 *In situ hybridization*

II.8.6.1 General solutions

5 M NaCl

0.75 M NaCl

1 M Tris pH 7.5

1 M Tris pH 8.0

1 M Tris pH 9.5

0.5 M EDTA pH 8.0

1 M $NaHCO_3$

1 M Na_2CO_3

1 M $MgCl_2$

II.8.6.2 Probe synthesis and hydrolysis

4 M LiCl

2x Carbonate buffer	80 mM $NaHCO_3$ 120 mM Na_2CO_3
10x Neutralization buffer	10% Acetic acid

II.8.6.3 Dewaxing and rehydration

FAA (Formaldelhyde Acetic Acid)	50% Ethanol 5% Glacial Acetic Acid 3.7% Formaldehyde
10x TE	100 mM Tris 10 mM EDTA

1x TE

Proteinase K buffer	0.1 M Tris pH 7.5 0.05 M EDTA

II.8.6.4 Hybridization

10x PBS	1.3 M NaCl 30 mM NaH_2CO_3 70 mM Na_2HPO_4 adjust to pH 7.0 with HCl

1x PBS

1x PBS-G	2 mg / mL Glycine in 1x PBS
10x in situ salts	3 M NaCl 100 mM Tris pH 8.0 50 mM EDTA 53.7 mM NaH_2PO_4 46.3 mM Na_2HPO_4
50 x Dehnardt´s solution	1% Ficoll 1% Polividon 25 1% BSA
50% Dextrane sulfate	
tRNA	25 mg tRNA 0.5 mL H_2O
Hybridization buffer	50% (deionized) formamide, 10% dextrane sulfate, 1x *in situ* Salts 1x Denhardt's solution 0.5 mg/mL tRNA

II.8.6.5 Washing

20x SSC	3 M NaCl 0.3 M Na-citrate
2x SSC	
Soaking solution	2x SSC in 50% Formamide

II.8.6.6 Detection and colour reaction

10x TBS	1 M Tris pH 7.5 1.5 M NaCl
1x TBS-T	0.3% Triton to 1xTBS
TNM-50	100 mM Tris pH 9.5 100 mM NaCl 50 mM $MgCl_2$

II.8.7 Seed sterilization

Bleach	0.6% Sodium hypochlorite 1% Triton X-100

II.8.8 Dexamethasone / hormonal treatment

Dex induction medium	10 μM dexamethasone 0.01% EtOH 0.015% Silwet L-77 w/ or w/o 10 μM cycloheximid w/ or w/o 0.01% EtOH
Mock induction medium	0.01% EtOH 0.015% Silwet L-77 w/ or w/o 10 μM cycloheximid w/ or w/o 0.01% EtOH
Cytokinin treatment medium	50 μM BAP in 0.01% DMSO 0.015% Silwet L-77
Mock hormone treatment medium	0.01% DMSO 0.015% Silwet L-77

II.8.9 GUS staining

Staining buffer	0.2% Triton X-100
	50 mM $NaPO_4$
	2 mM Potassium-Ferrocyanide
	2 mM Potassium-Ferricyanide
	2 mM X-Gluc

II.9 Instruments

Confocal microscope TCS SP5	(Leica Microsystems; Mannheim, Germany)
Confocal microscope Nikon A1	(Nikon Instruments; Tokyo, Japan)
Digital Camera AxioCam HRC	(Carl Zeiss; Oberkochen, Germany)
Digital Camera Nikon D60	(Nikon Corporation; Tokyo, Japan)
DNA Engine/Chromo4 RT Detector	(Bio-Rad; Hercules, USA)
Dyad DNA Engine	(Bio-Rad; Hercules, USA)
FLIM-Photomultiplier	(Hamamatsu; Shizuoka, Japan)
Gelsystem PerfectBlue wide	(PEQLAB Biotechnologie GmbH; Erlangen, Germany)
Gelsystem PerfectBlue Midi S	(PEQLAB Biotechnologie GmbH; Erlangen, Germany)
Heating block neoBlock Duo	(neoLab Migge Laborbedarf; Heidelberg, Germany)
Incubation Shaker Innova® 44	(New Brunswick Scientific; Edison, USA)
Incubator Binder BD-Serie	(Binder; Tuttlingen, Germany)
Laboratory freezer	(ThermoScientific; Waltham, USA)
Laboratory refrigerator	(Liebherr; Mannheim, Germany)
Microscope Axio Imager.M1	(Carl Zeiss; Oberkochen, Germany)
Microtome RM2235	(Leica Microsystems; Mannheim, Germany)
Milli-Q® water system	(Merck Millipore; Billerica, USA)
Nanodrop ND-1000	(Nanodrop, Wilmington, USA)
Orbital shaker GFL® 3011	(GFL; Burgwedel, Germany)
Paraffin embedding center EG1160	(Leica Microsystems; Mannheim, Germany)
Pipetus® Akku	(Hirschmann Laborgeräte; Eberstadt, Germany)
PicoHarp 300 TCSPC	(PicoQuant, Berlin, Germany)

Power Supply EPS 301	(GE Healthcare Bio-Sciences AB; Fairfield, USA)
Precision balance	(Kern & Sohn; Balingen, Germany)
Refrigerated centrifuge	
Eppendorf 5430R	(Eppendorf; Hamburg, Germany)
Sonicator Misonix S-4000	(Misonix; Farmingdale, USA)
Smart processor ASP200	(Leica Microsystems; Mannheim, Germany)
Stereomicroscope	(Nikon Corporation; Tokyo, Japan)
Table top centrifuge	
Eppendorf 5424	(Eppendorf; Hamburg, Germany)
Tissue Lyser II	(Qiagen; Hilden, Germany)
Vortex-Genie® 2	(Scientific Industries; Bohemia, USA)
Waterbath WNB 7	(Memmert; Schwabach, Germany)

II.10 Software

Microsoft office 2008	(Microsoft Corporation; Albuquerque, USA)
R	(https://cran.r-project.org/)
R Studio	(https://www.rstudio.com/)
Adobe creative suite 4	(Adobe Systems; San Jose, USA)
Gene Construction Kit 4.0.2	(Textco BioSoftware, Raleigh, USA)
Image J/ Fiji	(https://imagej.nih.gov/ij/)
Integrative Genomics Viewer	(Robinson et al., 2011)
Papers 2	(http://papersapp.com/)
MACS2.0	(Zhang et al., 2008)
SAM tools	(Li et al., 2009)
BED tools	(Quinlan and Hall, 2010)
Fast QC	(http://www.bioinformatics.babraham.ac.uk/projects/fastqc)
Tophat 2	(Kim et al., 2013)
Bowtie 2.1.0	(Langmead and Salzberg, 2012)
KNIME	(Berthold et al., 2008)
Matlab	(MathWorks, Inc; Natick, USA)

III. Methods

III.1 Working with *Arabidopsis*

III.1.1 Genotyping

For genotyping transgenic plants, tissue from young leaves (about 5 mm^2) was harvested, shock frozen in liquid nitrogen, ground using Tissue Lyser II (Qiagen, Hilden, Germany) and mixed with extraction buffer. The isolated supernatant was mixed with isopropanol and centrifuged. Pellets were cleaned with 70% EtOH and air-dried before being resuspended in TE buffer.

Plant DNA was used as template for genotyping PCR using the JumpStart™ REDTaq® ReadyMix™ (Sigma-Aldrich; St. Louis, USA).

III.1.2 Creation of transgenic lines

To create *Arabidopsis* transgenic lines, genomic sequences were cloned within a T-DNA and transformed in *Agrobacterium tumefasciens* strain ASE. Bacteria were grown for 2 days at 28°C, resuspended in infiltration medium and transformed to plants using the floral dipping method (Clough and Bent, 1998).

III.1.3 Plant growth and treatments

Plants were cultivated in chambers equipped with LED or white lights (Philips, Amsterdam, Netherlands) at approximately 200 μE, under long day conditions (16h light / 8h dark). Temperature was set to 23°C with 65% humidity.

For dexamethasone (dex) treatments, 25-30 DAG plant inflorescences were sprayed with mock or dex induction medium supplemented or not with cycloheximide, and 100 μl was locally applied using a pipette. Plants were treated only once.

For hormonal treatments, inflorescences were treated with cytokinin (50 μM BA) weekly during three weeks or with gibberellic acid (50 μM GA) once every 5 days during two weeks. Control treatments were conducted in parallel.

Inflorescence plastochron was measured by counting newly formed stage 15 flowers once every 3 days. The rate of lateral organ formation was then calculated.

For assessing the number of organ primordia, confocal pictures were analysed by counting the number of primordia up to flower stage 3.

Root meristems were analysed by growing plants under white light, long day conditions (16h light / 8h dark) at 23°C. For dex treatments, 3DAG or 6DAG seedlings were transferred from regular ½ MS plates to plates supplemented with mock (0.01% EtOH) or dex induction medium.

III.1.4 Histology

For GUS staining, plant tissues were harvested in 90% aceton, prefixed for 20 minutes and washed with cold staining buffer without X-Gluc. Tissues were next transferred to staining buffer and incubated at 37°C in the dark. GUS signal was regularly checked and stopped before over-staining by transferring tissues in 70% EtOH.

In situ hybridization experiments were performed as previously described in Medzihradszky et al., 2014.

III.2 Working with DNA

III.2.1 Cloning

pCLV3:HEC1-linker-GR, *pCUC2:HEC1-linker-GR* and *p16:HEC1-linker-GR* were constructed by overlap-extension PCR of HEC1-CDS with 33 aa Serine-Glycin linker and GR tag and recombined into pDONOR221 and pGreenIIS destination vectors using the Gateway cloning system (Thermo Fisher Scientific; Waltham, USA). To generate *pKNOLLE:fast-mFluorescentTimer-NLS*, fast m-FluorescentTimer CDS fused to N7 NLS was recombined into pGreenIIS destination vetors containing 2.1 kb the regulatory regions upstream of the *KNOLLE* start codon. *pCLV3:SPT, pCLV3:GUS, pCLV3:HEC1, pDEST22-HEC1* and *p16:mCherry-GR-linker-NLS* were generated similarly using the Gateway cloning system (Thermo Fisher Scientific; Waltham, USA).

pGBKT7-HEC1 was generated by ligating *HEC1* CDS with EcoRI and PstI overhangs to pGBKT7 vector. *pGADT7-SPT* and *pGADT7-ALC* were generated by ligating *SPT* and *ALC* CDS with EcoRI and BamHI overhangs into pGADT7 vector.

HEC and MP constructs for BiFC and small-scale yeast-two-hybrid were generated by Juan-José Rippoll, University of San Diego, USA.

All other constructs used in this study were generated using the Green Gate system (Lampropoulos et al., 2013). After cloning genomic sequences of interest in entry modules plasmids using BsaI restriction enzyme, six entry modules containing respectively promoter, N-terminal tag, CDS, C-terminal tag, terminator and a selective cassette were mixed with a destination vector and successively digested by BsaI and ligated (Lampropoulos et al., 2013).

III.2.2 Yeast-two-Hybrid assay

III.2.2.1 Small-scale yeast-two-hybrid assay

Bait construct pGBKT7-HEC1 was transformed in Ah109 yeast strain as described in Gietz and Schiestl, 2007, and tested for auto-activation by mating with Y187 strain carrying empty pGADT7 vector. Diploid colonies were resuspended in water and equal volumes were dropped on -L,T selective minimal medium to test for colonies growth and on -H,L,T medium with an increasing concentration of 3-Amino-1,2,4-triazole (3-AT) to test for the degree of auto-activation.

To test the interaction between HEC1 and SPT or ALC, HEC1 bait strain was mated with SPT or ALC prey strain (pGADT7-SPT or pGADT7-ALC in Y187) and selected on –H,L,T supplemented with 20mM 3AT.

Small-scale interaction test between HEC factors and MP was performed by Juan-José Rippoll, University of San Diego, USA as described in (José Ripoll et al., 2015).

III.2.2.2 Yeast-two-hybrid screening

Bait stain was mated with a prey strain carrying a floral cDNA library (Detlef Weigel, University of Tubingen, Germany) as described in Matchmaker^{TM} gold yeast two-hybrid system user manual (Clontech; Mountain View; USA). Diploid colonies were selected on –H,L,T medium supplemented with 15mM 3AT, isolated, resuspended in water and dropped on –H,L,T + 15mM 3AT medium for confirmation. DNA was extracted according to a modified version of the Smash and grab protocol (Hoffman and Winston, 1987). Cell pellets were resupended in breaking buffer, phenol/chloroform/isoamyl solution with glass beads and vigorously vortexed for one to two minutes. The aqueous phase was next transferred to a new tube and DNA was precipitated with 100% ethanol. After centrifugation DNA pellet was washed with 70% ethanol, air-dried and resuspended in TE buffer. Isolated plasmids were used as template for PCR amplification. Resulting amplified PCR products were used for further identification of the candidate cofactor by DNA sequencing.

For REGIA library screening, HEC1 bait strain was generated by transforming pDEST32-HEC1 in pJ69-4a yeast strain. Bait strain was transformed with pDEST22 vector and selected on –H,L,T media supplemented with a gradual concentration of 3-AT to test for auto-activation. Next, pJ69-4a strain was mated with pJ69-4A prey stain containing the REGIA library (Castrillo et al., 2011). Diploid colonies were selected on –H,A,T medium and on –H,L,T supplemented with 1mM and 5mM 3-AT (Richard Immink, Wageningen University, Netherlands).

III.2.3 Primers

A detailed list of primers can be found in the Appendix section.

III.3 Working with chromatin

III.3.1 Chromatin immuno-precipitation

ChIP experiments were conducted using a modified protocol of (Gendrel et al., 2005). Two grams of seedlings from wild type or stable and functional *hec1* lines expressing *p35S:HEC1-linker-GFP* was harvested 12 days after germination. Nuclei extraction was conducted by successive resuspension in extraction buffer 1, 2 and 3 and filtering of nuclei through nylon meshes, before lysis with nuclei lysis buffer. Sonication was performed at 4°C during 20 minutes with cycles of 30 seconds of sonication, and 45 second of pause. Size of the sheered chromatin was checked on agarose gel for individual samples and DNA content was measured and adjusted to the same concentration using nuclei lysis buffer. Input samples (10 µl) were isolated at this step and frozen at -80°C. Immuno-precipitation was performed with Anti-GFP: GFP-trap® (Chromotek; Planegg, Germany) overnight at 4°C on a rotating wheel. Beads were then collected by gentle centrifugation at 1000 rpm for 30 seconds and successively washed with low salt wash buffer, high salt wash buffer, LiCl wash buffer and TE buffer. DNA was eluted by incubating samples in elution buffer at 65°C for 15 minutes by vortexing vigorously before transferring the supernatant to individual tubes. For reverse crosslinking, 5M NaCl was added to input and IP samples and incubated overnight at 65°C. DNA extraction was performed using MiniElute Reaction Cleanup kit (Qiagen; Hilden, Germany). Quantitative PCR was next performed with ABsolute qPCR SYBR Green mix (ThermoScientific; Waltham, USA) using input and immunoprecipitated (IP) samples. Relative enrichment of IP over input samples was calculated for target and control loci.

For ChIP-seq, 10 to 12 individual ChIP samples were pooled per replicate (biological triplicate). DNA was precipitated with 50 µl NaAc, 10 µl Acrylamid and 1 ml ethanol by overnight incubation at -80°C. DNA was collected by centrifugation during one hour at 4°C and DNA pellets were air-dried under sterile bench, before resuspension in sterile water.

III.3.2 ChIP-sequencing

Library preparation and next generation sequencing were conducted at the core sequencing facility in Bioquant, Heidelberg University. ChIP libraries were generated with the Rubicon Thru-Plex DNA-seq kit, given the low sample DNA concentration; maximum volume for input was used.

Sequencing was performed on HiSeq2500 and NextSeq 500 sequencers (Illumina, Inc; San Diego, USA). Raw data have been deposited at NCBI GEO under the series number GSE94311.

III.4 Working with RNA

III.4.1 RNA extraction and qRT-PCR

Twenty inflorescences per replicates were harvested by dissecting inflorescences till flower stage 4 and shock frozen in liquid nitrogen. Experiments were performed in biological triplicate. RNA was extracted using RNAeasy plant mini kit (Qiagen; Hilden, Germany) according to manufacturer´s instructions. cDNA was prepared using the cDNA synthesis kit after DNase treatment (Thermo Fischer Scientist, Waltham, Massachusetts, USA). qPCR was performed using SYBR Green kit (ThermoScientific; Waltham, USA).

III.4.2 RNA-sequencing

Library preparation and next generation sequencing were conducted at the core sequencing facility in Bioquant, Heidelberg University. RNA samples were poly-A selected using the NEB Poly (A) Magnetic isolation module (7490), and libraries were synthesized with1 μg input using the NEBnext Ultra Direction RNA Prep Kit (E7420) for Illumina and the NEBnext Multiplex Oligo's for Illumina (E7335).

Sequencing was performed on HiSeq2500 and NextSeq 500 sequencers (Illumina, Inc; San Diego, USA). Raw data have been deposited at NCBI GEO under the series number GSE94311.

III.5 Microscopy

III.5.1 Image acquisition

Part of the method was previously described and written for Gaillochet & al 2017, under preparation.

Confocal images were acquired on Nikon A1 Confocal with a CFI Apo LWD 25x water immersion objective (Minato, Tokyo, Japan).

Inflorescence meristems were dissected in water, by cutting the stem and removing flower primordia up to flower stage 3-4. Shoot meristems were counter-stained with DAPI or propidium iodide by incubation during 2-3 minutes, mounted on 2% agarose plates and covered with water during at least 15 minutes to prevent sample movement under the objective. Gynoecia from flower stage 8 to flower stage 12 were prepared using a similar method. Root meristems were analysed by cutting the root and counterstained with propidium iodide for 3 to 5 minutes. Samples were mounted on glass slides with a cover slip. For time series analysis, 5 to 15 plants were analysed daily; imaging settings were established at the first day and kept for the entire experiment.

III.5.2 Image analysis

Image processing and analysis was performed using Fiji software (Schindelin et al., 2012). A ROI crossing the centre of the SAM on a maximum projection image was used to generate WUS, CLV3 and TCS intensity plot profiles. Size of the domain was estimated by measuring the width of the profile with intensity higher than one quarter of the maximum intensity. For shoot meristem size measurement, 3-D reconstructed images were analysed by averaging the diameter of 3 segments starting from P1, P2 and P3.

To measure cell surface area, MorphoGraphX was used according to author's instructions (Barbier de Reuille et al., 2015).

To quantify the number of cells in the CZ of the shoot meristem, a customized workflow using the KNIME Image Processing platform (KNIP) (Berthold et al., 2008) was established by Dr. Christian Wenzl. Ubiquitously expressed nuclear GFP marked SAM cells and was used in combination with CZ domain specific reporter in a stable plant line expressing *pUBQ10:3xGFP-NLS* and *pCLV3:mCherry-NLS*. Images were segmented after background subtraction using a 3D seeded watershed algorithm implemented in the KNIP package (Berthold et al., 2008). A volume mask was then generated with a 3D seeded watershed and used to exclude primordia cells from the analysis. CLV3 signal intensity was measured from segmented nuclei with threshold set at 35% of the maximum mean value.

To assess cell proliferation in the SAM, we developed an imaging tool by driving a Fluorescent-Timer protein under a cell cycle-dependent promoter and combined this with an ubiquitous nuclear GFP in a stable line expressing *pKNOLLE:fast-mFluorescentTimer-NLS* and *pUBQ10:3xGFP-NLS*. As the timer protein matures

from a blue to a red form, newly dividing cells are marked by high blue to green signal ratio. As cells age this ratio decreases. Using this feature, we categorized cells in four different classes depending on the normalized blue to green ratio, and monitored the cell age as a proxy for cell division activity (from oldest to youngest: Class 1: 0-0.3, Class 2: 0.3-0.53, Class 3: 0.53-0.76, Class 4: 0.76-1). To calculate proliferation rates at the central and peripheral domain of the meristem, a sphere of radius r was fitted through the centroids cells in the L1 layer of the meristem. Selected cells were located within 35 μm from a manually selected center point P. The size of the central domain was defined by one third of the radius of the sphere, all cells with a distance to P smaller were considered to belong to this central domain whereas cells with a larger distance were classified as peripheral cells.

Lateral to medial PIN1-GFP intensity ratio in the gynoecium was measured as described in Schuster et al., 2015.

Dr. Christoph Schuster performed electron microscopy experiments at the Microscopy Core Facility, Sainsbury Laboratory, Cambridge, UK.

III.5.3 Bi-fluorescence complementation assay

Dr. Juan Jose Ripoll, University of San Diego conducted the BiFC experiments as described in Ripoll et al., 2006.

III.5.4 FRET-FLIM

For FRET-FLIM assays, *Nicotiana benthamiana* leaves were co-infiltrated with *p35S:HEC1-GFP* and *p35S:mCherry-NLS* or *p35S:SPT-mCherry.* Cell nuclei were analysed 48 to 60 hours after infiltration on a Leica TCS SP5II microscope equipped with a PicoHarp 300 TCSPC (PicoQuant, Berlin, Germany) system and an integrated FLIM-PMT (Hamamatsu). Nuclei from similar signal intensities were recorded with a 63x water immersion objective. Fluorescence lifetime was acquired after excitation with a 40MhZ pulsed laser at 100 repetitions and images recorded at 256x256 resolution. Fluorescent lifetime was calculated using the Symphotime software (PicoQuant, Berlin, Germany). Nuclei regions were manually selected and decay function was estimated together with the GFP lifetime. Tail fitting was applied to the analysed nuclei using a fixed threshold.

III.6 Computational analysis

III.6.1 Bioinformatic analysis

Part of these methods were previously described and written for Gaillochet & al, 2017, under preparation.

All sequencing files were first checked for quality using FastQC (Andrews S., 2010); available online at: http://www.bioinformatics.babraham.ac.uk/projects/fastqc.

For RNA-seq analysis, we used TOPHAT2 (Kim et al., 2013) with default settings for aligning reads and calling peaks, samtools for converting BAM to SAM, HT-seq (Anders et al., 2015) for constructing read tables (Anders et al., 2015; Li et al., 2009) and EdgeR for calculating differential gene expression with $p<0.05$ as a cut-off (Robinson et al., 2009). All RNA-seq data sets were obtained experimentally except *p35S:NGA3* RNA-seq dataset, which was published in (Martínez-Fernández et al., 2014).

For ChIP-seq analysis BOWTIE2 was used with default settings for aligning reads and MACS2 for calling peaks by limiting the number of duplicate reads to 2 ("keepdup 2") (Langmead and Salzberg, 2012; Zhang et al., 2008). Bedtools multiinter function generated the list of HEC1 bound regions by overlapping 200 bp regions surrounding the peak summits of two biological replicates (Quinlan and Hall, 2010). Peak annotation in relation to gene model was performed with Homer (Heinz et al., 2010) and peaks were visualised with Integrative Genomic Viewer (IGV)(Robinson et al., 2011).

MEME-ChIP with JASPAR core 2016 as motif input was used to identify *de novo* motif enrichment in 500 bp regions surrounding the peak summit (Bailey et al., 2009).

To assess the distribution of distances between G-boxes and ARE under HEC1 bound-regions and in open chromatin regions, bed files with the position of G-box and ARE were generated using IGV and further processed with bedtools functions "intersect" and "closest" (Quinlan and Hall, 2010; Robinson et al., 2011). Histograms were generated with R studio (https://www.r-project.org/).

The relative distribution of G-boxes and ARE on the regulatory regions of HEC1-response genes and on open chromatin domains was calculated by annotating bed files with Homer and intersecting the datasets with Microsoft Excel ("VLOOKUP") (Heinz et al., 2010; Zhang et al., 2012).

DNA-binding regions of HEC1, SPCH (Lau et al., 2014), PIF3, PIF5 (Pfeiffer et al., 2014), KAN1 (Merelo et al., 2013) and LFY (Moyroud et al., 2011) were overlapped

on a 50 bp region centered on the peak summits. An overlap of 40 or more bases was considered as a shared binding region.

HEC1 and SPT mRNA expression patterns were obtained from the AtGenExpress atlas (Schmid et al., 2005). Gene ontology (GO) enrichment analysis among high confidence HEC1 response genes was performed with AgriGO (Du et al., 2010).

HEC1 protein-protein interaction network was reconstructed using the Arabidopsis Interactome web tool (Arabidopsis Interactome Mapping Consortium, 2011). First-level PPI clusters and GO analysis were obtained with STRING tool (Mering, 2004).

III.6.2 Computational modelling

The computational model was built in collaboration with Thomas Stiehl.

Dr. Thomas Stiehl wrote scripts, performed model simulations and wrote the model description. Further details can be found in the Appendix.

IV. Results

All figures in this section were originally generated for research articles that are published or are still under preparation.

IV.1 Characterization of HEC function in the shoot meristem

IV.1.1 *HEC* genes control cellular fate transition

In order to investigate the impact of HEC function on cell behaviour, we developed an image analysis pipeline that allowed us to quantify the number of cells in specific domains of the shoot meristem. Using this analytical tool, we found that shoot meristems from HEC-loss of function plants (*hec1,2,3* triple mutant) displayed a reduced total cell number, correlating with their smaller SAM compared to wild type plants (Figure 4A-D). Consistently, cell size was not modified in *hec1,2,3* plants, further supporting the idea that their reduced cell number caused the smaller SAM (Figure 4E-F).

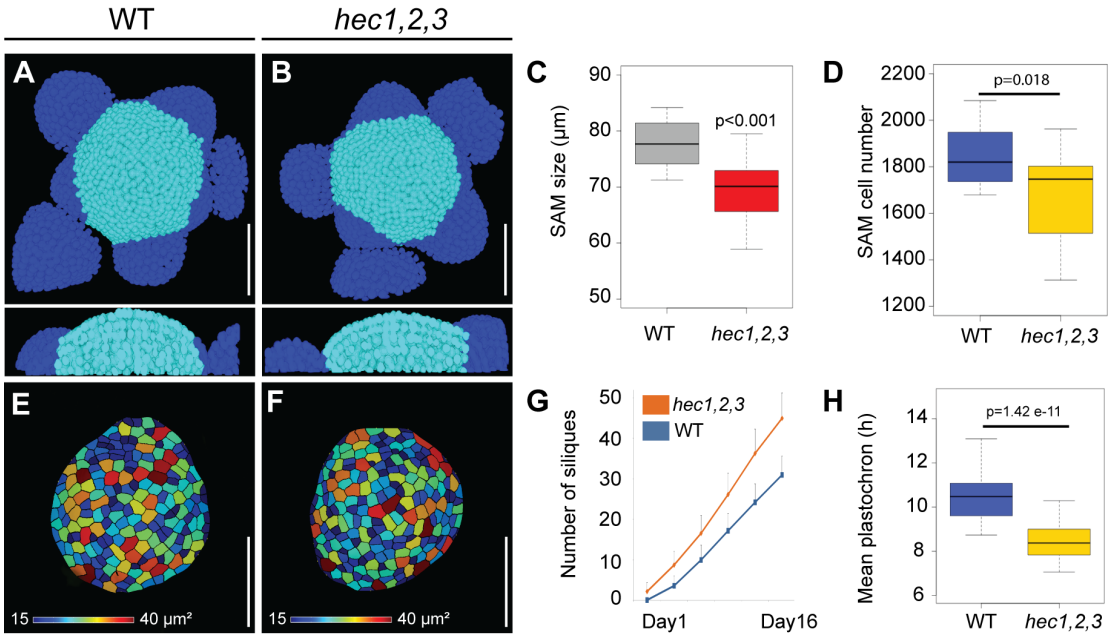

Figure 4: HEC function regulates the size and the number of cells in the SAM
(A-B) Representative views of 3D-reconstructed shoot meristems after nuclei segmentation from WT (A) and *hec1,2,3* (B). Light blue: SAM cells; dark blue: primordia cells. **(C)** Shoot apical meristem size at 28 days after germination (DAG) (n=15) **(D)** Quantification of SAM cell number in WT (n=19) and *hec1,2,3* (n=21). **(E-F)** Representative cell area of segmented L1 layer from WT (E) and *hec1,2,3* (F) SAM (n>3) **(G)** Cumulated number of siliques over time after bolting in WT (n=46) and *hec1,2,3* (n=42). **(H)** Mean inflorescence plastochron in WT (n=46) and *hec1,2,3* (n=42). Statistical test: Student t-test (C, H), Wilcoxon signed-ranked test (D). Scale bar: 50 *µ*m

Intriguingly, although *hec1,2,3* displayed a smaller stem cell system, plants produced lateral organs at a faster rate, as shown by a significant decrease in the time separating the successive formation of lateral organs (plastochron) compared to wild type (Figure 4G, H). These data suggested that rather than exclusively regulating stem cell function as we previously described (Schuster et al., 2014), HEC factors might also carry a broader function in the SAM to coordinate cell fate transitions during stem cell differentiation.

The progression of stem cell lineages is a highly dynamic process, taking place in spatially restricted domains of the SAM. Thus, to investigate the role of HEC function on cellular fate transitions at high spatio-temporal resolution, we created an inducible version of the HEC1 protein by tagging it with the rat glucocorticoid receptor (HEC1-GR).

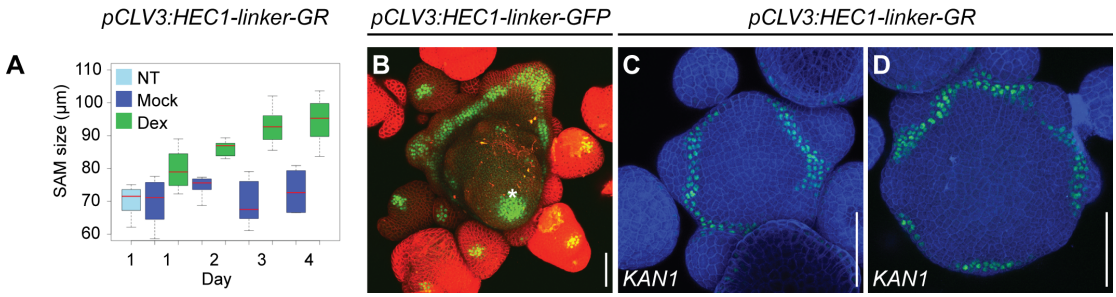

Figure 5: HEC function in the CZ promotes SAM enlargement
(A) Time series quantification of shoot meristem sizes after mock and dex induction (n>6 per condition). Plants not treated (NT) were used as control **(B)** Shoot meristem expressing *pCLV3:HEC1-linker-GFP*. Note the establishment of a ring-like stem cell domain at the base of the meristem (n>10). The asterisk marks the central zone **(C-D)** Boundary region as marked by *pKAN1:KAN1-GFP* in shoot apical meristems expressing *pCLV3:HEC1-linker-GR*, four days after mock (C) or dex (D) treatment (n=2). Scale bar: 50 µm

First, we confirmed the functionality of the construct by inducing HEC1 in the central zone using dexamethasone treatment (Figure 5A). In line with constitutive expression of HEC1 in this domain, the SAM progressively increased in size whereas cellular behaviour was not modified upon mock treatment, confirming the quality of our inducible strategy (Figure 5A-D). Furthermore, given the low cell-to-cell mobility of HEC1-GFP protein from the CZ or the epidermis (Figure 6A-K), this system also allowed us to assess the local activity of HEC function within its specific expression domains in the SAM.

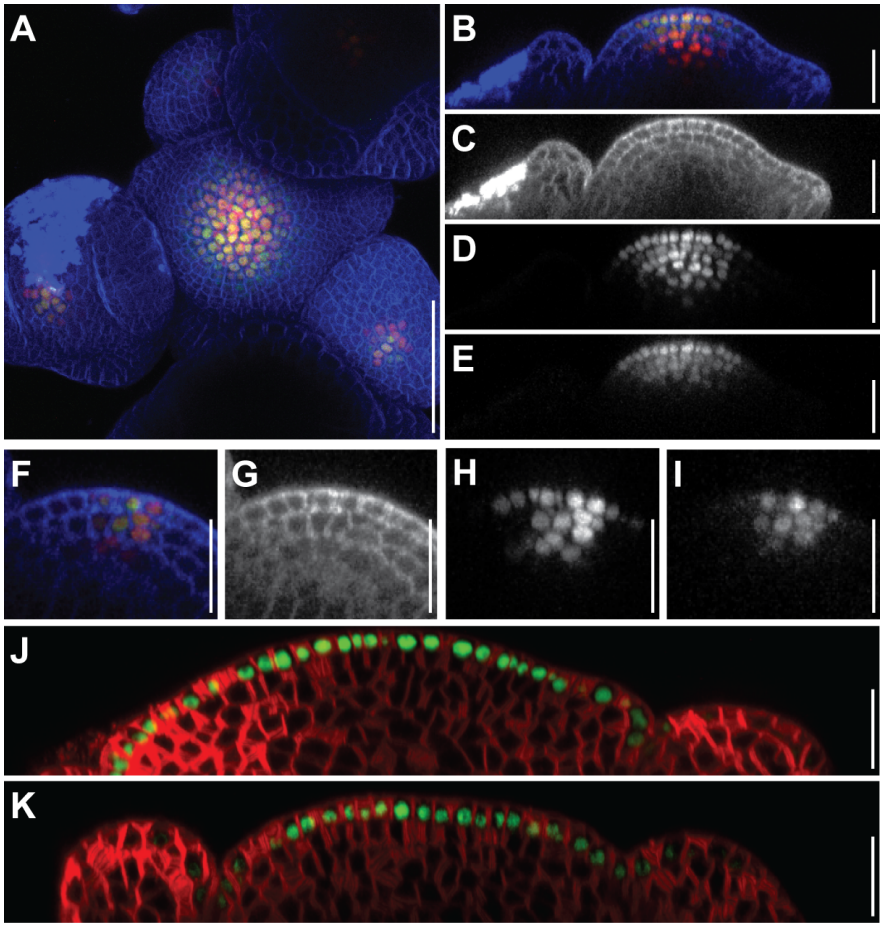

Figure 6: HEC1-GFP displays reduced cell-to-cell movement in the SAM
(A-E) Representative view of axillary meristem before fasciation expressing *pCLV3:HEC1-linker-GFP* and *pCLV3:3xmCherry-NLS* (n=4). Top view of the merged channels (A), side view of the merged channels (B), blue (C), red (D) and green (E) channels. **(F-I)** Representative views of flower stage 3 expressing *pCLV3:HEC1-linker-GFP* and *pCLV3:3xmCherry-NLS*. Merged channels (F), blue (G), red (H), green (I) channels. **(J-K)** Side view of shoot meristem expressing *pML1:2xGFP-NLS* (J) and *pML1:HEC1-linker-GFP* (K). Scale bar: 50*μ*m (A), 20*μ*m (B-K)

Next, to investigate the dynamics of HEC regulatory function in the SAM, we monitored central zone (CZ) and organising centre (OC) cell identities using *pCLV3:mCherry-NLS*, *pWUS:3xYFP-NLS* and *pWUS:WUS-linker-GFP* (Figure 7-8). HEC1 induction in the CZ led to an expansion of both CZ and OC domains, correlating with an increase SAM size (Figure 7-8). Interestingly, although the size of the CZ and OC domains increased, we observed a decrease in WUS and CLV3 reporter intensities three days after induction (Figure 9), likely as a result of feedback loop of regulation limiting the expression of the core stem cell regulatory network.

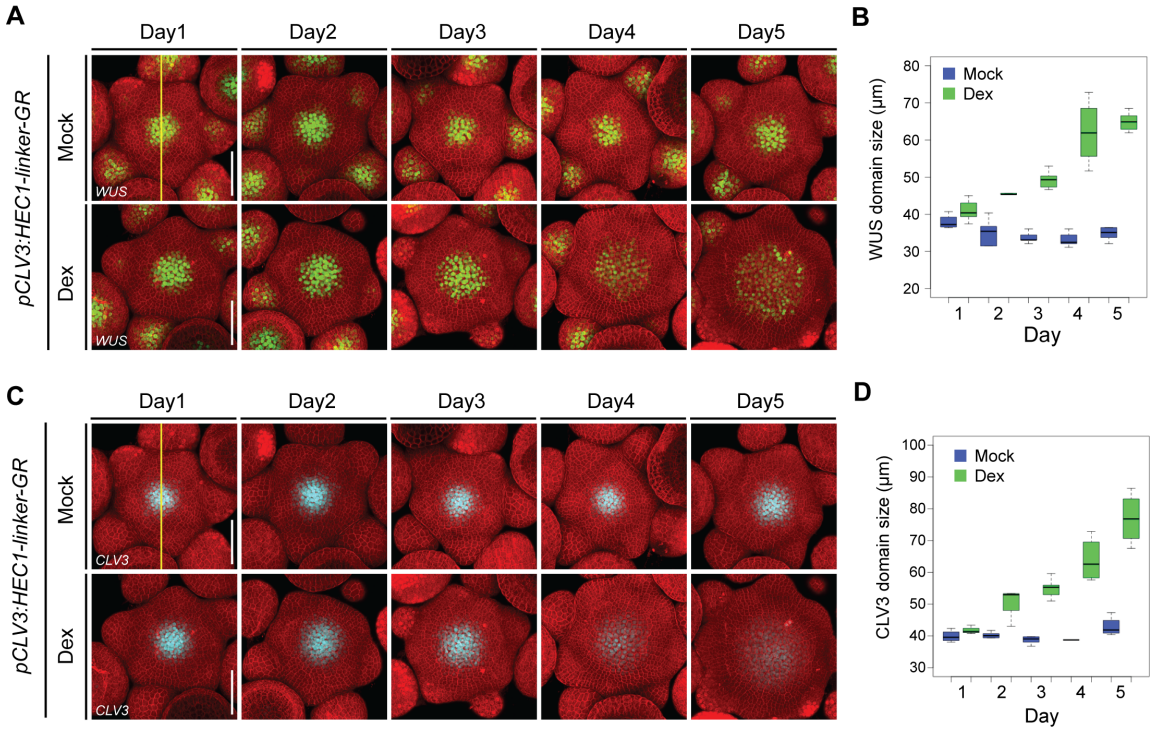

Figure 7: HEC function in the CZ expands WUS and CLV3 signalling domains
(A-B) Development of the OC domain (*pWUS:3xYFP-NLS)* in shoot meristems after *pCLV3:HEC1-linker-GR* mock or dex induction (n=5 per condition). Representative view of individual meristems (A). Quantification of WUS domain size (B). **(C-D)** Development of the CZ domain (*pCLV3:mCherry-NLS*: cyan) in shoot meristems after *pCLV3:HEC1-linker-GR* mock or dex induction (n=5 per condition). Representative view of individual meristems (C). Quantification of CLV3 domain size (D). Yellow line: ROI selected to quantify WUS and CLV3 domain sizes (A,C). Scale bar: 50 *µ*m

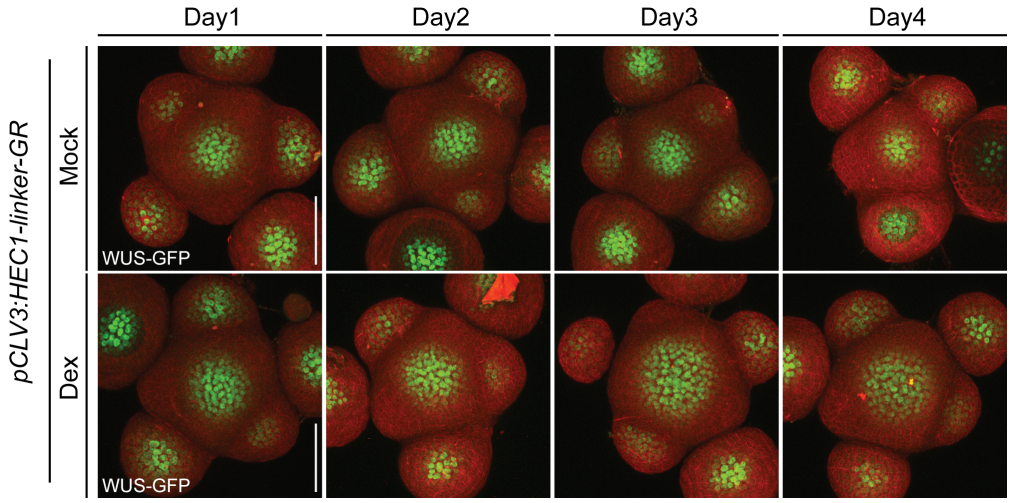

Figure 8: HEC function in the CZ expands WUS distribution domain.
Development of WUS protein distribution in individual *wus-1* / *pWUS:WUS-linker-GFP* shoot meristems after *pCLV3:HEC1-linker-GR* mock or dex induction (n>6 per condition). Scale bar: 50 *µ*m

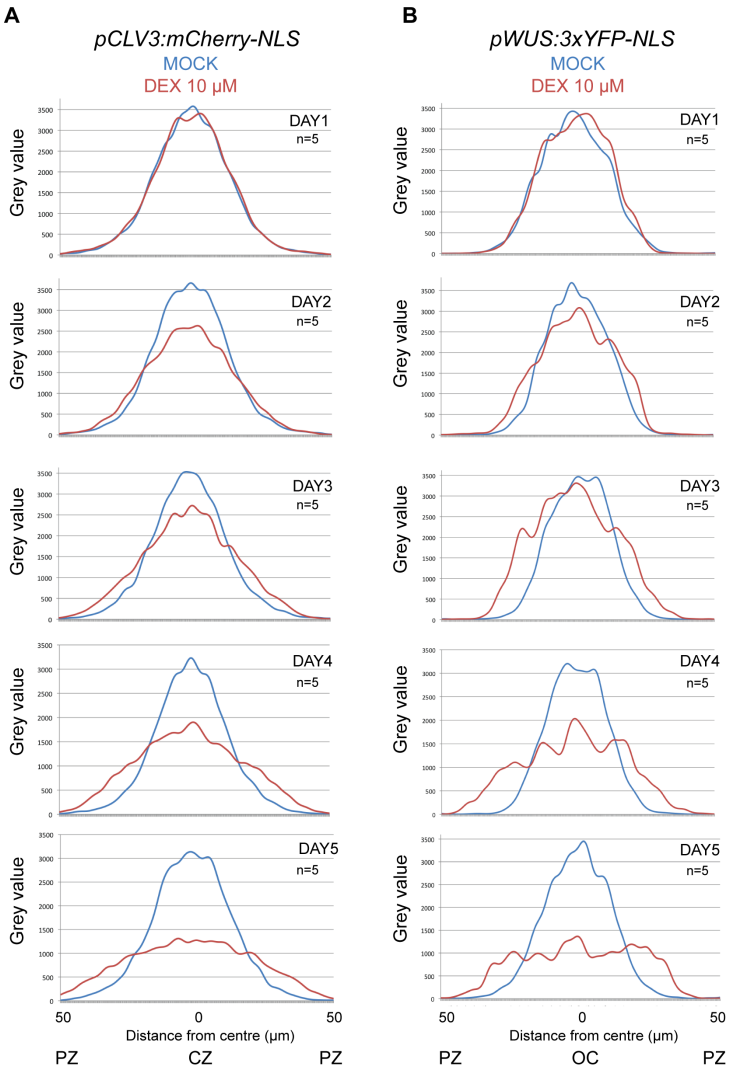

Figure 9: HEC-driven SAM expansion represses the WUS-CLV signalling system
Development of the OC (*pWUS:3xYFP-NLS*) and CZ (*pCLV3:mCherry-NLS*) signalling domains after *pCLV3:HEC1-linker-GR* mock or dex induction (n=5 per condition)

The observed expansion of the CZ domain could reflect three independent mechanisms controlled by HEC1: 1) De-differentiation of early peripheral zone cells 2) Local increase in cell proliferation at the CZ or 3) Delayed transition from CZ to PZ cell identity.

First, to test whether HEC re-specified early PZ cells into stem cells, we analysed the ratio between the number of CLV3 cells and the total number of SAM cells. Early PZ re-specification would cause an increase in this ratio, as the CZ domain would expand faster than the SAM. Although we observed an increase in the number of CZ cells after HEC1 induction, the ratio between CZ and SAM cells remained constant over time, suggesting that HEC1 does not re-specify early PZ cells and that the expansion of the SAM size scales with the CZ (Figure 9,10).

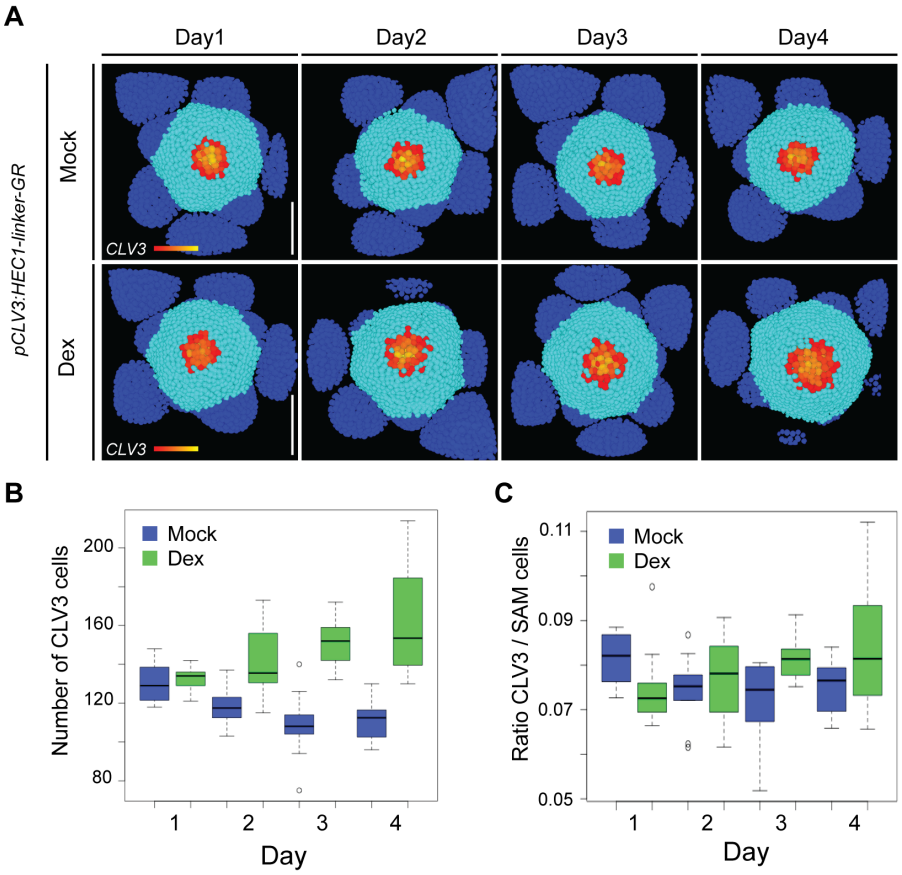

Figure 10: HEC1 function in the CZ does not re-specify early PZ cell fate
(A-C) Development of *pCLV3:HEC1-linker-GR* shoot meristems expressing *pCLV3:mCherry-NLS / pUBQ10:3xGFP-NLS* after mock or dex treatment (n>9 per condition). Reconstructed images of meristems (A). Red, orange and yellow highlight CLV3 cells; light blue represent PZ and BZ cells and dark blue show primordia cells. Time series quantification of CLV3 cell number after mock or dex treatment (B). Time series quantification of CLV3 / total cell number ratio after mock or dex treatment (C). Scale bar: 50 μm

To quantify cell division activity in the CZ, we developed a novel imaging tool by driving a fast fluorescent timer under a cell-cycle dependent promoter (*pKNOLLE:fastFluorescentTimer-NLS*) and combined this reporter in plants with an ubiquitously expressed nuclear GFP (*pUBQ10:3xGFP-NLS*) that allowed segmentation and calibration of the timer signal (Figure 11). As fluorescent timers mature from emitting in blue to red, newly dividing cells displayed a high blue to green ratio that decreased over time after division. By quantifying the blue to green signal ratio, we measured the time after cell division and used this parameter as a proxy for mitotic activity. After HEC1 induction in the CZ, we observed that most of the mitotic active cells, contributing to the increase in the SAM size were localized at the peripheral zone. This pattern of cell division was similar to control plants (Figure 11A-B).

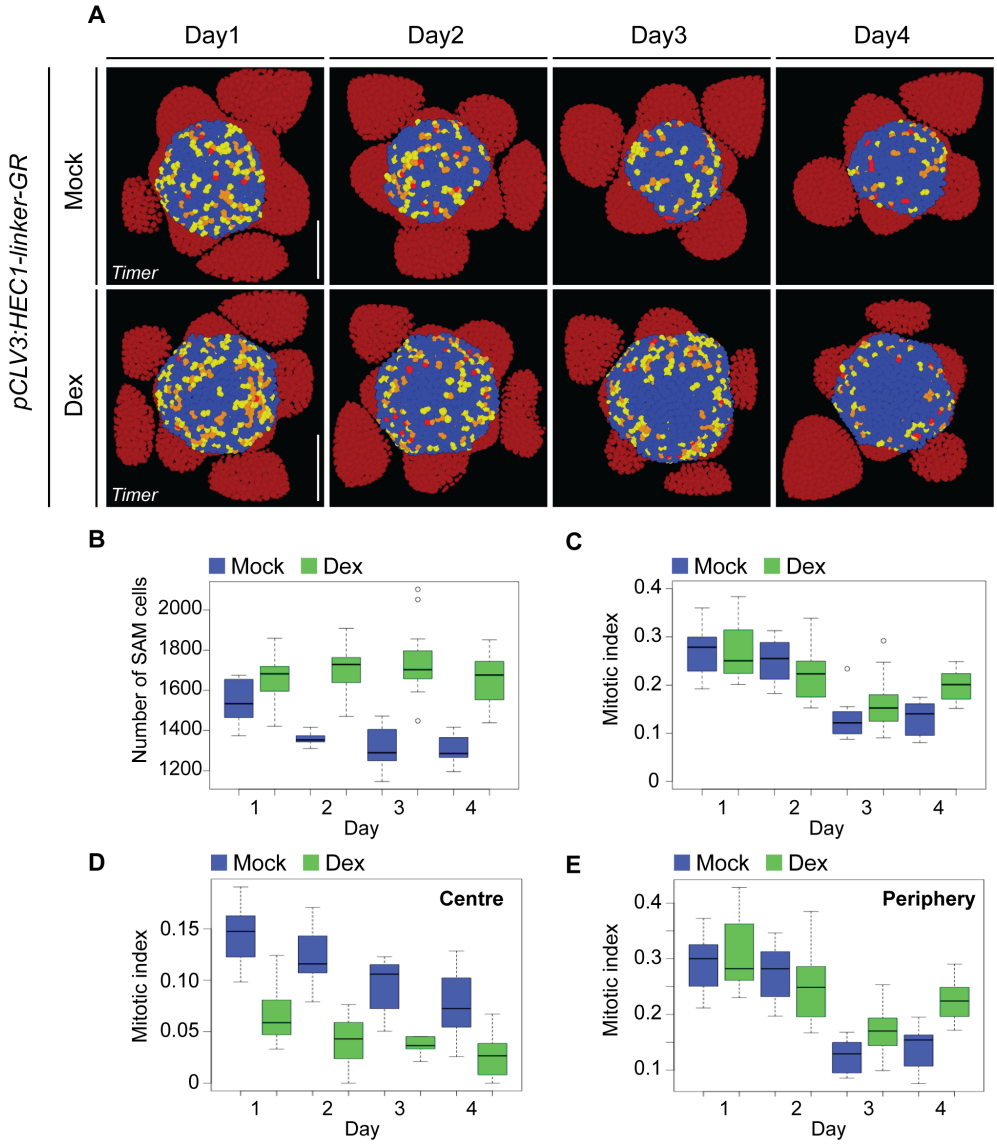

Figure 11: HEC1 function in the CZ does not locally promote cell proliferation
(A-E) Development of cell proliferation activity as marked by *pKNOLLE:mFluorescentTimer-NLS / pUBQ10:3xGFP-NLS* in *pCLV3:HEC1-linker-GR* shoot meristems after mock or dex treatment (n>7 per condition). Representative meristems after image segmentation (A). Light red, orange and yellow depict young dividing cells; blue marks older cells; dark red highlights primordia cells. Quantification of total SAM cell number (B), SAM mitotic index (number of young cells / total SAM cell number) (C), mitotic index at the centre (D) or at the periphery of the SAM (E). Scale bar: 50 μm

Importantly, the mitotic index decreased at the centre of the SAM whereas it increased at the periphery, demonstrating that HEC did not locally promote cell proliferation at the CZ but rather promoted cell proliferation non-cell autonomously at the PZ (Figure 11C-E). By excluding the scenarios that HEC function is re-specifying early PZ cell fate, or promoting CZ cell proliferation; our data suggested that HEC mainly delayed cellular fate transition from the CZ to the PZ.

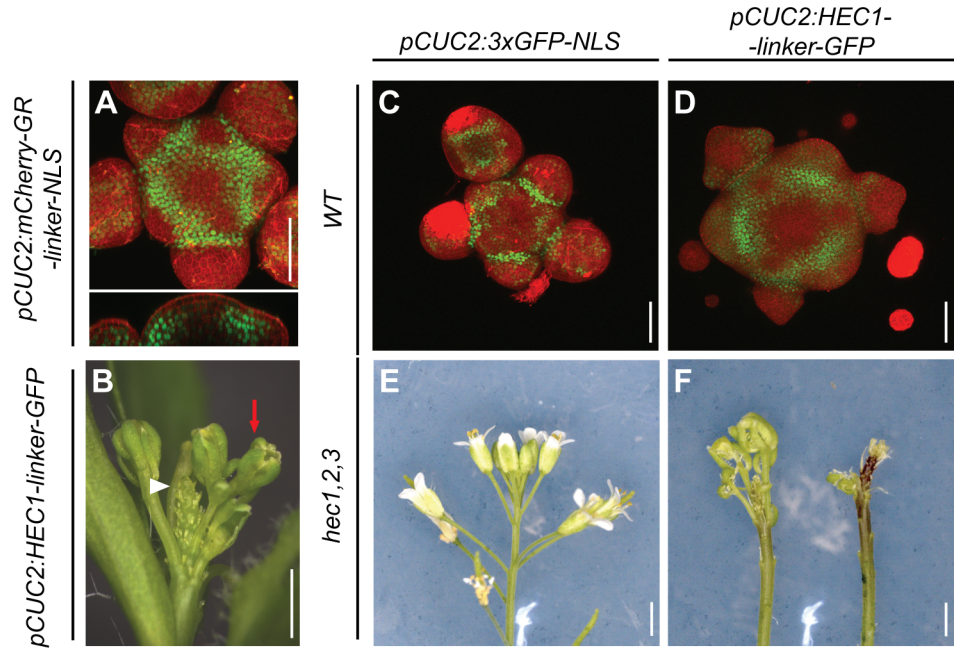

Figure 12: HEC function at the SAM periphery interferes with floral initiation
(A) Representative activity of *pCUC2:mCherry-GR-linker-NLS* in the shoot meristem (n>3). Green signal marks mCherry-NLS. **(B)** *pCUC2:HEC1-linker-GFP* inflorescence 30 DAG (n>30). Note the inhibition of flower primordia formation (white triangle) and flower morphological defects (red arrow). **(C)** Shoot meristem expressing *pCUC2:3xGFP-NLS* 28 DAG (n>5). GFP signal marks the boundary zone. **(D)** Shoot meristem expressing *pCUC2:HEC1-linker-GFP* 28 DAG (n>10). Note the enlargement the SAM and early defects in flower primordia formation. **(E-F)** *hec1,2,3* inflorescences expressing *pCUC2:3xGFP-NLS* (E) or *pCUC2:HEC1-linker-GFP* (F)

These results were in line with *hec1,2,3* phenotypes of a smaller SAM producing more lateral organs and suggested that HEC function could coordinate the timing of cell fate differentiation across the SAM. To test this idea, we investigated whether HEC factors could influence cell fate progression at another key developmental transition domain of the SAM, between the PZ and primordia. First, we constitutively expressed HEC1-GFP under the CUC2 promoter, which is active in the late PZ and boundary zone (BZ) (Figure 12A). Strikingly, locally promoting HEC function in this region strongly interfered with the formation of lateral organs in both wild type and *hec1,2,3* backgrounds (Figure 12B-F).

Similarly, inducing *pCUC2:HEC1-GR* at the periphery of the SAM gradually inhibited the formation of lateral organs and led to the formation of pin-like inflorescences after prolonged induction (Figure 13A-B).

Together, these data showed that HEC function locally controlled cell fate transition in distinct domains of the SAM and thus suggested that HEC factors might regulate the dynamics of stem cell differentiation across multiple domains of the SAM.

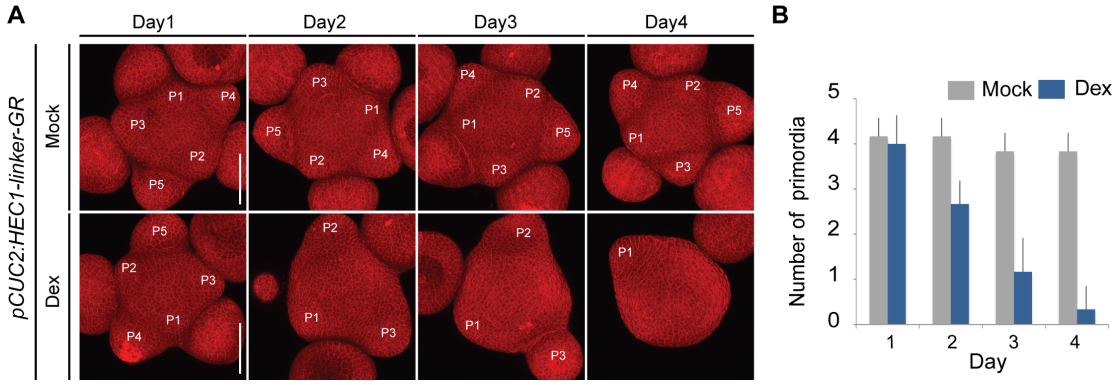

Figure 13: HEC function at the SAM periphery blocks flower primordia initiation
(A-B) Development of shoot meristems expressing *pCUC2:HEC1-linker-GR* after mock or dex treatment (n=6 per condition). Representative views of individual meristems, the successive flower primordia are labelled from P1 to P5 (A). Primordia number quantification (B). Scale bar: 50 μm

IV.1.2 HEC function control stem cell differentiation dynamics

Having shown that HEC factors could control the fate transition from CZ to PZ and further on to primordia, we next wanted to test whether this regulatory function could be sufficient to explain the phenotypes observed after loss and gain of HEC function. To tackle this question, we built a computational model from experimentally defined parameters and simulated different regulatory scenarios on meristem dynamics. In particular, the model allowed us to investigate the dynamics of HEC-loss of function, for which we had only limited experimental data.

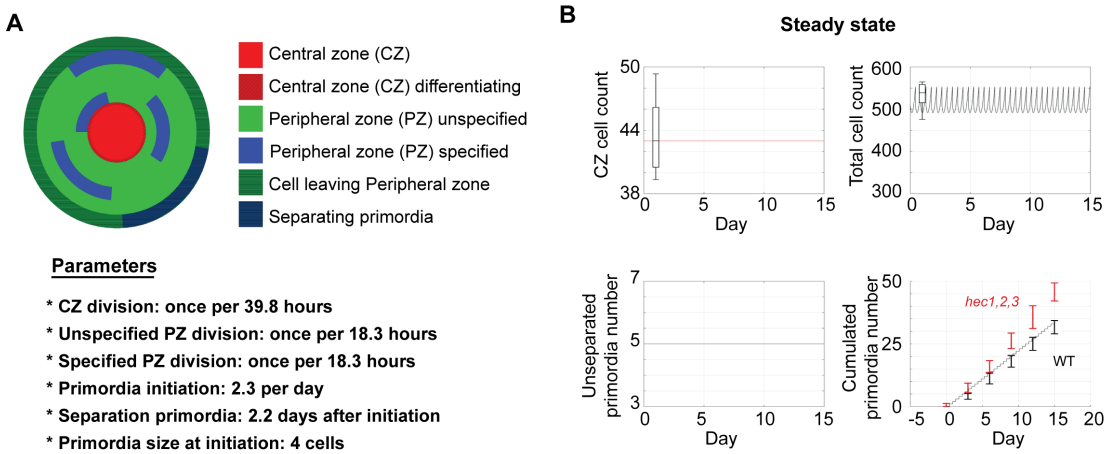

Figure 14: Computational model for investigating SAM dynamics
(A) Spatial representation of the computational model and parameters description. **(B)** Model calibration and quantification of CZ cell count, total cell count, number of unseparated primordia and cumulated number of primordia at steady state. Simulations were performed by Dr. Thomas Stiehl

First, we developed a 2-dimensional cell population-based model and adjusted parameters using quantified data obtained from live-cell imaging. At the centre, CZ cells divided (once per 39.82 hours; (Reddy et al., 2004) and were displaced towards the peripheral zone where they proliferated faster (once per 18.35 hours; (Reddy et al., 2004) before exiting the meristem upon primordia differentiation (Figure 14A-B). At the exit of the CZ domain, a population of PZ cells is committed to primordia fate (2.27 primordia initiated per day), (Figure 4H), grow and separate from the meristem (2.2 days after initiation; (Besnard et al., 2014) (Figure 14A-B). Using these set of parameters, the system reached a steady state where simulated values for the number of CZ cells, the total number of SAM cells, the number of unseparated primordia and the number of cumulated primordia fitted well our experimental data (Figure 14B).

We next investigated HEC-loss of function dynamics and tested whether increasing the transition rate between the CZ and PZ and further on to the primordia could reproduce *hec1,2,3* phenotypes. Interestingly, although we observed a decrease in the number of SAM cells similar to *hec1,2,3* plants and a slight decrease in the number of CZ cells, our simulations did not lead to an increased number of cumulated primordia. Thus, these data showed that increasing the transition rate only was not sufficient to fit our *in vivo* observations (Figure 15A). Thus, we tested the impact of increasing primordia intiation rate together with increased CZ to PZ fate transition. We observed in these simulations that the number of CZ and SAM cells together with the cumulated number of primordia reproduced well our experimental measurements. These simulations also predicted an increased number of unseparated primordia (Figure 15B). To directly test this prediction experimentally, we introduced *pDR5v2:3xYFP-NLS* reporter in the *hec1,2,3* mutant background and quantified the number of auxin maxima as a proxy for the number of unseparated primordia (Figure 15C). Although we observed a significant increase in the number of DR5 signalling domains, this increase was not sufficient to explain the higher number of cumulated primordia in our simulation and therefore suggested that HEC function coordinated multiple developmental processes.

Thus, we then fixed the parameter value for the primordia initiation rate and modulated the time separating primordia initiation and separation. Importantly, this simulation recapitulated our *in vivo* observations (Figure 15C). In addition, these simulations allowed us to compute that in *hec1,2,3* plants, primordia were initiated at

a rate 15% higher than in wild type and that after initiation, primordia separated on average 10 hours faster (52 hours in wild type, 42 hours in *hec1,2,3*).

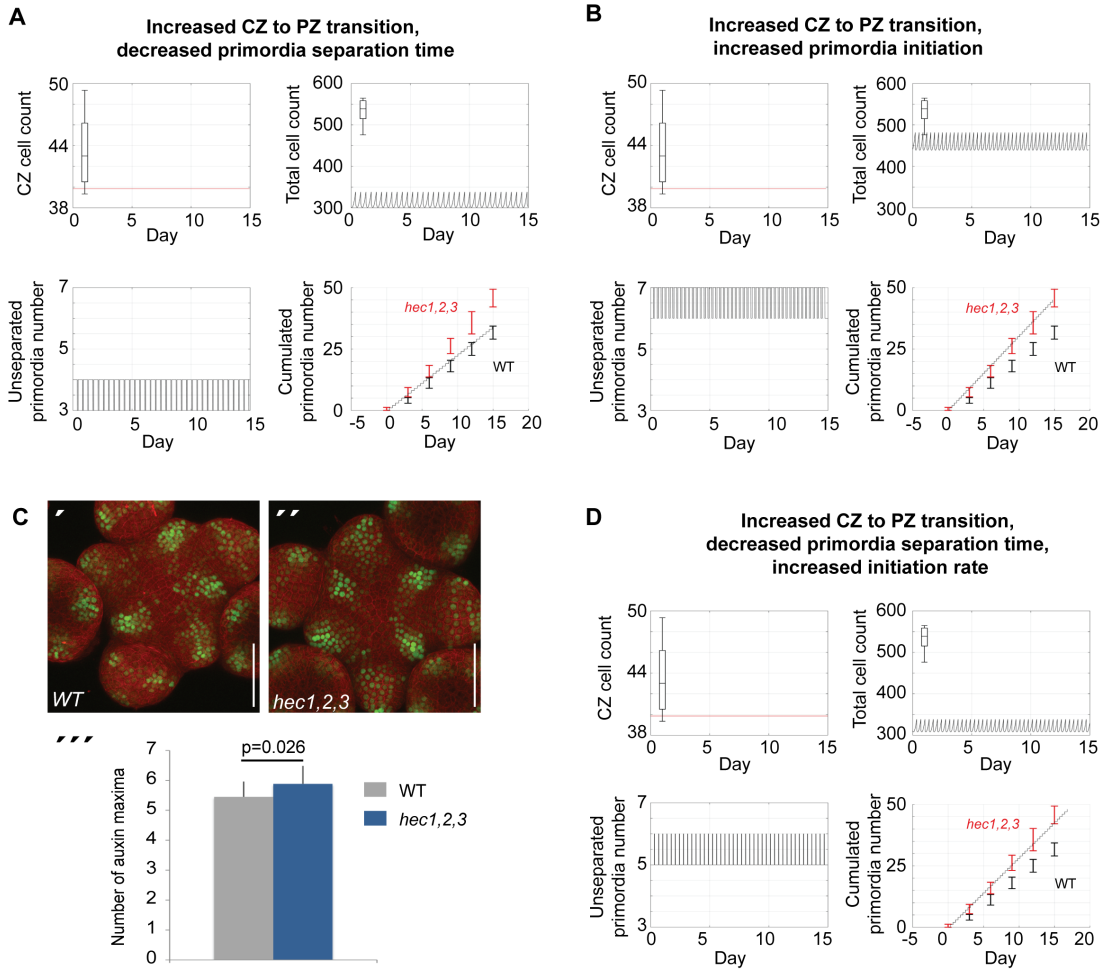

Figure 15: HEC function controls cell differentiation dynamics in the SAM
Computational simulations displaying *in silico* estimation (line) and observed *in vivo* quantification (boxes) for CZ cell number, total cell number, CZ/total cell ratio, number of unseparated primordia and cumulated number of primordia **(A-B)** Simulation of *HEC* loss-of function on SAM cell behaviour. Effects caused by increasing cell differentiation between CZ and PZ and decreasing primordia separation time (A). Simulation of effects caused by increasing CZ to PZ transition and increasing primordia initiation rate (B). **(C)** Analysis of *pDR5v2:3xYFP-NLS* in WT (´) and *hec1,2,3* (´´) SAMs. Quantification of auxin maxima in WT (n=20) and *hec1,2,3* (n=17)(´´´). **(D)** Simulation of effects caused by increasing CZ to PZ transition, increasing primordia initiation rate and decreasing their separation time. Cell numbers in (A, B, D) refer to a single cellular layer and correspond to one third of the respective quantified cell numbers. Scale bar: 50μm (E). Statistical test: Student t-test (E´´´). Simulations were performed by Dr. Thomas Stiehl

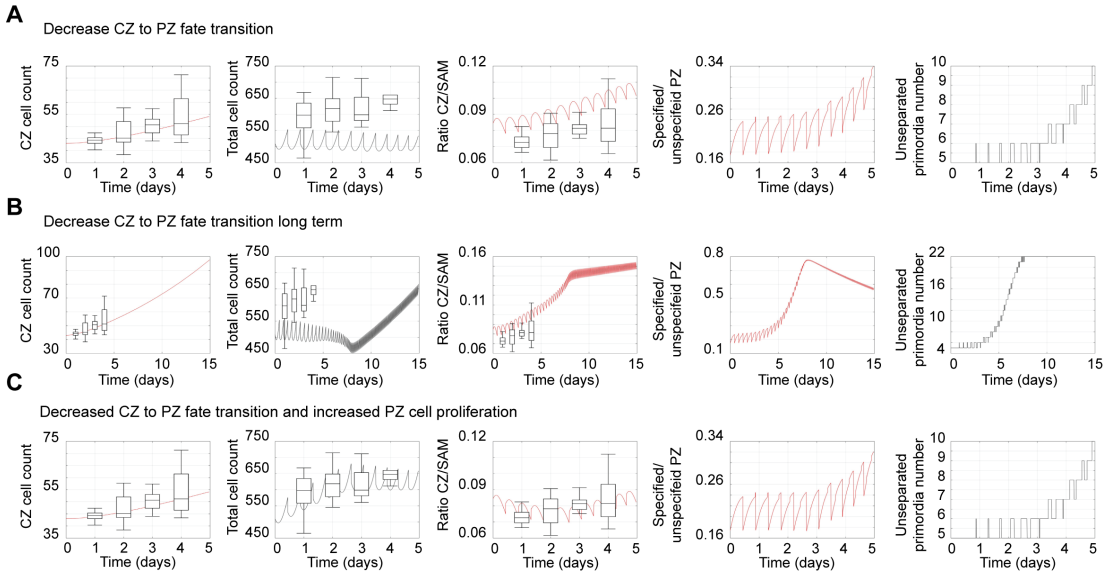

Figure 16: HEC gain-of-function coordinates cell fate transition with PZ cell proliferation
Computational simulations displaying *in silico* estimation (line) and observed *in vivo* quantification (boxes) for CZ cell number, total cell number, CZ/total cell ratio, specified / unspecified PZ cells and number of unseparated primordia **(A-C)** Simulation of changes in SAM behaviour by induction of *pCLV3:HEC1-GR*. Short term effects caused by reducing cell differentiation between CZ and PZ alone (A) . Long term effects caused by reducing cell differentiation between CZ and PZ alone (B). Note the delay in the increase of the total cell count. Changes caused by reducing cell differentiation between CZ and PZ and increasing PZ proliferation rate by 10% (C). Simulations were performed by Dr. Thomas Stiehl

To further confirm the quality of our model in characterizing HEC function, we simulated gain-of function scenarios in the CZ and compared the results from simulations to our quantitative live-cell imaging data (Figure 16). We first tested whether the reduction in the transition from CZ to PZ was sufficient to explain the expansion of the CZ and the SAM. Although the increase in the number of CZ cells nicely fitted our *in vivo* observations, the increase in the total number of cells was delayed compared to our experiments, suggesting that another developmental parameter changed upon HEC1 induction (Figure 16A-B).

As we previously measured an increase in the mitotic index at the PZ, we simulated a reduced cell transition rate with an increased proliferation rate at the periphery. This new scenario could recapitulate our experimental results, further supporting the quality of our model in faithfully capturing the SAM dynamics upon modulation of HEC activity (Figure 16C).

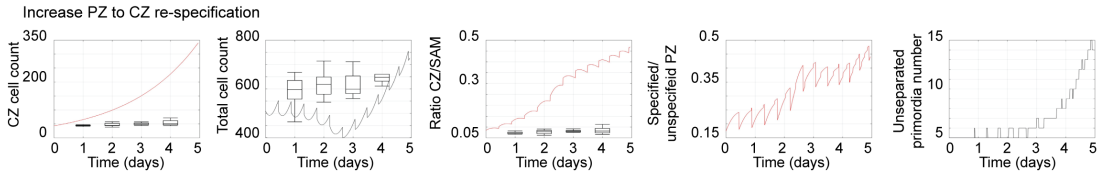

Figure 17: HEC gain-of-function does not respecify early PZ cells
Simulation of HEC1 loss-of-function by local increase of CZ to PZ fate transition, decreased PZ proliferation and increased primordia initiation. Simulations were performed by Dr. Thomas Stiehl

In addition, our previous experiments excluded that HEC function could respecify early PZ into CZ cell identity (Figure 10). To further confirm this result, we simulated an early PZ cell respecification scenario. Interestingly, the simulation showed an early dramatic increase in the number of CZ cells followed by a late increase in the total number of cells, which clearly diverged from our *in vivo* data and thus further confirmed our experimental results (Figure 17).

Taken together, the iterative use of experimental and computational methods revealed that HEC function controls the dynamics of stem cell differentiation at the SAM by coordinating cell fate transition and cellular behaviour across different domains of the meristem.

IV.1.3 HEC function balances phytohormonal responses

Having characterized the role of HEC genes on the dynamics of stem cell differentiation in the SAM, we investigated the molecular mechanisms driving this activity. Given the crucial role of cytokinin and auxin in controlling fate acquisition and cell behaviour in meristematic tissues (reviewed in (Gaillochet and Lohmann, 2015), we analysed both hormonal responses in HEC-loss and gain-of function plants.

First, we recorded cytokinin responses using the *pTCSn:erGFP* reporter (Zürcher et al., 2013). Interestingly, TCS signal in *hec1,2,3* was strongly reduced and the spatial pattern was more heterogeneous than in wild type meristems (Figure 18A-C). In contrast, HEC1 induction in the CZ caused an expansion of the cytokinin-signalling domain that was concomitant with an increase in the SAM size (Figure 18D-F).

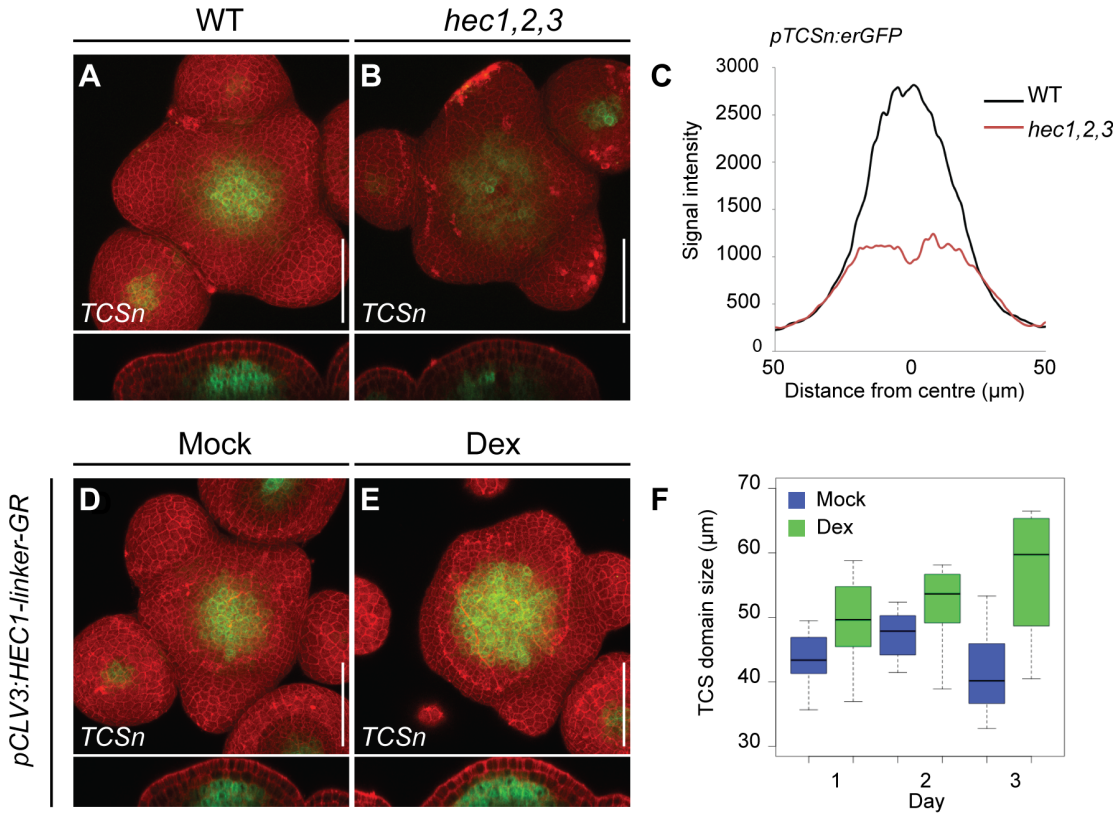

Figure 18: HEC function promotes cytokinin signalling
(A-B) Cytokinin response (*pTCSn:erGFP*) in WT (A) and *hec1,2,3* (B) shoot meristems (n>13 per genotype). **(C)** TCSn signal intensity in WT and *hec1,2,3* SAM (n>13). **(D-E)** Development of cytokinin responses (*pTCSn:erGFP)* in *pCLV3:HEC1-linker-GR* shoot meristem (n>6 per condition). Representative TCSn expression three days after mock (D) or dex (E) treatment. **(F)** Quantification of cytokinin signalling domain size after mock or dex treatment (n>6). Scale bar: 50 *µ*m

TCS measurements suggested that the defects in cytokinin response observed in *hec1,2,3* plants might lead to a smaller SAM size. Thus, we tested whether *hec,1,2,3* meristem defects could be rescued by promoting cytokinin responses. We first used a pharmacological approach and exogenously applied cytokinin on *hec1,2,3* and wild type shoot meristems. Although both lines displayed an increased SAM size, the size difference between *hec1,2,3* and wild type was suppressed after treatment (mock: p=0.007, BA: p=0.11) (Figure 19A). To complement this approach, we genetically promoted cytokinin signalling by introducing the *ahp6-1* mutation in both backgrounds (Besnard et al., 2014; Mähönen et al., 2006). In line with an increased cytokinin signalling, *ahp6-1* mutants displayed larger meristems than wild type plants (Figure 19B). Interestingly, *ahp6-1* mutation in *hec1,2,3* background restored their SAM size to that of wild type plants, indicating that loss of HEC function could be compensated by increasing cytokinin responses (Figure 19B). Together these data showed that HEC function was required and sufficient to promote cytokinin signalling,

which in turn modulated SAM size. Mechanistically, these results also suggested that by promoting cytokinin signalling HEC function could enhance *WUS* expression, which in turn could delay the transition from CZ to PZ cell identity (Yadav et al., 2010).

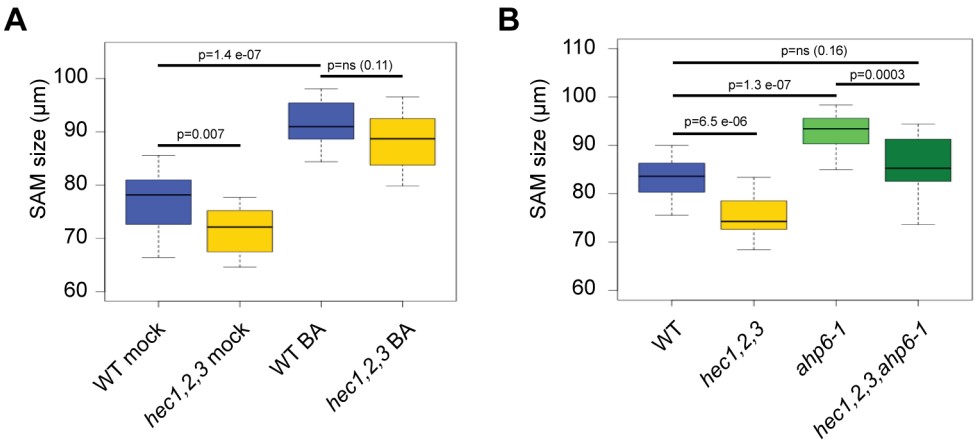

Figure 19: Promoting cytokinin signalling rescues *hec1,2,3* reduced SAM size
(A) SAM size after cytokinin treatment in WT (n>13) and *hec1,2,3* (n>13) **(B)** SAM size after introducing *ahp6-1* mutation in WT (n>14) and *hec1,2,3* (n>14). Statistical test: Student t-test.

Second, we analysed auxin sensing and response at the SAM by monitoring the auxin reporters R2D2 and *pDR5v2:3xYFP-NLS* respectively (Liao et al., 2015). Interestingly, auxin sensing and responses were not dramatically altered in *hec1,2,3* compared to wild type, demonstrating that auxin signalling does not require HEC function at the SAM (Figure 15C, 20A-B).

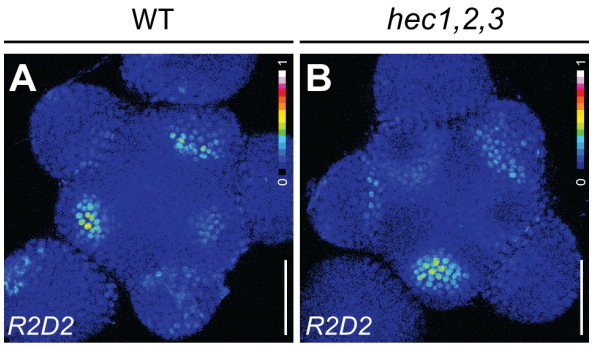

Figure 20: HEC genes are not required for auxin sensing in the SAM
(A-B) Representative expression of R2D2 in WT (n=10) (A) and *hec1,2,3* (n=7) (B) shoot meristems (intensity-based colour coding). Scale bar: 50 µm

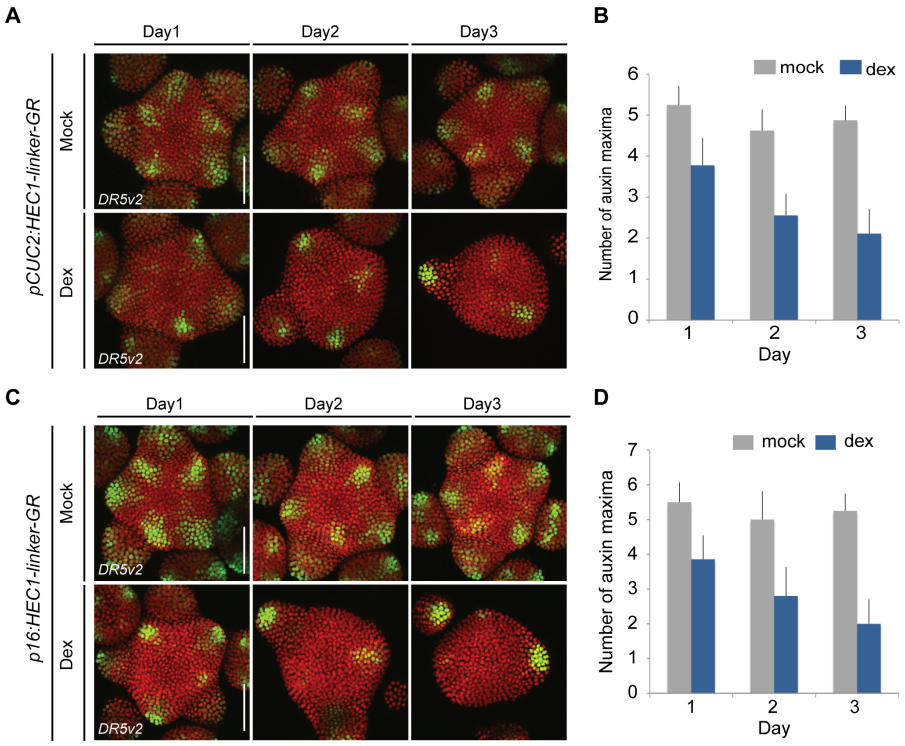

Figure 21: HEC function represses auxin signalling at the SAM periphery
(A-B) Development of auxin response (*pDR5v2:3xYFP-NLS*) in *pCUC2:HEC1-linker-GR / pRPS5A:dtTomato-NLS* shoot meristems after mock or dex treatment (n>7 per condition). Representative DR5v2 expression (A). Quantification of auxin maxima number (B). **(C-D)** Development of auxin responses (*pDR5v2:3xYFP-NLS*) in *p16:HEC1-linker-GR / pRPS5A:dtTomato-NLS* shoot meristems after mock or dex treatment (n>4 per condition). Representative DR5v2 expression (C). Quantification of auxin maxima number (D). Scale bar: 50 μm

However, the increased number of auxin maxima in *hec1,2,3,* together with the faster initiation rate predicted from our computational model, suggested that HEC function could regulate the dynamics of auxin maxima initiation. In line with this idea, HEC1 induction at the PZ using *pCUC2:HEC1-linker*-GR or ubiquitously using *p16:HEC1-linker-GR* lines (Schuster et al., 2014) gradually restricted the number of auxin maxima initiated at the SAM (Figure 21A-D).

To test the local impact of *HEC* genes on auxin responses, we induced HEC function in the stem cells and recorded R2D2 and DR5v2. Interestingly, boosting HEC1 activity in the CZ did not interfere with auxin responses at the periphery but led to a local reduction in auxin perception as shown by an increased R2D2 signal, indicating that HEC function locally repressed the auxin feedback system (Figure 22A-D). Together, the analysis of cytokinin and auxin responses revealed that HEC factors locally controlled phytohormonal responses in distinct domains the SAM and suggested that this regulation might coordinate cellular fate transitions during stem cell differentiation.

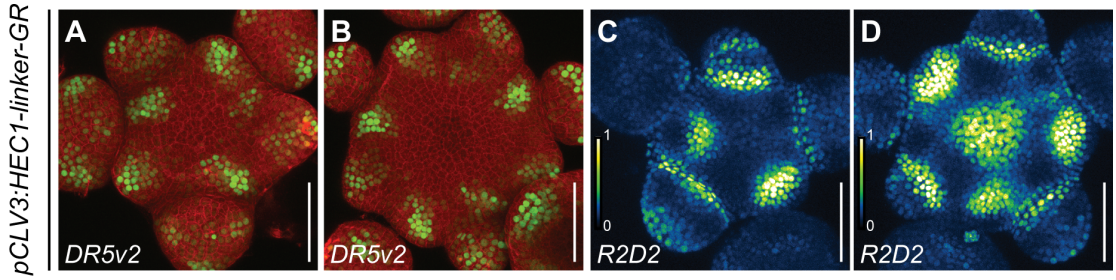

Figure 22: HEC function locally represses auxin signalling
(A-B) Auxin response (*pDR5v2:3xYFP-NLS*) in *pCLV3:HEC1-linker-GR* SAM three days after mock (A) or dex (B) treatment (n>7 per condition) **(C-D)** Auxin sensing (R2D2) in *pCLV3:HEC1-linker-GR* SAM three days after mock (C) or dex (D) treatment (n>5 per condition). Scale bar: 50 μm

To independently test the interaction between HEC function and hormonal signalling pathways in regulating cell fate acquisition, we ectopically promoted HEC activity in the root apical meristem, a region where HEC factors are not expressed (Figure 23A-F). In contrast to the SAM, auxin response is required for positioning the root stem cell niche, whereas cytokinin signalling triggers cell differentiation (reviewed in (Gaillochet and Lohmann, 2015). Interestingly, we observed that already one day after HEC1 induction, the RAM size decreased compared to control roots (Figure 23C-G). This was followed by ectopic periclinal divisions in the cortical layer and a complete suppression of the elongation zone two and three days after induction respectively (Figure 23F, H-I). Importantly, these phenotypes correlated with changes in the balance between cytokinin and auxin responses as we observed at the elongation zone an increase in cytokinin responses and a repression of auxin signalling one day after HEC1 induction (Figure 24A-D). These results showed that HEC function was sufficient to control the balance between cytokinin and auxin responses to shift stem cell differentiation trajectories.

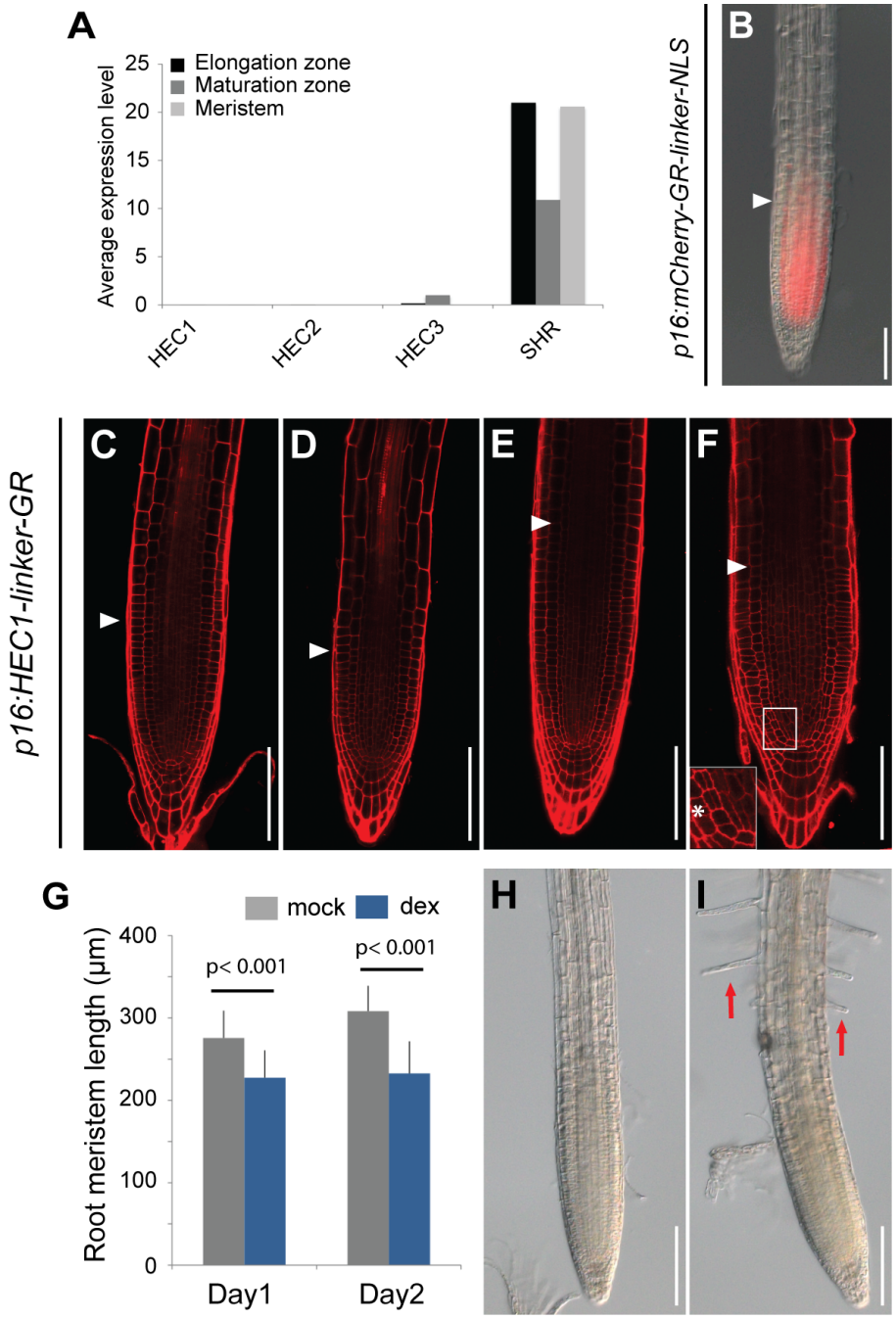

Figure 23: HEC misexpression in the root meristem modulates cell fate progression
(A) Average expression level of *HECATE* genes and *SHORTROOT* (*SHR*) in different root domains as calculated in Li et al., 2016 **(B)** Representative image of *p16:mCherry-GR-linker-NLS* root three days after dex treatment (n=15). White arrowhead marks the transition zone **(C-D)** 5 DAG root meristem of *p16:HEC1-linker-GR* one days after mock (C) or dex (D) treatment. (**E-F)** 6 DAG root meristem of *p16:HEC1-linker-GR* two days after mock (E) or dex (F) treatment. Also note ectopic periclinal division at the cortex layer of dex-treated plants (white asterisk). White triangles mark the limit between the proximal meristem and the elongation zone (mock: n=18, dex: n=21). **(G)** Quantification of RAM size in *p16:HEC1-linker-GR* after mock or dex treatment (n>17 per condition). **(H-I)** bright field view of 5 DAG *p16:HEC1-linker-GR* root meristem one days after mock (H) or dex (I) treatment. Red arrows highlight root hair differentiation. Statistical test: Student t-test (G). Scale bar: 100µm

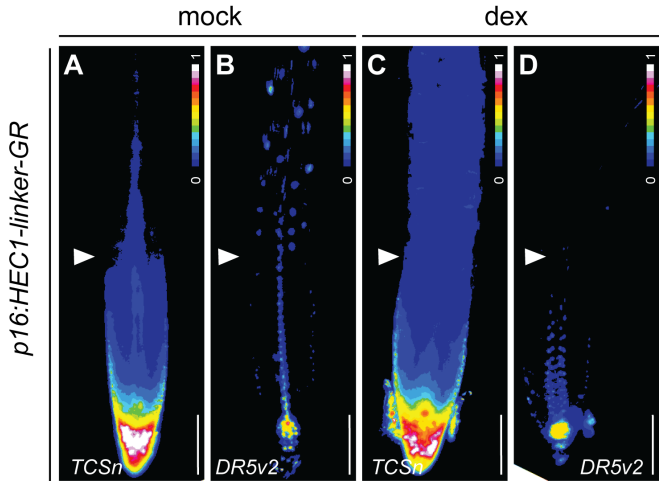

Figure 24: HEC misexpression in the RAM modulates the auxin-cytokinin balance
(A-D) Intensity-based representation of cytokinin (*pTCSn:erGFP-NLS*) (A, C) and auxin responses (*pDR5v2:3xYFP-NLS*) (B, D) in *p16:HEC1-linker-GR* root meristems one day after mock (A, B) or dex (C, D) treatment. (n>8 per genotype and condition). White arrowheads mark the region where HEC1 modulates the balance between auxin and cytokinin signalling. Scale bars: 100μm.

To further test the potential of HEC function to modulate hormonal responses in other developmental contexts, we analysed leaves and vegetative shoot meristems after ectopic HEC1 induction (Figure 23B; (Schuster et al., 2015). In line with HEC broad regulatory potential, we observed that leaves radialized after three days of induction whereas pin-like structure formed at the vegetative SAM after ten days, suggesting that auxin responses were strongly reduced in those tissues (Figure 25A-D).

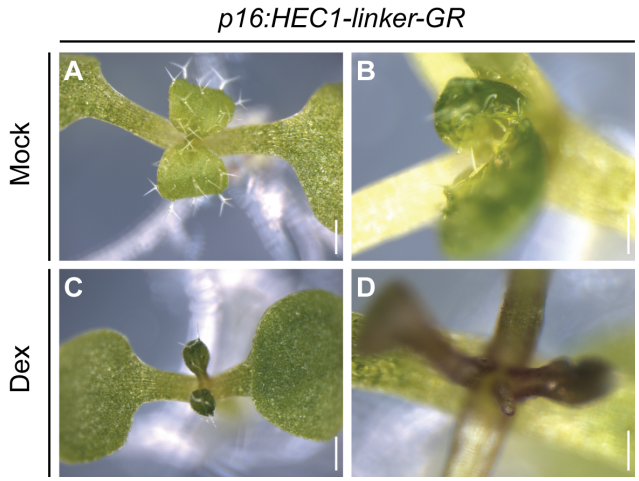

Figure 25: HEC misexpression in seedlings interferes with leaf initiation and patterning
(A-B) Seedlings 6 days after germination expressing *p16:HEC1-linker-GR* after three days of mock (A) or dex (B) induction (n> 10 per condition). **(C-D)** 13 DAG seedlings expressing *p16:HEC1-linker-GR* after ten days of mock (C) or dex (D) treatment (n> 10 per condition). Scale bar: 500 μm (A, C); 200 μm (B, D)

Taken together, these data revealed that HEC factors act as key regulators to control the balance between auxin and cytokinin responses under various developmental and cellular contexts.

IV.1.4 Molecular network underlying HEC activity

IV.1.4.1 HEC function controls auxin regulatory feedback

After having characterized the role of HEC factors in balancing cytokinin and auxin signalling at the SAM, we further investigated the molecular network mediating their activity. To this end, we used genome-wide profiling approaches and analysed HEC1 target genes (Figure 26A, B).

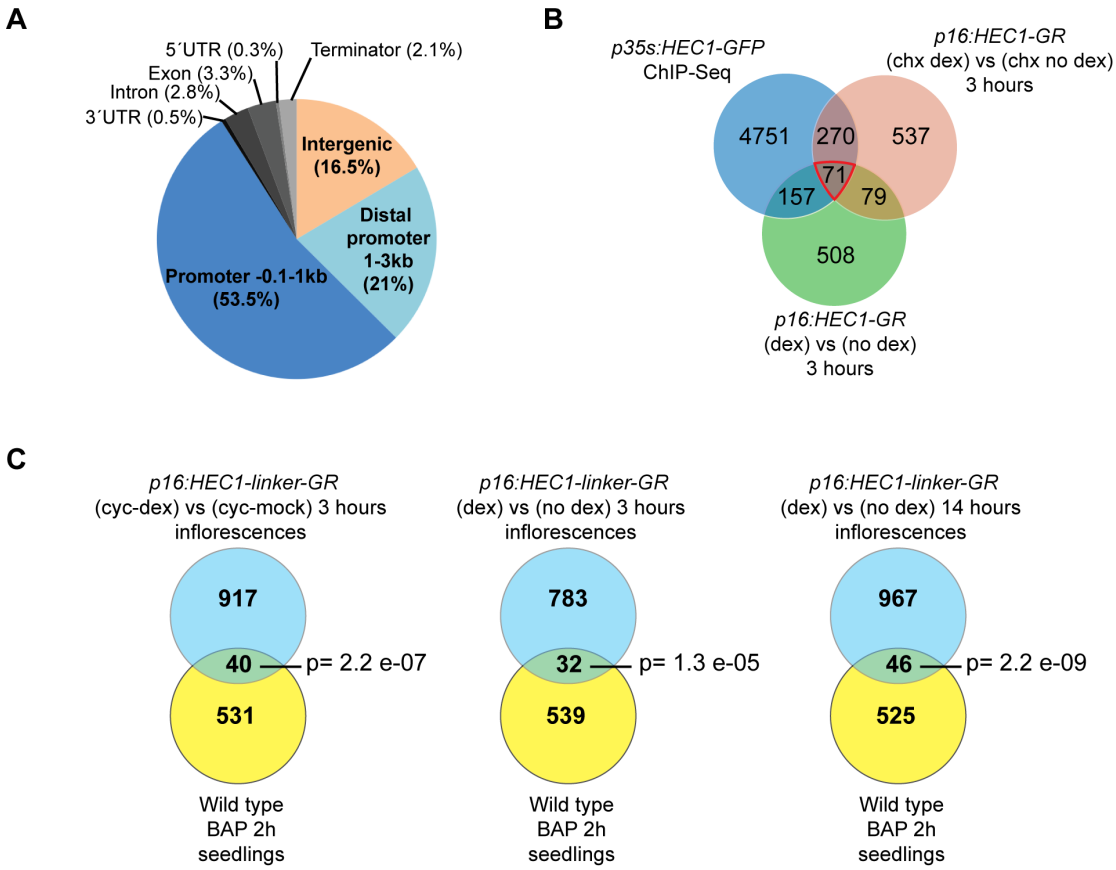

Figure 26: Genome-wide analysis of HEC1 regulatory potential
(A) HEC1 genome-wide DNA-binding pattern relative to gene model. **(B)** Venn diagram overlapping HEC1-bound genes and HEC1-response genes (inflorescence stage). **(C)** Overlap between HEC1 response genes and cytokinin response genes (Bhargava et al., 2013)

First, we assessed HEC1 genome-wide DNA-binding pattern by chromatin-immunoprecipitation followed by sequencing (ChIP-seq) at seedling stage, using a functional *p35:HEC1-linker-GFP* expressing line (Figure 26A). We identified 6930 regions bound by HEC1, belonging to 5250 genes, with 74.5% of the binding peaks located within 3kb upstream of the transcriptional starting site (Figure 26A). We then analysed HEC1-early response genes by RNA-sequencing after *p16:HEC-linker-GR* induction in inflorescences (Figure 26B). Using this approach, we detected 957

differentially regulated genes three hours after HEC1 induction and 815 regulated genes by co-inducing with the translational inhibitor cycloheximide (Figure 26B). By combining these three datasets, we defined a list of 71 high confidence direct HEC1-response genes (Figure 26B). In line with HEC function controlling cytokinin responses, we found a significant overlap between HEC- and cytokinin response genes (Bhargava et al., 2013), suggesting that these two pathways converge at the molecular level. In contrast, the canonical cytokinin and auxin signalling components, including ARF and Aux-IAAs, were not significantly enriched in our datasets, suggesting that HEC function does not directly orchestrate phytohormonal response but rather acts indirectly or target specific components of the pathways (Supplementary table 1, Appendix: Supplementary table 1).

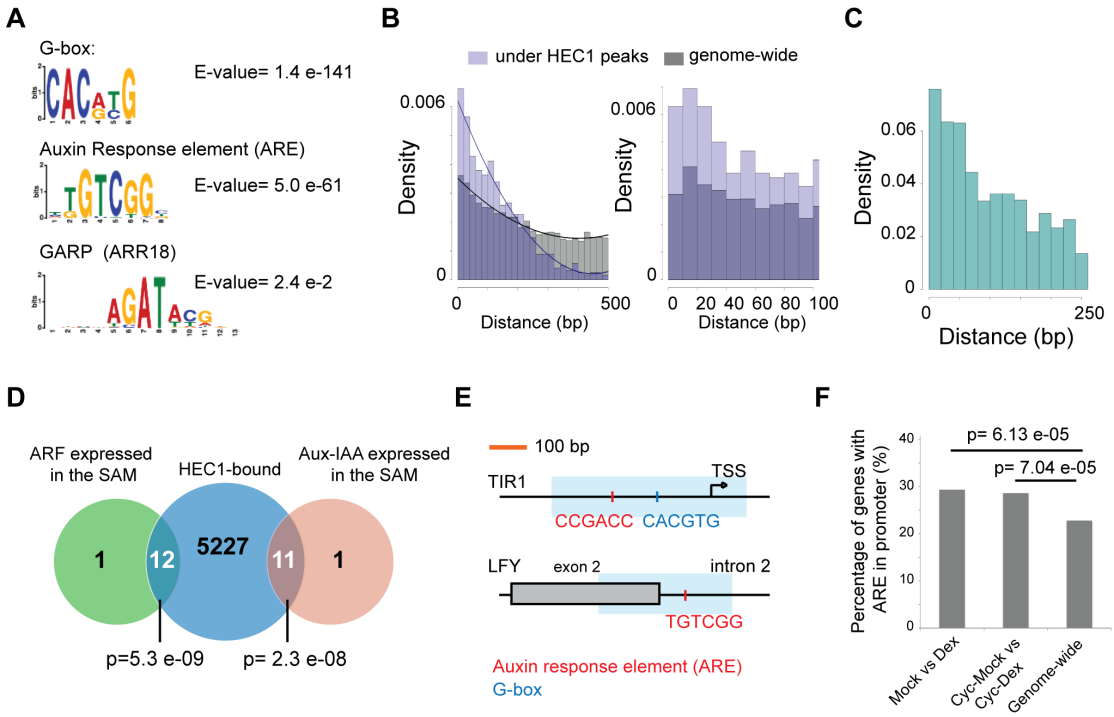

Figure 27: HEC1 genomically associates with ARFs and their target genes
(A) *De novo* motif enrichment under HEC1-bound regions. **(B)** Distribution of genomic distances between G-box and ARE under HEC1 peaks (light purple) and on the genome-wide scale (grey). Fitting curves depict polynomial second order fit. **(C)** Distribution of genomic distances between HEC1 peak summit and ARE. **(D)** Venn diagram overlapping HEC1-bound genes and auxin signalling components expressed in the SAM (Vernoux et al., 2011). **(E)** Schematic of genomic loci bound by HEC1. Light blue box depicts HEC1 binding region; blue and red line show G-box and ARE motifs respectively. **(F)** Percentage of HEC-response genes carrying an ARE in their promoter compared to genome-wide scale. Statistical test: Hypergeometric test (D), Fischer test two-sided (F). (Panel B, and C were generated by Dr. Andrej Miotk)

To further define HEC1 regulatory signatures, we carefully analysed the ChIP-seq dataset and identified HEC1 genomic associations (Figure 27). Consistent with HEC1 belonging to the bHLH transcription factor family, we detected a strong enrichment of the G-box motif under its bound genomic regions (E-value=1.4 e-141) (Lau et al., 2014; Pfeiffer et al., 2014). Interestingly, we also found that the auxin response element (ARE), a motif bound by ARFs, was significantly enriched under HEC1 peaks (E-value= 5.0 e-61) (Figure 27A). In contrast, the GARP motif bound by the type-B ARR ARR18 was only mildly enriched (E-value=2.4 e-2), demonstrating the specificity, among phytohormonal pathways, of the association between HEC1 and ARF targets (Figure 27A).

These results also suggested that HEC1 could directly modulate ARF function at the regulatory regions of ARF target genes. In line with this idea, we found that G-box and ARE motifs were closely associated under HEC1 peaks compared to their genome-wide distribution (Figure 27B) and that the greater proportion of ARE were located within 50bp of HEC1 peak summits (Figure 27C). Strikingly, we found a significant enrichment of HEC1 binding at the promoter regions of ARFs (p=5.3 e-9) and Aux-IAAs (p=2.3 e-08) expressed in the SAM (Vernoux et al., 2011). (Figure 27D, Figure 28A-B). Furthermore, HEC1 bound the regulatory regions of the auxin receptor TIR1 and LFY, whose activity is tightly intertwined with auxin signalling during flower primordia initiation (Figure 27E) (Yamaguchi et al., 2013).

Finally, we found that the proportion of genes carrying an ARE in their promoter was significantly increased among HEC1 response genes compared to their distribution on the genome-wide scale (Figure 27F). Taken together, these results showed that HEC factors and ARF closely associated at the genomic level, and further suggested that they could control auxin responses in competition, independently or in complex.

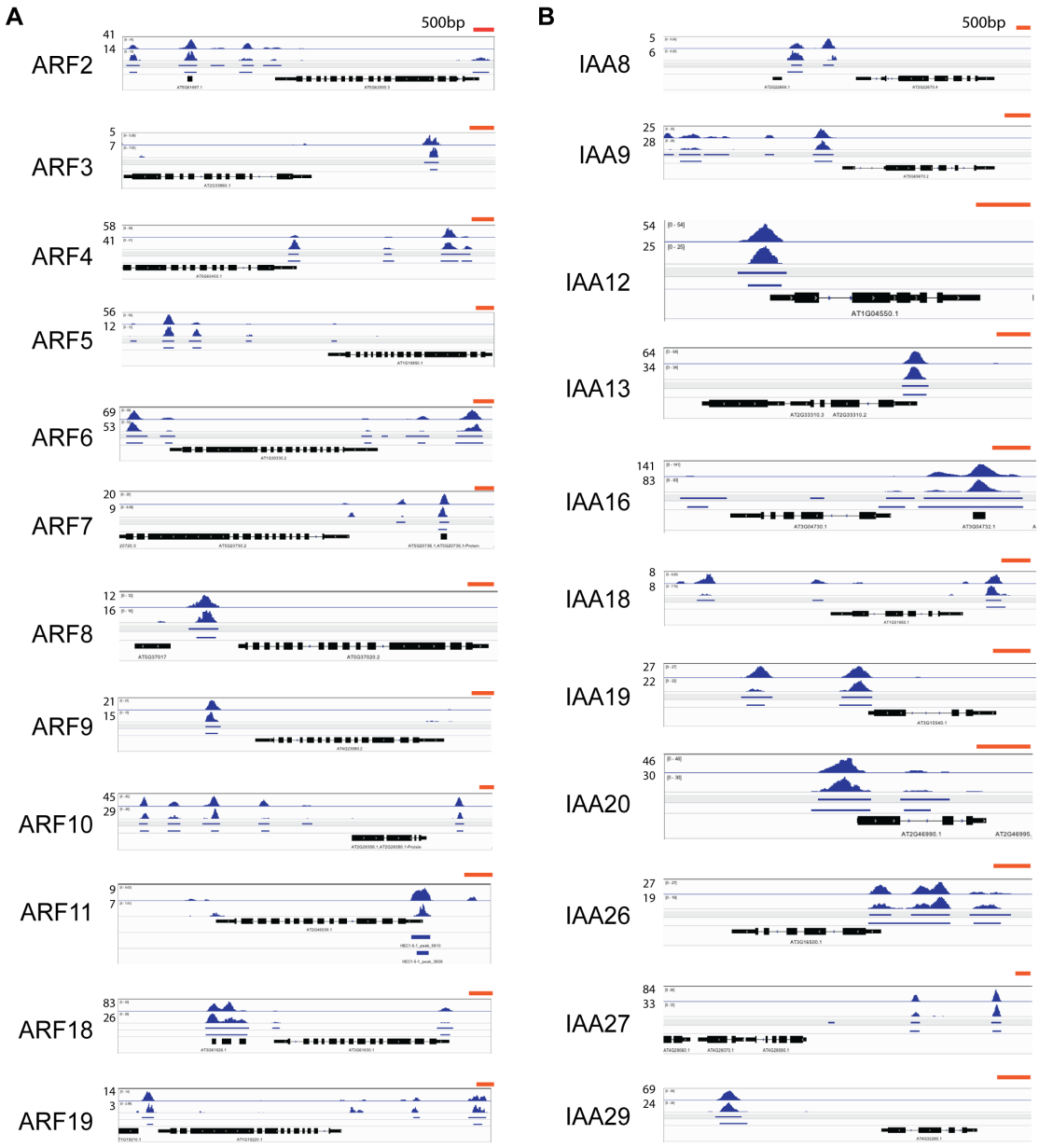

Figure 28: HEC1 binds the regulatory regions of auxin signalling components
Visualisation of HEC1-binding peaks at the regulatory region of auxin signalling components expressed in the SAM (Vernoux et al., 2011) for two ChIP-seq biological duplicates. Orange line depicts 500bp

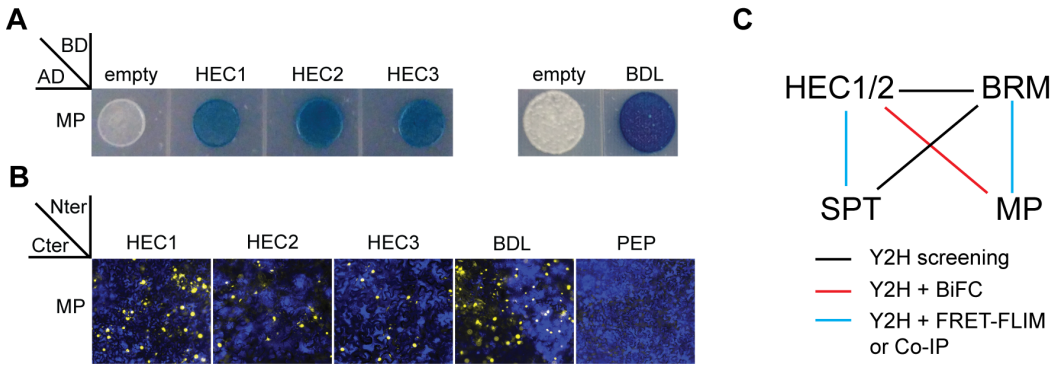

Figure 29: HEC factors physically interact with MP
(A) Yeast-two hybrid assay testing physical interaction between HEC factors and MP. Blue colonies indicate physical interaction. BDL is used as a positive control **(B)** Bi-Fluorescence complementation assay testing physical interaction between HEC factors and MP. Yellow nuclear signal reveals physical interaction. BDL was used as a positive control and PEP as a negative control. **(C)** Protein-protein interaction network showing association between HEC factors, SPT, MP and BRHAMA (Efroni et al., 2013). Experiments in (A-B) were conducted by Dr. Juan Jose Rippoll, UC San Diego

To test whether HEC factors could directly form a complex with ARFs in the SAM, we assessed the physical interaction between HEC1,2,3 and MP, a key ARF for flower primordia initiation (Bhatia et al., 2016; Hardtke and Berleth, 1998). Using yeast-two-hybrid (Y2H) assays and bi-molecular fluorescence complementation (BiFC) assays, we found that HEC proteins physically associated with MP (Figure 29), supporting the idea that these factors could interfere with the auxin feedback system through complex formation. This idea was also supported by the ability of HEC1, HEC2 and SPT to physically interact with BRM, a key MP cofactor during primordia initiation (Figure 29C). The formation of a larger complex suggests that HEC function could slowly uncouple auxin response, perception and transport, which consequently could modulate cell fate decisions at the SAM periphery. In line with this idea, *MP* expression was not changed at early time points, but significantly decreased 14 hours after HEC1 induction (Figure 30A). This regulation was consistent with a lower MP-GFP signal at the PZ and BZ upon HEC1 induction, further demonstrating the relevance of this interaction for primordia initiation (Figure 30B). Accordingly, we observed strong repression of auxin perception and changes in PIN1-GFP polarity after inducing HEC1 at the PZ-BZ (Figure 31A-D).

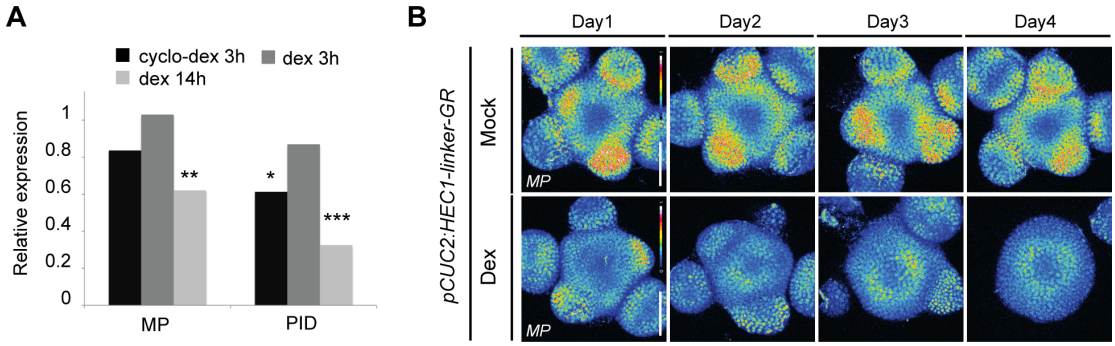

Figure 30: HEC downregulates MP expression
(A) MP and PID relative expression after *p16:HEC1-linker GR* induction in inflorescences. **(B)** Time series of *pMP:MP-GFP* (intensity-based representation) in individual *pCUC2:HEC1-linker-GR* shoot meristems after mock or dex treatment (n>6 per condition). Statistical test: Fischer´s exact test (EdgeR), * p<0.05, ** p<0.01, *** p<0.001. Scale bar: 50 μm (B)

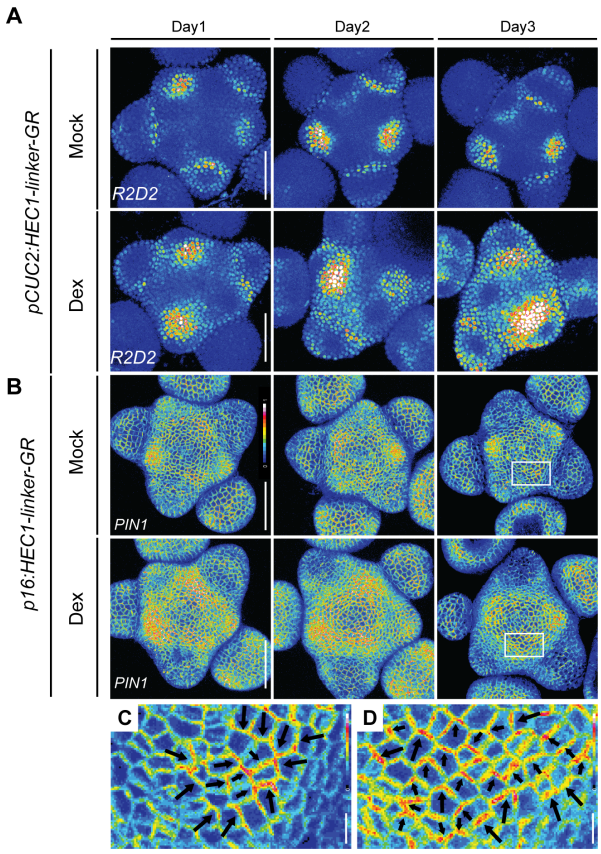

Figure 31: HEC factors can uncouple the auxin feedback system at the SAM
(A) Time series of auxin signalling input in individual *pCUC2:HEC1-linker-GR / R2D2* shoot meristems after mock or dex treatment. Higher R2D2 intensity signals mark low auxin sensing regions (n>4 per condition). **(B)** Time series of *pPIN1:PIN1-GFP* in individual *p16:HEC1-linker-GR* shoot meristems after mock or dex treatment (mock: n>4; dex: n>9 per condition). **(C-D)** Magnified views of white boxes in (B) depicting *pPIN1:PIN1-GFP* (intensity-based representation) after *p16:HEC1-linker-GR* mock (C) or dex (D) induction. Black arrows depict hypothetical auxin flow. Scale bar: 50 μm (A-B), 5 μm (C-D)

In turn, the progressive uncoupling of the auxin feedback system correlated with the expansion towards the centre of the PZ-BZ cell identity marker CUC2, denoting changes in cellular identities (Figure 32).

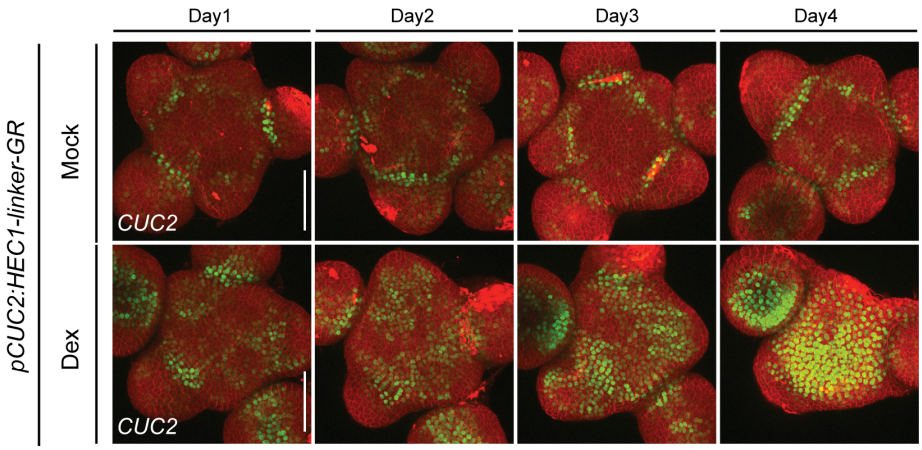

Figure 32: HEC function interferes with boundary zone fate acquisition
Development of boundary zone reporter (*pCUC2:3xGFP-NLS*) after *pCUC2:HEC1-linker-GR* induction with mock or dex. Scale bar: 50 *µ*m

Together this data showed that HEC factors modulate the auxin feedback system at the SAM periphery, which in turn instruct primordia cell fate switch. Their close genomic association with ARFs and physical interaction with MP also suggested that the formation of HEC-MP complex could mediate this function.

To test whether the modulation of auxin signalling was mediating HEC function at the transition between PZ and primordia cell fate, we simultaneously induced HEC1 and stabilized the auxin feedback system by exogenously treating shoot meristems with auxin. First, we tested the feasibility of our strategy by analysing *MP* mRNA levels. Although MP expression was significantly reduced upon HEC1 induction with dex, auxin co-treament rescued its expression level to those of controls, confirming that our strategy to stabilize auxin responses was successful (Figure 33). Interestingly, we also observed a significant increase in SPT expression after HEC1 induction and auxin treatment, suggesting that auxin positively regulated *SPT* expression (Figure 33).

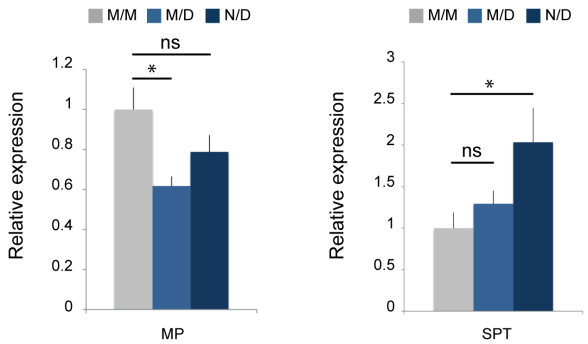

Figure 33: Auxin treatment rescues *MP* RNA level upon HEC induction
Relative expression of *MP* and *SPT* 24 hours after *p16:HEC1-linker-GR* induction (M/M:mock/mock, M/D: mock/dex, N/D: NAA/dex). Statistical test: Welch t-test
* p<0.05, ** p<0.01, ***p<0.001

Next, we analysed the phenotypic outcome of stabilizing the auxin regulatory loop while increasing HEC activity. Strikingly, although HEC1 induction inhibited the formation of primordia, HEC1 co-induction with auxin fully suppressed this phenotype, leading to the formation of primordia and lateral organs similarly to control plants (Figure 34E-H). Importantly, the suppression of pin-like inflorescence phenotypes was not a mere consequence of changes in the *CUC2* promoter activity, nor resulted from the downregulation of *SPT* expression (Figure 33, 34A-D). Taken together, these data demonstrated that HEC function modulates primordia cell fate decision by controlling auxin responses.

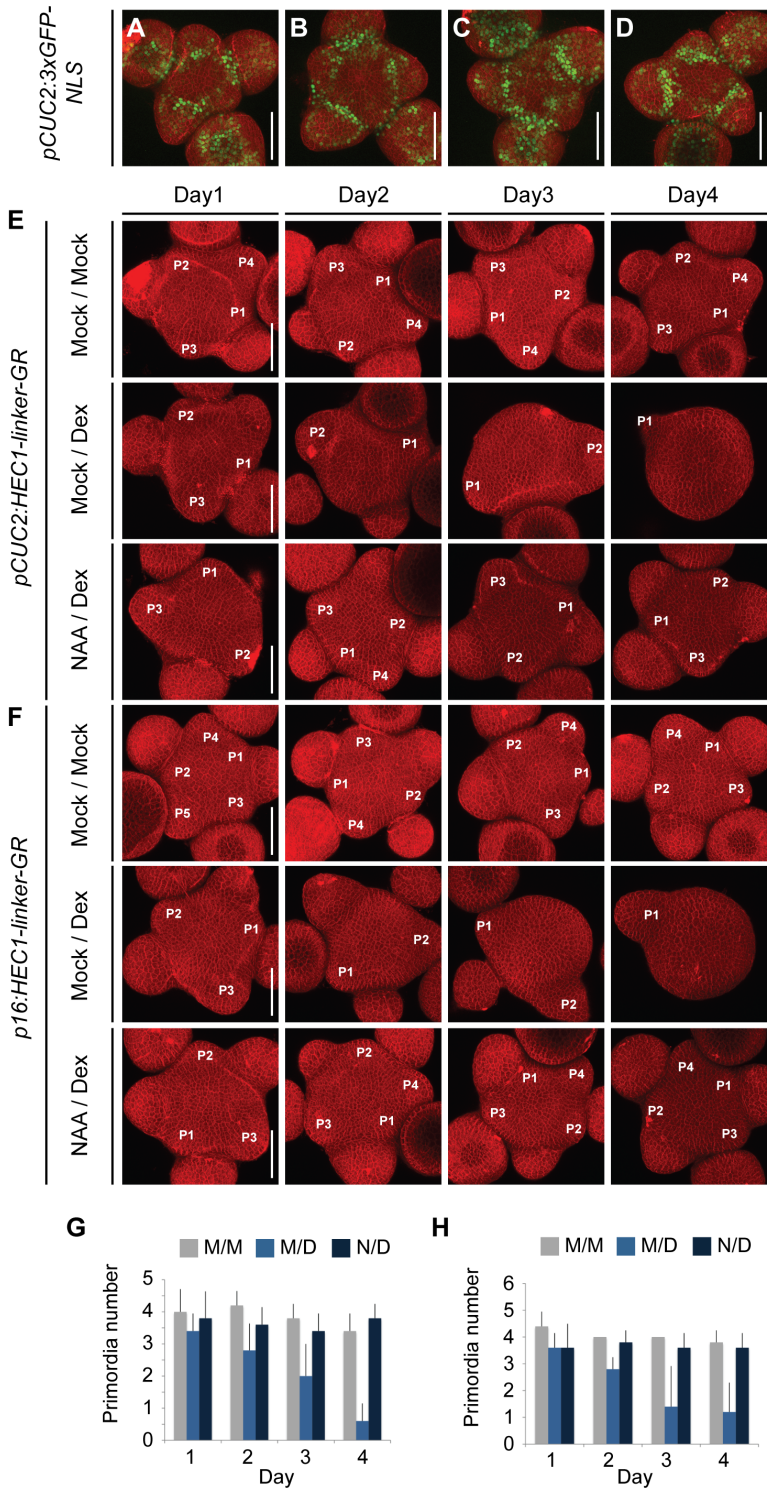

Figure 34: Auxin treatment suppresses HEC function at the SAM periphery
(A-D) Representative view of shoot meristems expressing *pCUC2:3xGFP-NLS* following 24 hours (A,B) or 48 hours (C,D) of mock (A,C) or NAA (B,D) treatment (n>3 per condition) **(E-F)** Development of *pCUC2:HEC1-linker-GR* (E) or *p16:HEC1-linker-GR* (F) shoot meristems after mock/mock, mock/dex or NAA/dex treatment (n=5 per condition and time point). Primordia are marked till flower stage 2. **(G-H)** Time series quantification of primordia number in *pCUC2:HEC1-linker-GR* (G) or in *p16:HEC1-linker-GR* (H) after mock/mock (M/M), mock/dex (M/D) or NAA/dex (N/D) treatment (n=5 per condition and time point). Scale bar: 50μm

IV.1.4.2 HECATE and SPATULA interact during SAM development

Our genome-wide analysis allowed us to further define the molecular interaction between HEC factors and hormonal signalling pathways. Given the domain-specific activity of HEC1 on hormonal responses at the SAM, we wanted to further understand the molecular mechanisms controlling that process and hypothesized that its association with distinct protein cofactors could define its functional specificity. Importantly, bHLH transcription factors typically form protein homo- and hetero-dimers through their bHLH domains (Toledo-Ortiz et al., 2003) and it was previously shown that HEC factors can physically interact with another bHLH transcription factor SPT (Gremski et al., 2007). Therefore, we investigated whether the interaction between HEC factors and SPT could mediate HEC domain-specific activity.

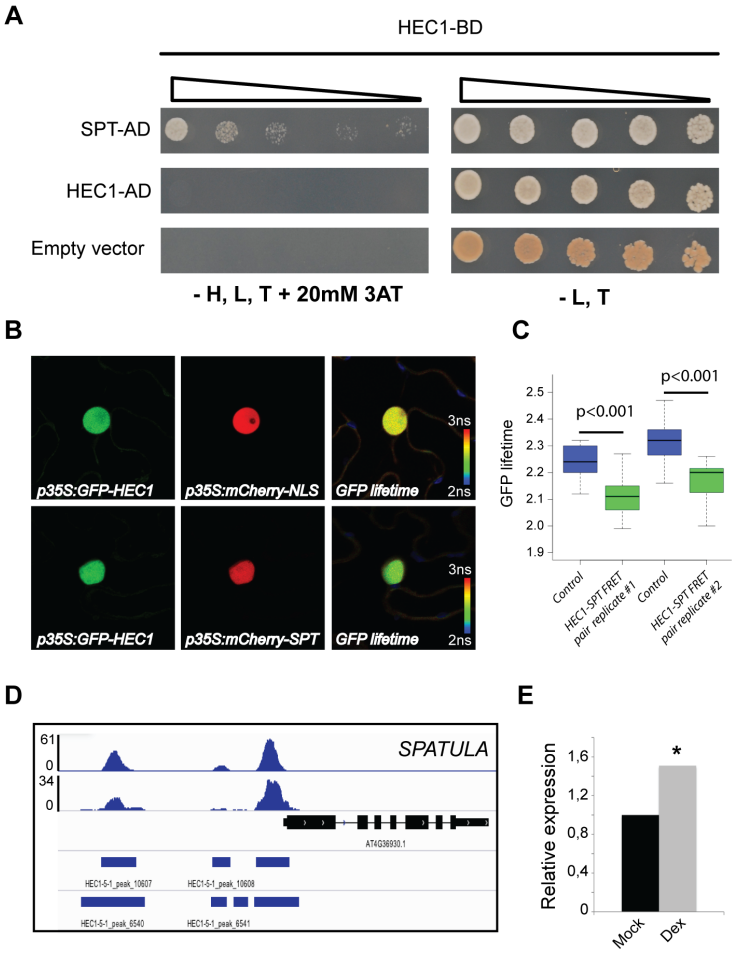

Figure 35: HEC and SPATULA form a regulatory unit
(A) Yeast-two hybrid assay testing HEC1 homo- and heterodimerisation with SPT. Growth on –H,L,T supplemented with 3AT indicates physical interaction. **(B-C)** FRET-FLIM assay testing the physical interaction between HEC1 and SPT. Nuclei expressing GFP-HEC1, mCherry-SPT and mCherry-NLS (B). Intensity based images depicts GFP lifetime. GFP lifetime quantification, decrease in GFP lifetime reveals physical interaction (C). **(D)** Visualisation of HEC1 DNA-binding pattern at SPATULA loci. **(E)** *SPT* relative expression after *p16:HEC1-linker-GR* induction in inflorescences. Statistical test: Fischer´s exact test (EdgeR), * p<0.05

Using Y2H assays, we first confirmed the physical interaction between HEC1 and SPT, and additionally showed that HEC1 was not able to homo-dimerize (Figure 35A). We then used fluorescence energy resonance transfer (FRET)- fluorescence lifetime imaging microscopy (FLIM) assays to test HEC1-SPT interaction *in planta* and observed a significant reduction in the GFP lifetime upon co-transfection of *HEC1-GFP* construct with *SPT-mCherry* compared to controls, showing that HEC and SPT form a complex *in planta* (Figure 35C). Interestingly, we found from our genome-wide analysis that HEC1 directly bound and positively regulated the expression of SPT (Figure 35D, E), suggesting that HEC1-SPT form a regulatory module that can self-amplify its activity.

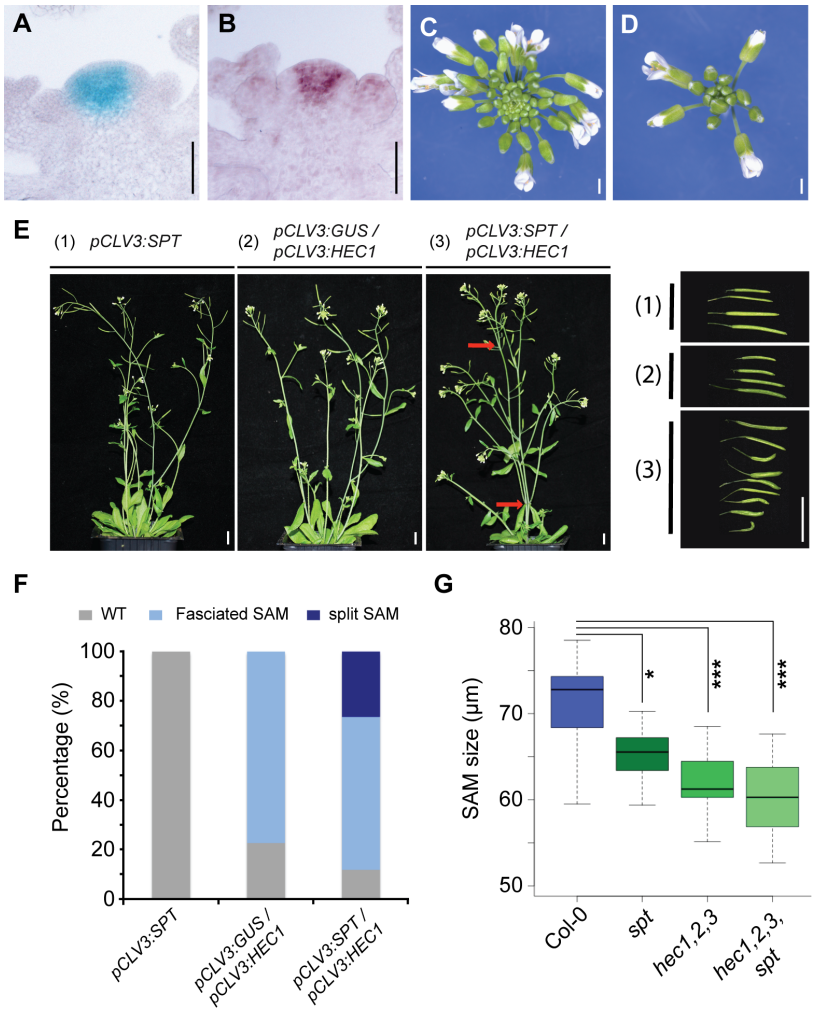

Figure 36: HEC-SPT complex formation mediates HEC function in the CZ
(A) *pSPT:GUS* expression in the SAM. **(B)** *SPT* in situ hybridization in the SAM. **(C-D)** Wild type (C) and *spt-12* (D) inflorescences expressing *pCLV3:HEC1*. **(E)** Inflorescences and siliques expressing *pCLV3:SPT* (1) *pCLV3:GUS* and *pCLV3:HEC1* (2) *pCLV3:SPT* and *pCLV3:HEC1* (3). **(F)** Phenotypic quantification testing the interaction between HEC1 and SPT functions in the SAM. **(G)** Quantification of shoot meristem size. Statistical test: Student t-test. Scale bars: 50*µ*m (A-B); 1mm (C-D); 1cm (E)

To test this hypothesis in the SAM, we first recorded *SPT* expression pattern by in situ hybridization. *SPT* was expressed in the CZ and the PZ of the SAM (Figure 36A, B), similarly to *HEC1* (Schuster et al., 2015). Using genetic approach, we tested the functional interaction between HEC and SPT in the CZ by expressing *pCLV3:HEC1* in the *spt* mutant background. Strikingly, SAM expansion phenotypes observed upon HEC1 gain-of-function in the CZ were fully suppressed in the *spt* mutant background, demonstrating that SPT was required for HEC function in the CZ (Figure 36C, D). To further test their genetic interaction, we combined HEC1 and SPT gain-of-function (Figure 36E,F). In line with their combinatorial activity as part of a protein complex, the co-expression of *pCLV3:SPT* and *pCLV3:HEC1* gave rise to two novel phenotypes: split meristems and smaller fruits, which were never observed by expressing *pCLV3:SPT* or *pCLV3:HEC1* alone (Figure 36E, F). In addition, *spt* mutants displayed significantly smaller shoot meristems compared to wild type, further confirming the role of SPT in regulating SAM activity. Interestingly, introducing *spt* mutation in the *hec1,2,3* background did not further enhance the defects in SAM size, suggesting that in the wild type situation, HEC levels are limiting the activity of the HEC-SPT complex (Figure 36G). To test whether the interaction with SPT could also modulate HEC function at the SAM periphery, we assessed the role of HEC-SPT complex at the transition between PZ and primordia. Similarly to the CZ, the inhibition of lateral organs upon *p16:HEC1-linker-GR* induction was fully suppressed in *spt-12* mutant background, demonstrating that SPT was also required for HEC function at the PZ (Figure 37A, B). Together, these results excluded the hypothesis that SPT could instruct HEC functional specificity in the SAM, but instead underlined the relevance of the HEC-SPT protein complex in controlling cell fate transitions at the SAM.

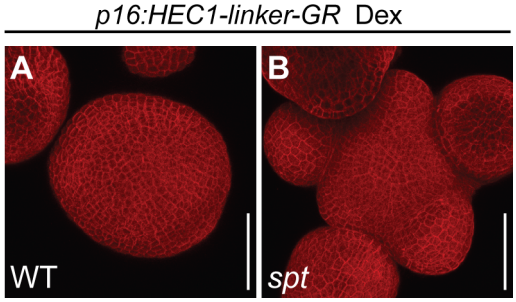

Figure 37: HEC-SPT complex modulates flower primordia initiation
(A-B) Wild type (A) and *spt-12* (B) shoot meristems four days after *p16:HEC1-linker-GR* dex induction. Scale bar: 50 μm

IV.1.5 Theoretical model of HEC function at the SAM

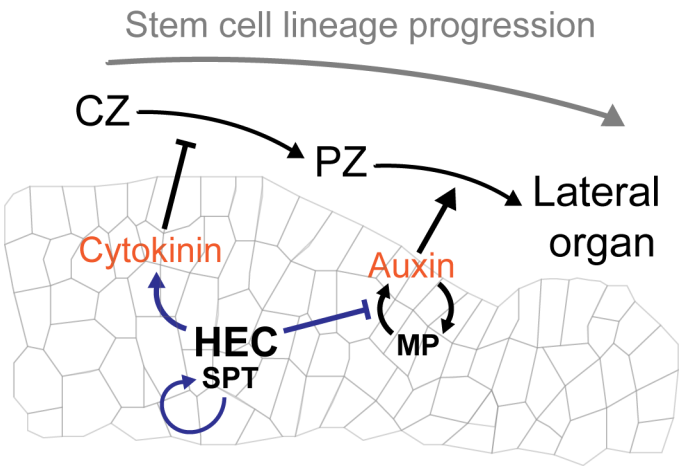

Figure 38: Theoretical model showing HEC regulatory functions at the SAM

Our multi-scale analysis of the shoot apical meristem revealed that *HEC* genes control the dynamics of SAM cell differentiation by locally coordinating cytokinin and auxin responses. During this process, HEC factors positively regulate cytokinin signalling at the centre of the SAM and pace the auxin regulatory loop dynamics at the periphery by possibly directly associating with MP. Both activities at the CZ and PZ require the transcription factor SPT, which forms a protein complex with HEC1 and self-amplifies its activity (Figure 38).

IV.2 Characterization of HEC function in the gynoecium

Our analysis of the shoot meristem allowed us to unravel key regulatory functions of *HEC* genes. First, we showed that HEC factors coordinated cytokinin and auxin responses and found that HEC factors were interacting with auxin signalling components to modulate the dynamics of the auxin feedback system. Secondly, we showed that HEC and SPT form a protein complex that is crucial to mediate HEC function.

Given the previously described role of *HEC* genes and *SPT* and the key role of phytohormonal signalling during gynoecium development (Gremski et al., 2007; Heisler et al., 2001; Sundberg and Østergaard, 2009), we hypothesized that some of the regulatory functions identified in the SAM could also act in the gynoecium. Therefore, we investigated whether HEC-SPT complex could regulate phytohormonal homeostasis during gynoecium development.

IV.2.1 HEC and SPT functionally interact in the gynoecium

To characterize the interaction between HEC and SPT, we first analysed their expression pattern across plant development using data from the AtGenExpress Atlas (Figure 39).

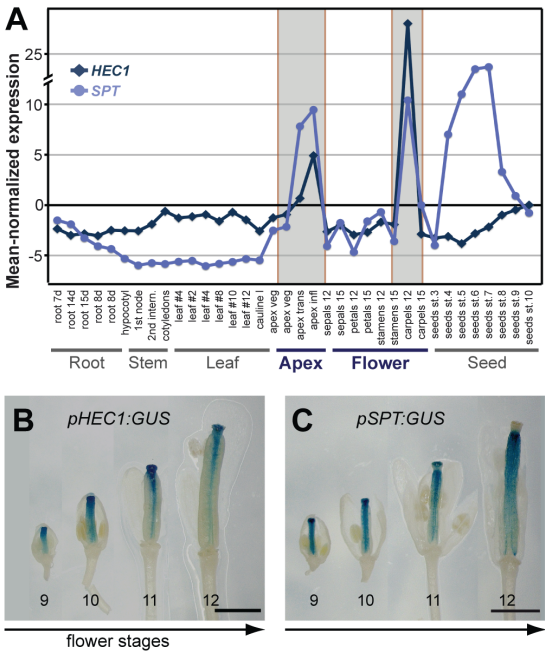

Figure 39: HEC and SPT are co-expressed in the gynoecium
(A) Normalised *HEC1* and *SPT* expression across *Arabidopsis* development (AtGenExpress atlas; Schmid et al., 2005). **(B-C)** GUS staining showing *pHEC1:GUS* (B) and *pSPT:GUS* (C) expression in the developing gynoecium. Scale bar: 1 mm (figure modified from Schuster et al., 2015)

In line with their functional interaction in the SAM, HEC1 and SPT were co-expressed in the inflorescence apex. In addition, their transcripts were also detected in carpels at stage 12 and 15 (Figure 39A) (Schmid et al., 2005). To confirm these results, we stained gynoecium from stage 9 to stage 12 expressing *pHEC1:GUS* and *pSPT:GUS* using ß-glucoronidase assays. We found that HEC1 and SPT were co-expressed at the apical part of the gynoecium across multiple developmental stages (Figure 39B, C), suggesting that HEC and SPT co-regulate style development.

To further dissect this functional interaction, we used genetic approaches and compared WT, *hec1,2,3*, *spt* and *hec1,2,3,spt* gynoecia from stage 9 to stage 13 using scanning electron microscopy (SEM). In wild type plants, the style fused and stigmatic papillae started to develop from stage 11 on and were fully developed by stage 13 (Figure 40A, E, I, M). In contrast, the style in *hec1,2,3* (Figure 40B, F, J, N) and *spt* (Figure 40C, G, K, O) mutants did not a fuse at that stage, subsequently leading to defects in stigmatic tissue differentiation. These style fusion phenotypes were strongly enhanced in *hec1,2,3,spt,* as apical parts of the gynoecium did not fuse and ovules could grow externally (Figure 4O, H, L, P). Together these data demonstrated that HEC and SPT function genetically interact during the formation of the style and stigmatic tissues.

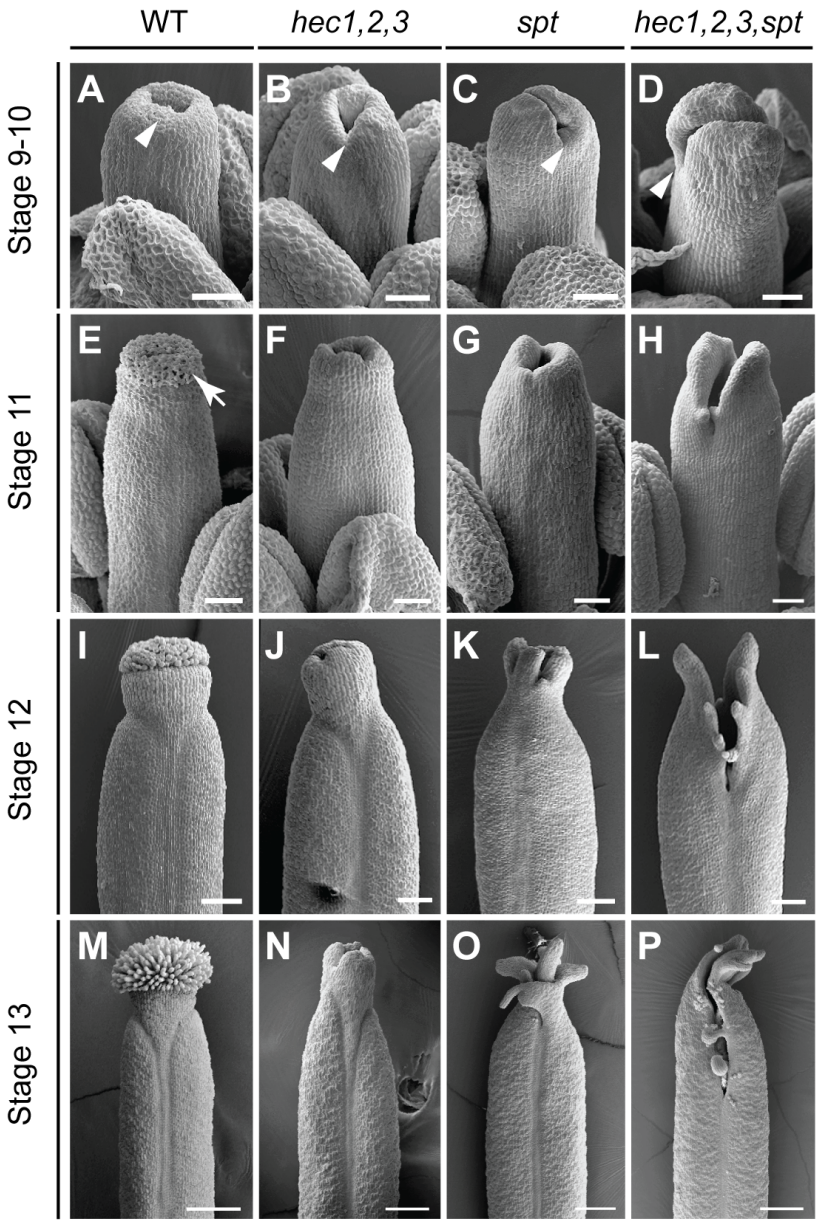

Figure 40: HEC and SPT functionally interact to specify style and stigma
(A-P) Scanning electron microscopy of wild type (A, E, I, M); *hec1,2,3* (B, F, J, N); *spt* (C, G, K, O) and *hec1,2,3,spt* (D, H, L, P) gynoecium at stage 9-10 (A-D), stage 11 (E-H), stage 12 (I-L), stage 13 (M-P). Arrowheads highlight the style fusion. Arrow marks stigma formation. Scale bar: 50 µm (A-H); 100 µm (I-L); 200 µm (M-P). Electron microscopy was performed by Dr. Christoph Schuster; figure modified from (Schuster et al., 2015).

IV.2.2 HEC function controls auxin transport and responses at the style

After having characterized the role of HEC and SPT during style formation, we wondered what regulatory program were they controlling. Therefore, we analysed our genome-wide profiling datasets to identify putative downstream target genes mediating HEC activity in this context.

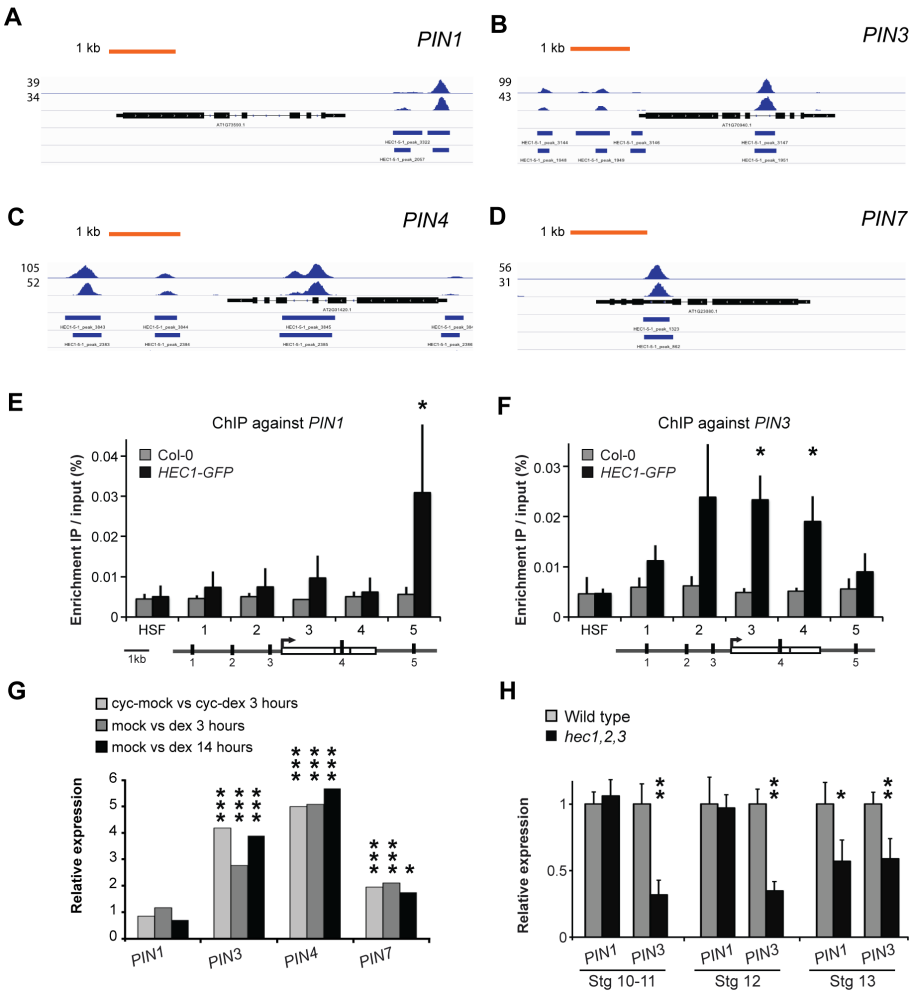

Figure 41: *HEC1* directly promotes the expression of *PIN* genes
(A-D) HEC1 ChIP-seq visualisation showing DNA-binding pattern at PIN1 (A), PIN3 (B), PIN4 (C) and PIN7 (D) loci. **(E-F)** HEC1 ChIP-qPCR showing DNA-binding enrichment at the *PIN1* (E) and *PIN3* (F) loci. **(G)** Relative expression of *PIN* genes after *p16:HEC1-linker-GR* induction as measured by RNA-seq. **(H)** *PIN* mRNA expression at multiple gynoecium developmental stages as measured by qRT-PCR. Biological triplicate were performed. Statistical test: Wilcoxon signed-rank test, *p<0.05; **p<0.01; ***p<0.001 (E, F, H). Fischer´s exact test (EdgeR), * p<0.05, ** p<0.01, *** p<0.001 (G). qRT PCR experiments in (H) were performed by Dr. Christoph Schuster

From the high confidence HEC1 early response genes, we identified PIN genes among the top targets. From our ChIP-seq dataset, HEC1 bound *PIN1*, *PIN3*, *PIN4* and *PIN7* regulatory regions (Figure 41A-D). Using ChIP-qPCR, we detected

significant HEC1 enrichment at the regulatory regions of PIN1 and PIN3, confirming the genome-wide binding data (Figure 41E,F). To analyse PIN transcriptional regulation upon HEC1 induction, we examined our RNA-seq datasets. In line with their direct binding, we found that *PIN3*, *PIN4* and *PIN7* were significantly upregulated 3 hours after HEC1 induction in inflorescences. Using *hec1,2,3* gynoecium, we next measured *PIN1* and *PIN3* expression levels across gynoecium developmental stages (from stage 10 to stage 13) (Figure 41H). Consistent with our genome-wide analysis at the inflorescence stages, we detected a significant reduction in *PIN1* expression at stage13 and a decrease in *PIN3* expression at all stages tested, demonstrating that HEC function directly promotes *PIN* expression in the context of the gynoecium (Figure 41H).

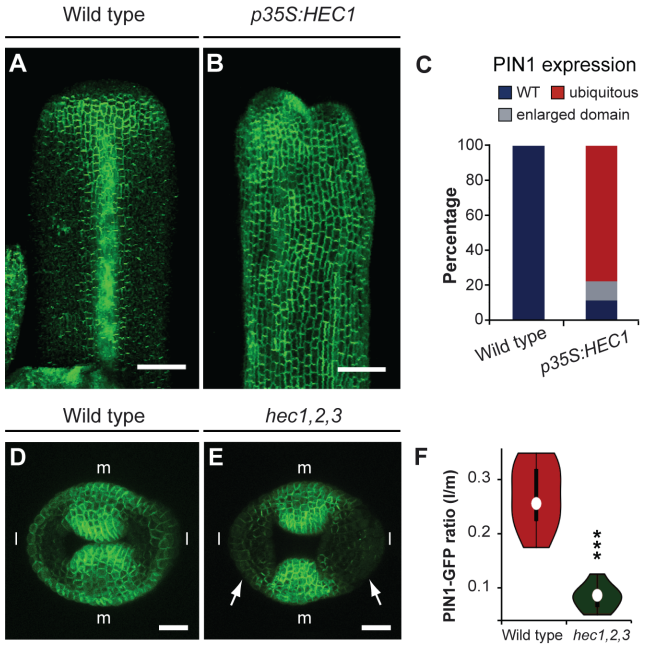

Figure 42: HEC function shapes PIN1 distribution domains
(A-B) PIN1-GFP distribution (*pPIN1:PIN1-GFP*) in wild type (A) and *p35S:HEC1* (B) stage 9-10 gynoecium. **(C)** Phenotypic quantification of PIN1 distribution in T1 plants. **(D-E)** PIN1-GFP distribution in wild type (D) and *hec1,2,3* (E) style region at stage 9-10. **(F)** Lateral (l) to medial (m) PIN1 distribution ratio in wild type and *hec1,2,3* style regions. Statistical test: Student t-test (F) Scale bar: 50 μm (A,B) 20μm (D,E). Figure modified from (Schuster et al., 2015)

Given the important role of auxin distribution and signalling at the apical part of the gynoecium to specify style structures (Moubayidin and Østergaard, 2014), our results suggested that the defects observed in HEC gain- and loss-of-function might be caused by irregular PIN distribution. To directly test this, we monitored the distribution of PIN1-GFP in gynoecia expressing *pPIN1:PIN1-GFP*. In wild type

plants, PIN1 accumulated laterally along the developing septum and was localized radially all across the developing style, with stronger localisation at the medial part compared to the lateral side (Figure 42A, D). In contrast, we observed that PIN1-GFP accumulated ubiquitously in gynoecia expressing *p35S:HEC1*, whereas it was reduced at the lateral side of the developing style in *hec1,2,3* (Figure 42A-E). Importantly, the reduction in PIN1 accumulation in *hec1,2,3* significantly modified the medial to lateral PIN1 distribution ratio at the style and thus likely impaired auxin flow and distribution in that region (Figure 42F). Interestingly, PIN1-GFP level and patterning was not modified in the shoot apical meristem upon loss-of HEC function (Figure 43). Furthermore, PIN1 expression did not respond to HEC1 induction in our inflorescence RNA-seq dataset (Figure 41). Collectively, these results indicated that HEC function directly regulates PIN1 levels specifically in the gynoecium.

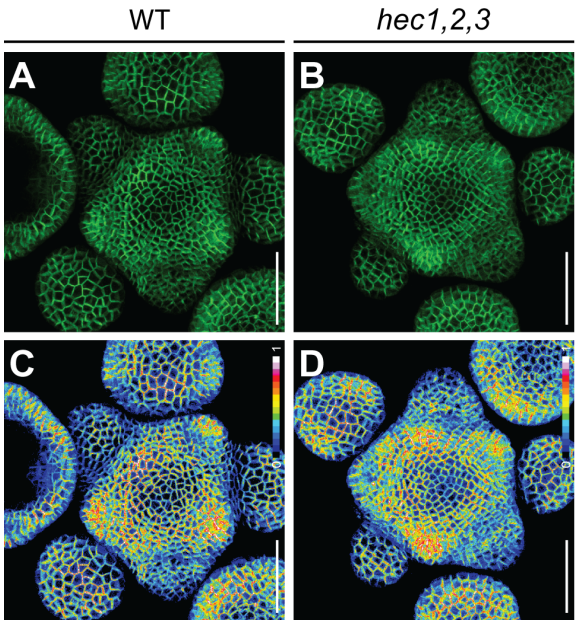

Figure 43: HEC genes are not required for PIN1 expression in the shoot apical meristem.
(A-D) Representative views of wild type (A, C) and *hec1,2,3* (B, D) expressing *pPIN1:PIN1-GFP*. PIN1-GFP is depicted in green (A, B) or using intensity-based representation (C, D). Scale bar: 50 μm

To test whether the changes in PIN cellular distribution could influence auxin distribution and in turn the patterns of auxin response, we monitored the auxin signalling reporter *pDR5:3xYFP-NLS* at the style region. At stage 8-9 in wild type, four auxin maxima marked the two lateral and medial part of the style (Figure 44A), and upon development, these foci progressively radialized, giving rise to a circular signal at stage 10 (Figure 44C,E). In contrast to wild type, auxin signalling foci did not radialize in *hec1,2,3*. Given the role of auxin responses in instructing the switch from a bilateral to a radialized structure during style differentiation (Moubayidin and

Østergaard, 2014), these results suggested that the impaired auxin responses in *hec1,2,3* later gave rise to the defects in style fusion observed at stage 13 (Figure 44B,D,F).

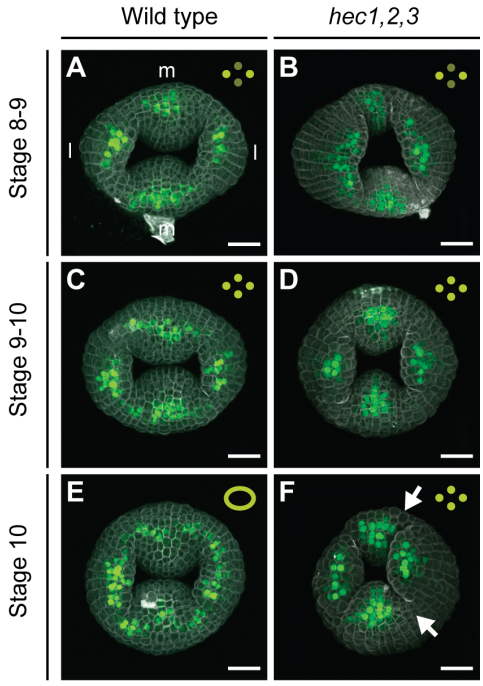

Figure 44: HEC function controls the radialisation of auxin responses at the style
(A-F) Auxin response (*pDR5:3xYFP-NLS*) in wild-type (A, C, E) and *hec1,2,3* (B, D, F) style at stage 8-9 (A-B), stage 9-10 (C-D) and stage 10 (E-F). Scale bar: 20μm

IV.2.3 HEC function buffers phytohormonal balance in the gynoecium

Our analysis of the shoot apical meristem demonstrated that HEC factors played a crucial role in balancing auxin and cytokinin signalling. We next asked whether HEC and SPT could also control cytokinin responses at the gynoecium. To test this, we used a pharmacological approach and treated gynoecia with 50μM BA for 3 weeks (Figure 45). Although our control did not show any defects after the treatment, *hec1,2,3* and *spt* mutant plants displayed gynoecia with enhanced defects in style fusion, caused by an overproliferation of apical tissues. These results demonstrated that similarly to the SAM, HEC function buffers cytokinin signals at the gynoecium. Thus, HEC function also controls the hormonal balance between auxin and cytokinin at the gynoecium.

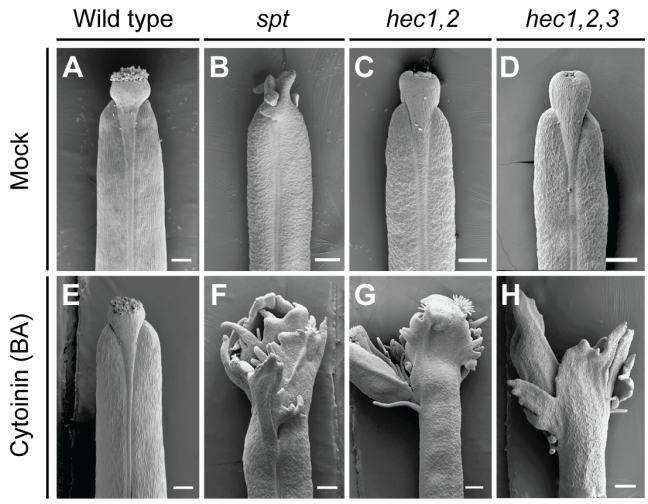

Figure 45: HEC and SPT buffer cytokinin responses at the style
(A-H) Scanning electron microscopy of wild type (A, E), *spt* (B, F), *hec1,2* (C, G) and *hec1,2,3* (D, H) gynoecium at stage 17b after mock (A-D) or cytokinin (E-H) treatment. Scale bar: 200μm. Electron microscopy was performed by Dr. Christoph Schuster; figure modified from (Schuster et al., 2015)

IV.2.4 Theoretical model for HEC function at the gynoecium

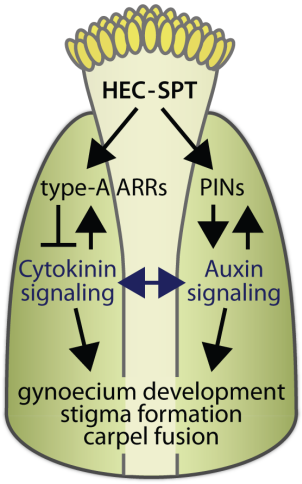

Figure 46: Theoretical model of HEC function during gynoecium patterning
(Figure designed by Dr. Christoph Schuster and modified from Schuster et al., 2015)

Our study of HEC function in the gynoecium revealed that the specification and the differentiation of the style and stigmatic structure integrate transcriptional and hormonal signals (Figure 46). During this process, HEC-SPT protein complex controls the distribution of PIN proteins, which in turn shape auxin distribution and the pattern of responses. In turn, auxin-signalling dynamics instructs style patterning and lead to its differentiation, including the formation of stigmatic papillae. In addition, HEC and SPT buffer cytokinin responses by restricting cell proliferation at the style region.

IV.3 A systems analysis of HEC regulatory networks

IV.3.1 Identification of putative HEC1 regulatory modules

The functional characterization of *HEC* genes in the SAM and in the gynoecium revealed that these factors control cell fate transition and organ patterning by modulating phytohormone signalling. More specifically, HEC factors coordinate shoot stem cell lineage progression by locally regulating cytokinin and auxin responses, whereas they regulate style differentiation by controlling auxin distribution and responses and by buffering cytokinin signals. Although we have delineated core molecular interactions mediating the role of *HEC* genes in modulating auxin responses in the SAM and gynoecium, many aspects of their regulatory function still remained elusive. In particular, the molecular mechanisms controlling HEC1 functional specificity were still unresolved. In order to bridge this gap, we first constructed a potential HEC1 regulatory network to identify relevant interactions.

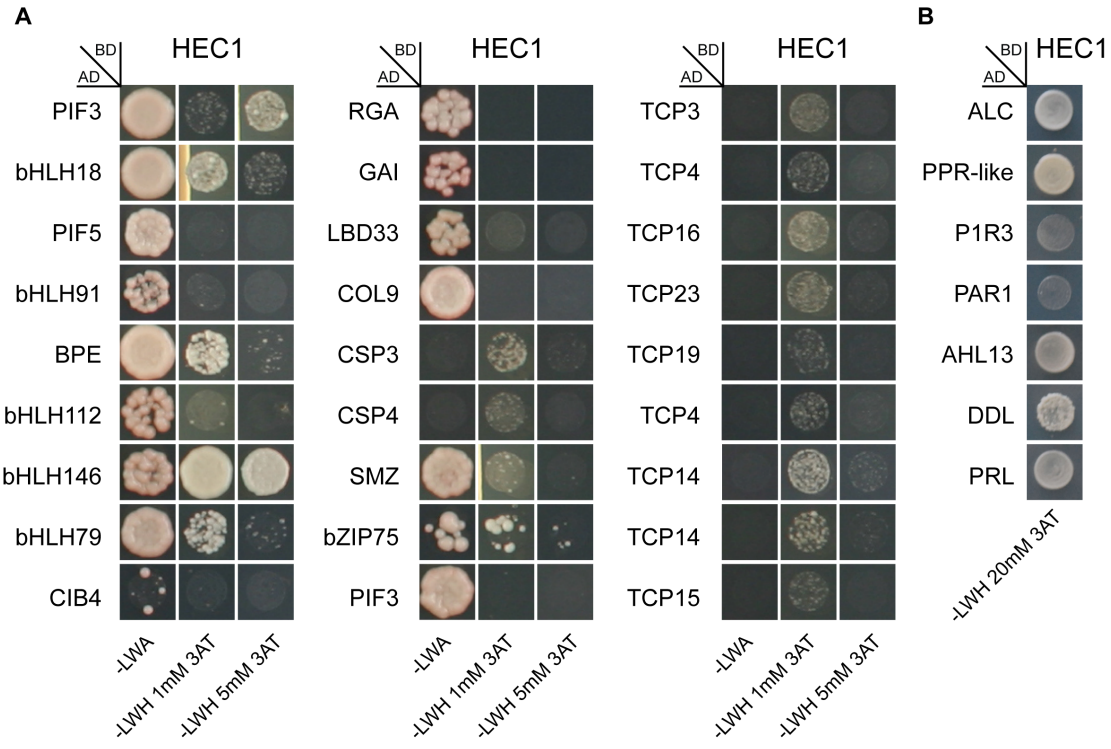

Figure 47: Identification of putative HEC1 cofactors by yeast-two-hybrid screening
(A) Positive clones obtained from Yeast-Two-Hybrid screening with the REGIA transcription factor library and replicated on 3 different selective media. **(B)** Positive clones obtained from Yeast-Two-Hybrid using a floral cDNA library and grown on selective medium. BD: binding domain; AD: activation domain

We hypothesized that HEC1 functional specificity could be encoded by the formation of distinct hetero-dimers depending on the developmental context. Thus, we

conducted Yeast-Two-Hybrid screenings using a floral cDNA library and a transcription factor library, and reliably identified 31 putative cofactors (Figure 47; Appendix: Supplementary table 2)(Castrillo et al., 2011). In line with HEC factors carrying a basic helix-loop-helix (bHLH) domain that act as an interface to mediate homo- and hetero-dimerizations (Toledo-Ortiz et al., 2003), 12 out of 31 putative cofactors were bHLH transcription factors, confirming the quality of our experimental approach. Interestingly, these factors belonged to a large spectrum of bHLH subfamilies (Appendix: Supplementary table 2)(Toledo-Ortiz et al., 2003), which suggested that HEC1 could participate in a wide range of protein complexes (Figure 47).

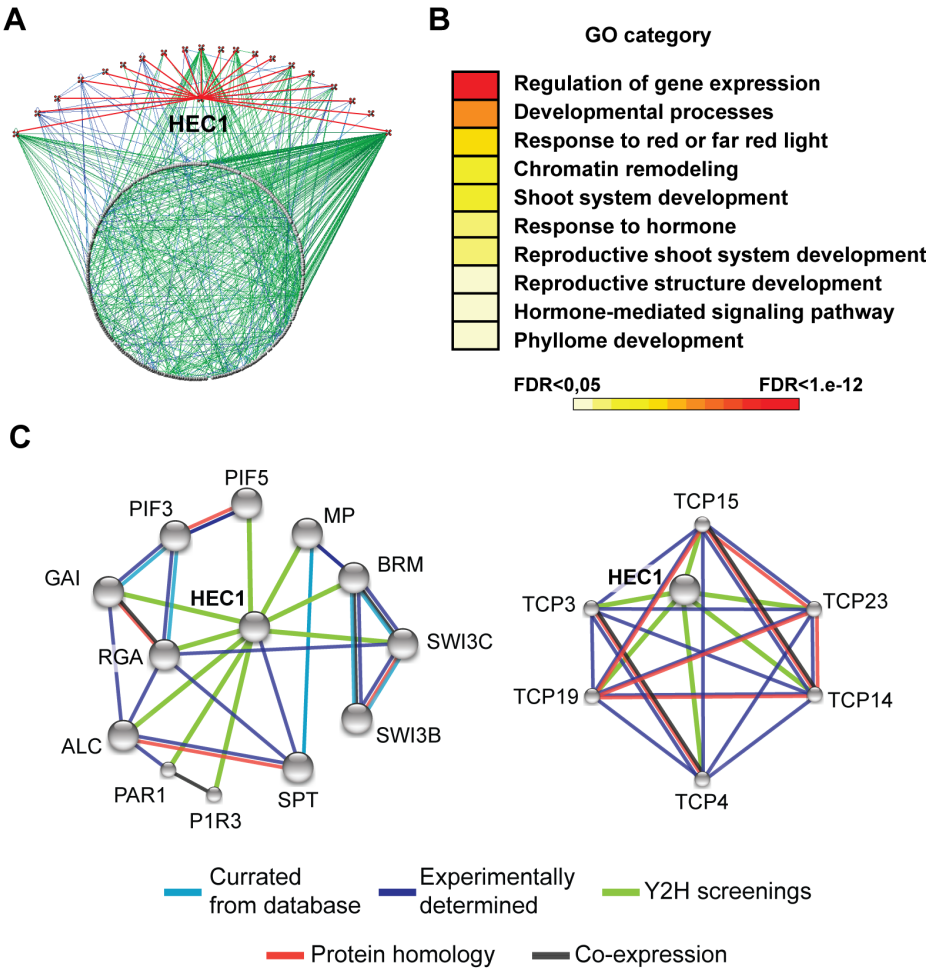

Figure 48: HEC1 participates in a highly connective protein-protein interaction network **(A)** Second level HEC1 protein-protein interaction network. 20 out of 37 HEC1 cofactors identified by Yeast-Two-Hybrid screenings clustered to form the network (Arabidopsis Interactome Mapping Consortium, 2011). **(B)** Over-represented gene ontology (GO) categories among HEC1 cofactors (FDR < 0,05). **(C)** First level HEC1 protein-protein interaction network reconstruction. Statistical test: Benjamini-Hochberg procedure (B), STRING tool: Szklarczyk et al., 2015

Next, we used the *Arabidopsis* interactome platform and publicly available datasets to reconstruct HEC1 second level protein-protein interaction network (Arabidopsis Interactome Mapping Consortium, 2011). Interestingly, we found that 20 of HEC1 cofactors were organized in a highly connective web, by sharing common cofactors (Figure 48A; Appendix: Supplementary table 2). To further identify functional regulatory modules we reconstructed protein association networks using the STRING tool (Szklarczyk et al., 2015). In line with previous characterization of HEC function, three of the most enriched Gene Ontology (GO) categories in the cofactors list were: regulation of gene expression (FDR = 7.2e-27); developmental process (FDR= 4.1e-08) and response to red and far red light (FDR= 4.4e-06)(Figure 48B)(Gremski et al., 2007; Schuster et al., 2014; Zhu et al., 2016). From the network reconstruction, we could cluster HEC1 cofactors in two main groups (Figure 48C). The first cluster included light signalling components: PHYTOCHROME INTERACTING FACTOR 3 (PIF3), PIF5, GIBBERELLIC ACID INSENSITIVE (GAI), REPRESSOR OF GA (RGA), PHY RAPIDLY REGULATED 1 (PAR1) (de Lucas et al., 2008; Feng et al., 2008; Pfeiffer et al., 2014; Zhou et al., 2014); key regulators of gynoecium development: SPT, ALCATRAZ (ALC), GAI, RGA (Arnaud et al., 2010; Fuentes et al., 2012; Heisler et al., 2001; Rajani and Sundaresan, 2001); chromatin remodeling factors: BRM, SWITCH SUBUNIT 3 (SWI3B), SWI3C (Vercruyssen et al., 2014); and hormonal signalling components: MP, RGA and GAI (Arnaud et al., 2010; Hardtke and Berleth, 1998). In contrast the second cluster included exclusively TEOSINTE BRANCHED, CYCLOIDEA AND PCF (TCP) transcription factors: TCP3, TCP4, TCP14, TCP15, TCP19 and TCP23, which were shown to play divergent function during development (Davière et al., 2014; Kubota et al., 2017; Lucero et al., 2015) (Table 1).

The functional diversity of potential cofactors and the high connectivity of the reconstructed clusters suggested that HEC1 could associate in multiple protein complexes carrying distinct functions during development. Mechanistically, this also suggested that the physical interaction with distinct transcription factors could determine DNA-binding affinity of the complex, and in turn could specify the spectrum of its target genes. To further investigate this idea, we analysed the DNA motifs enriched under HEC1 binding regions, which characterize the DNA binding signature of several transcription factor families (Figure 49A)(Bailey et al., 2009). In line with our protein-protein interaction data, two of the most enriched motifs were the TCP-binding motifs (E-value < 7.3 e-160) and G-boxes that are typically bound by TCP

and bHLH transcription factors (E-value<1.4e-141) respectively (Figure 49A)(Lau et al., 2014; Pfeiffer et al., 2014). Furthermore, we also found enrichment for the motif bound by SCHLAFMUTZE (SMZ) (E-value = 1.4e-05), which we previously identified as a putative HEC1 cofactor in the yeast-two-hybrid assay (Figure 49A; Appendix: Supplemental table 2). Together, these data showed that the reconstructed HEC1 protein-protein interaction networks correlated well with the patterns of HEC1 association to DNA and thereby suggested that its interaction with specific transcription factors could instruct the recruitment of the protein complex to distinct genomic sites and mediate HEC1 regulatory specificity.

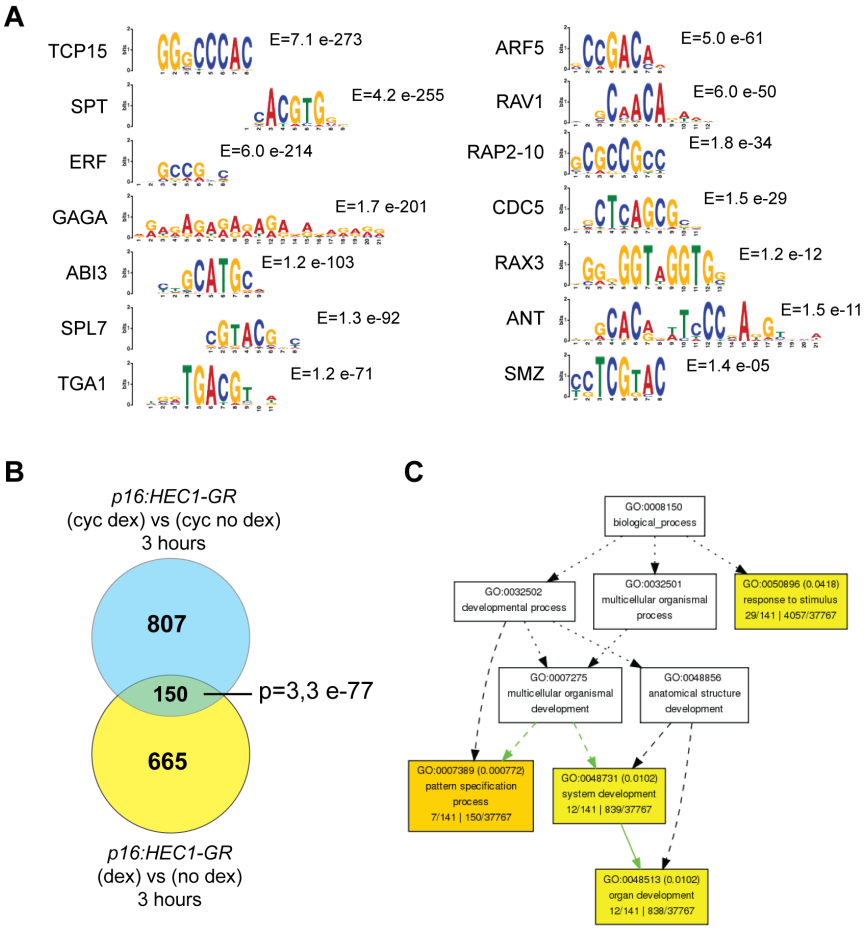

Figure 49: HEC1 regulatory signatures
(A) Enriched DNA-binding motifs associated with HEC1 binding regions obtained from MEME-ChiP (Bailey et al., 2009) **(B)** High confidence HEC1-early response genes as shown by overlap between *p16:HEC1-linker-GR* RNA-seq experiments 3 hours after dexamethasone (dex) treatment supplemented or not with cycloheximide (cyc). **(C)** Enriched GO categories among high confidence HEC1-early response genes (FDR < 0,05)

To further build a HEC1 regulatory network, we analyzed early HEC1-response genes in the inflorescence meristem obtained after HEC1 induction, and

supplemented or not with the translational inhibitor cycloheximide (cyc). By overlapping these two datasets, we identified 150 high confidence HEC1 response genes and defined their functional signatures by conducting a gene ontology (GO) analysis (Figure 49B-C)

Interestingly, only three distinct categories were significantly enriched: pattern specification process ($p < 2.3e-06$), organ development ($p < 8.6e-05$) and response to stimulus ($p < 5.0e-04$)(Figure 49C), including genes controlling: cell cycle (*SIAMESE*) (Kasili et al., 2010); auxin transport (*PIN3*, *PIN4* and *PIN7*) (Friml et al., 2002b; Friml et al., 2002a; Friml et al., 2003) ; gynoecium development (*CRABS CLAW*, *NGATHA1* (*NGA1*), *STYLISH2* (*STY2*))(Alvarez and Smyth, 1999; Kuusk et al., 2002; Trigueros et al., 2009); flower development (*WUSCHEL RELATED HOMEOBOX 3* (WOX3)(Vandenbussche et al., 2009), *EXCESS MICROSPOROCYTES1* (*EMS1*))(Feng and Dickinson, 2010); shoot development (*ERECTA-LIKE2*) (Uchida et al., 2013) and light signalling (*PHYTOCHROME A*, *PIF5*, *PHOTOTROPIN1*)(Khanna et al., 2004; Liscum and Briggs, 1995; Smith, 2000). These regulatory functions were consistent with the previously described roles of *HEC* genes, suggesting that our transcriptional profiles faithfully captured HEC regulatory functions (Schuster et al., 2014; Schuster et al., 2015; Zhu et al., 2016).

	Gene	Type of interaction	Reference
Light signalling	PIF3	Cofactor	(Ni et al., 1998)
	PIF5	Cofactor/ Target gene (-)	(Khanna et al., 2004)
	GAI	Cofactor	(Feng et al., 2008)
	RGA	Cofactor	(Feng et al., 2008)
	PAR1	Cofactor	(Roig-Villanova et al., 2007)
	PHYA	Target gene (+)	(Smith, 2000)
	PHOT1	Target gene (+)	(Liscum and Briggs, 1995)
Gynoecium development	SPT	Cofactor	(Heisler et al., 2001)
	ALC	Cofactor	(Rajani and Sundaresan, 2001)
	RGA	Cofactor	(Arnaud et al., 2010)
	GAI	Cofactor	(Arnaud et al., 2010)
	TCP15	Cofactor	
	PIF5	Cofactor/ Target gene (-)	(Reymond et al., 2012)
	PIN3	Cofactor	(Friml et al., 2002b)
	NGA1	Target gene (+)	(Trigueros et al., 2009)
	STY2	Target gene (+)	(Kuusk et al., 2002)
	CRC	Target gene (-)	(Bowman and Smyth, 1999)
Auxin signalling	MP	Cofactor	(Wu et al., 2015)
	BRM	Cofactor	(Wu et al., 2015)
	PIN3	Target gene (+)	(Friml et al., 2002b)
	PIN4	Target gene (+)	(Friml et al., 2002a)
	PIN7	Target gene (+)	(Friml et al., 2003)
HEC-TCP	TCP3	Cofactor	(Kubota et al., 2017)
	TCP4	Cofactor	(Kubota et al., 2017)
	TCP14	Cofactor	(Davière et al., 2014)
	TCP15	Cofactor	(Davière et al., 2014)
	TCP19	Cofactor	
	TCP23	Cofactor	

Table 1: Identification of HEC1 regulatory modules
Reconstructing HEC1 regulatory network allowed us to define four modules interacting with HEC function: light signalling, gynoecium development, auxin signalling and the TCP module of uncharacterized function. Furthermore, each module comprises cofactors and target genes that interact with HEC1. (+) : positively regulated genes; (-) : negatively regulated genes.

IV.3.2 Functional characterization of candidate genes

IV.3.2.1 miRNA-induced gene silencing (MIGS) approach

Having built a putative HEC1 regulatory network, we used this information as a springboard to investigate the regulatory function of key candidate genes.

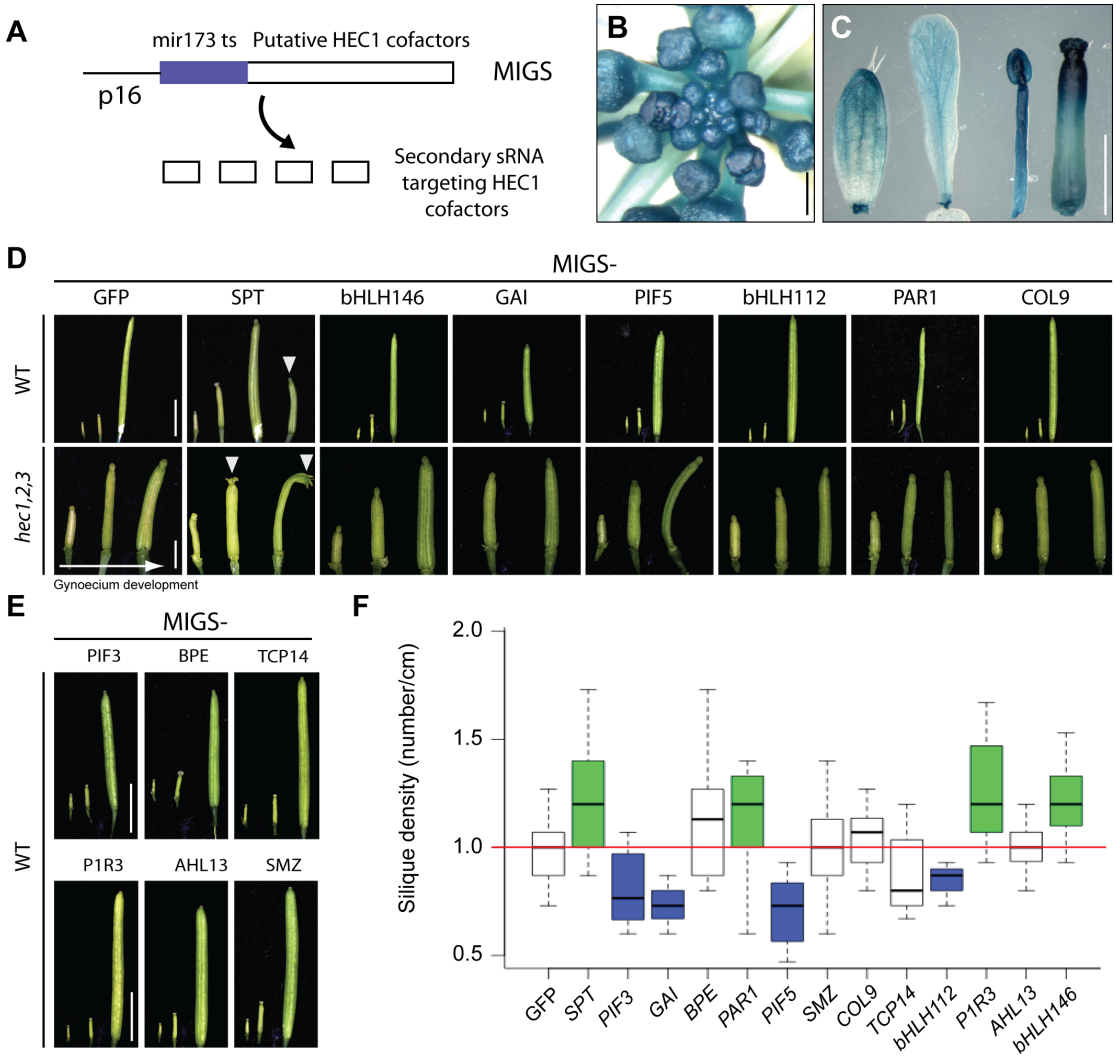

Figure 50: Functional characterization of putative HEC1 cofactors by MIGS
(A) Schematic of the MIGS approach. **(B-C)** GUS staining showing *p16:GUS* expression in inflorescence (B) and in individual flower organs (C). **(D-E)** Wild type and *hec1,2,3* stage 12, 15 and 17 gynoecium expressing MIGS constructs targeting HEC1 cofactors. **(F)** Silique density quantification in wild type inflorescences expressing MIGS constructs targeting HEC1 cofactors. Blue and green depicts significant changes (n>6) (Student t-test; p<0.05). MIGS data acquisition was performed by Lanxin Li under supervision. Scale bar: 1mm (B-C); 2mm (D: *hec1,2,3*); 5mm (D: WT, E)

First, we down-regulated the expression of multiple putative cofactors using the miRNA-induced gene silencing (MIGS) strategy (Felippes et al., 2012). The addition of the mir173 target sequence to the 5´of the transcript leads to the production of TAS transcripts that are recognized by miR173, triggering the synthesis of dsRNA by the RNA-dependent polymerases. The dsRNA is subsequently processed by DICER-LIKE proteins and produce 21 nucleotide tasiRNAs that trigger gene silencing (Felippes et al., 2012). We adapted this strategy to our tissues of interest by driving the mir173 target sequence followed by the coding sequence of putative cofactors under the p16 promoter (Figure 50A). Using *p16:GUS* staining, the activity of the p16 promoter was detected in all dividing tissues of the SAM or flower (Figure 50B, C). To test the functionality of our system, we down-regulated SPT in the *hec1,2,3* mutant background and in line with our previous genetic analysis, we observed strong defects in style fusion compared to control plants, indicating that our MIGS strategy was successful (Figure 50D). We next down-regulated putative HEC1 cofactors in the wild type or in the *hec1,2,3* background and analysed shoot and gynoecium development (Figure 50D-F). Although gynoecium development was not impaired in MIGS lines (Figure 50D, E), we observed significant deviations in the shoot architecture compared to control plants, suggesting that SAM activity was modified in those plants (Figure 50F). In particular, targeting SPT, PAR1, P1R3 and bHLH146 increased silique density, whereas targeting PIF3, GAI, PIF5 and bHLH112 decreased it (Figure 50F). Together these data suggested that HEC1 might functionally interact with multiple cofactors during shoot meristem activity.

IV.3.2.2 Functional characterization of putative HEC1 cofactors

After having conducted an untargeted approach to functionally characterize HEC1 cofactors, we specifically focused our attention on genes belonging to the reconstructed regulatory modules (Table 1) and used published studies to establish a list of promising candidate genes.

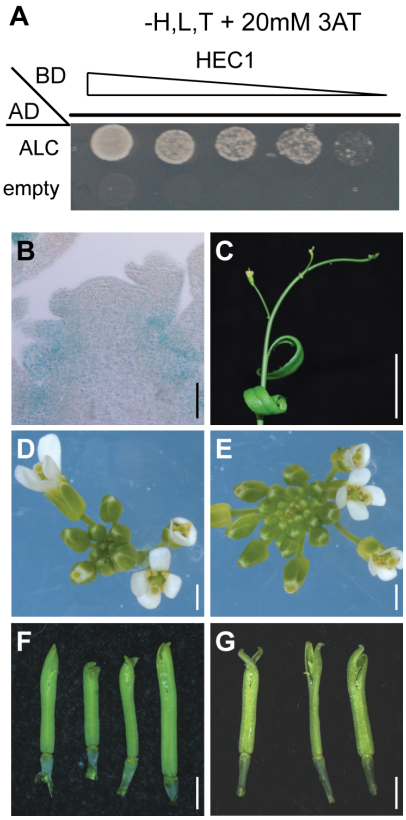

Figure 51: Functional characterization of ALCATRAZ-HEC1 interaction in the SAM and in the gynoecium
(A) Yeast-two-hybrid assay testing the interaction between HEC1 and ALCATRAZ. Clones were plated on selective medium using gradual dilution. **(B)** GUS staining showing *pALC:ALC-GUS* expression in a SAM transversal cross-section. **(C-E)** *alcatraz* inforescence expressing *p35S:HEC1* (C), *pCLV3:GFP-NLS* (D), *pCLV3:HEC1-linker-GFP* (E). **(F-G)** Gynoecium at stage 17b in *hec,1,2,3,spt* (F) and *hec2,3,spt,alc,p16:ts173_HEC1* (G). Scale bar: 50μm (B); 1mm (D-G); 1cm (C)

Given that SPT and ALC were previously shown to genetically and physically interact during style development (Arnaud et al., 2010; Groszmann et al., 2011) and that ALC was over-represented among the positive clones obtained from the floral Y2H screening, we hypothesised that HEC1 and SPT could form a functional protein complex with ALC. First we confirmed the physical interaction between HEC1 and ALC using small scale Y2H assay (Figure 51A). We then detected ALC expression at the SAM using plants expressing *pALC:ALC-GUS*. Unlike in the gynoecium, ALC expression pattern differed from HEC and SPT in the SAM and was mostly detected at the basal part of the flower petioles (Figure 51B)(Groszmann et al., 2011). To test whether ALC was required for HEC function in the SAM or flowers, we next expressed *pCLV3:HEC1* or *p35S:HEC1* in the *alc* mutant background (Figure 51C-E). In contrast to the suppression of HEC1-driven SAM phenotype in *spt*, the formation of enlarged SAM and pin-like inflorescences were not suppressed in the *alc* mutant background, demonstrating that ALC was not required for HEC function in the SAM (Figure 51C-E). Given that gynoecia in *hec1,2,3,spt* and *spt,alc* mutants were unable to fuse, giving rise to open style, we next tested whether HEC, SPT and ALC might functionally interact during this process. Interestingly, we observed slightly

enhanced defects in style fusion in *hec2,3,spt,alc,p16:ts173_HEC1* compared to *hec1,2,3,spt*, suggesting that the formation of a protein complex between HEC-SPT and ALC might control style development (Figure 51F,G).

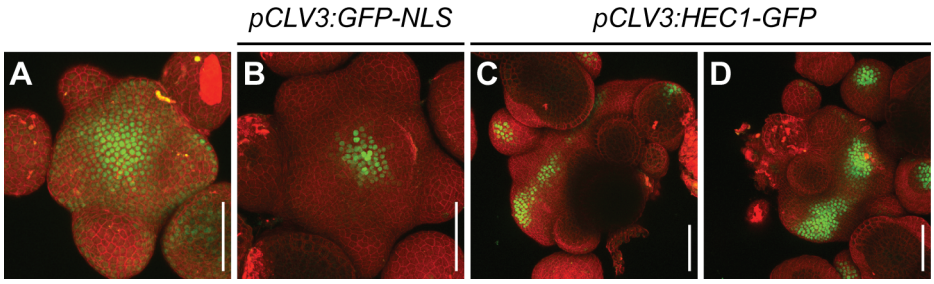

Figure 52: RGA and GAI are not required for HEC function in the SAM
(A) Wild type meristem expressing *pRGA:GFP-RGA*. **(B-D)** Wild type (B, C) and *rga,gai* (D) meristems expressing *pCLV3:GFP-NLS* (B) and *pCLV3:HEC1-linker-GFP* (C-D). Scale bar: 50 μm

In addition to ALC, we identified two DELLA proteins RGA and GAI physically interacting with HEC1 (Table 1). Importantly, these factors are key negative regulators of gibberellic acid signalling and were also previously shown to physically and genetically interact with SPT and ALC during gynoecium development (Arnaud et al., 2010). Thus, we investigated the role of DELLA proteins by testing whether their function was required for HEC activity in the SAM (Figure 52). Although RGA-GFP was expressed in the CZ, expressing *pCLV3:HEC1* in the *rga*, *gai* double mutant did not suppress SAM and CZ expansion, indicating that RGA and GAI were not required for HEC function in the CZ (Figure 52A-D). Therefore, we hypothesised that HEC and GA signalling might rather interact during fruit development and tested this idea by treating wild type and *hec1,2,3* gynoecia with gibberellic acid (Figure 53A, B). Although wild type silique size did not significantly change after treatment, we observed a significant increase in *hec1,2,3* silique size upon GA treatment, demonstrating that the hormonal treatment could partially rescue *hec1,2,3* growth defects. Given that GA degrades DELLA proteins, these results suggest that HECs may interact and mitigate DELLAs activity during gynoecium development.

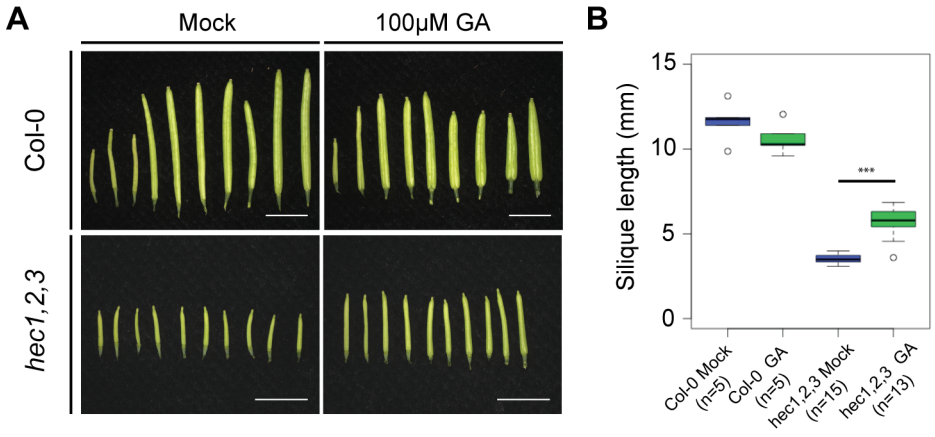

Figure 53: GA treatment partially rescues the reduced silique length in *hec1,2,3*
(A-B) Wild type and *hec1,2,3* stage 17b gynoecium treated with gibberellic acid. Representative pictures (A). Silique length quantification (B). Statistical test: Student-t-test; ***p<0.001. Scale bar: 5 mm (A)

IV.3.2.3 Functional characterization of putative HEC1 target genes

IV.3.2.3.1 NGATHA1 and NGATHA2 are relevant HEC1 targets in the SAM

To further investigate the regulatory function of genes belonging to the gynoecium regulatory modules, we next focused our attention on *NGA* genes that we identified as high confidence HEC1-response genes (Table 1).

NGATHA genes were previously shown to control style development, similar to HEC and SPT function and showed co-expression during gynoecium development (Trigueros et al., 2009). Therefore, we decided to test whether NGATHAs might also functionally interact with *HEC* genes to regulate SAM activity.

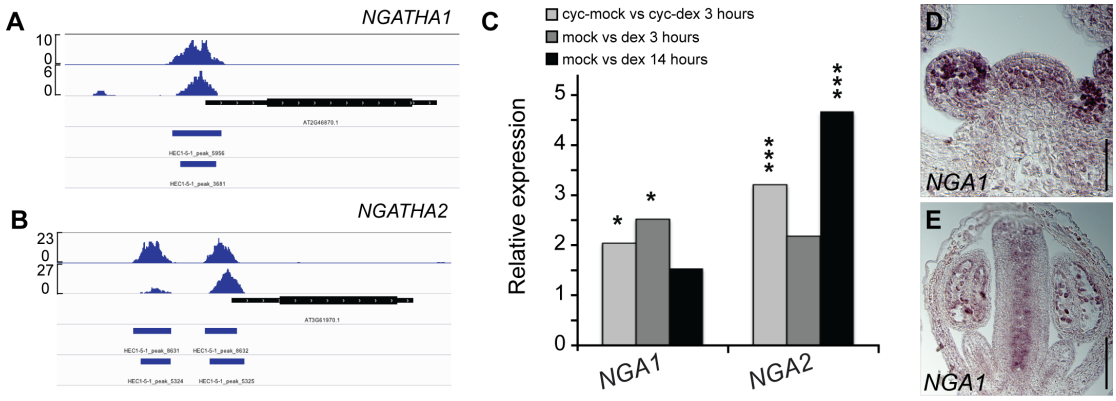

Figure 54: *NGA1* and *NGA2* are HEC1 direct target genes
(A-B) HEC1 DNA binding pattern at *NGA1* (A) and *NGA2* (B) loci as shown by ChIP-seq. **(C)** *NGA1* and *NGA2* relative mRNA expression after *p16:HEC1-linker-GR* induction as measured by RNA-seq. **(D-E)** *NGATHA1* expression as shown by in situ hybridization in the shoot meristem (D) or in gynoecium at stage 11-12 (E). Statistical test: Fischer´s exact test (EdgeR). Scale bar: 50*µ*m

From ChIP-seq and RNA-seq datasets, *NGA1* and *NGA2* were both bound and positively regulated by HEC1 (Figure 54A-C). Accordingly, *NGA1* expression pattern overlapped with *HEC1* in the SAM and in the gynoecium, suggesting that NGA1 could act downstream of HEC1 to regulate SAM homeostasis (Figure 54D-E; (Trigueros et al., 2009). We next investigated NGATHA function on stem cell activity by driving NGA1 and NGA2 expression specifically in the CZ using *pCLV3:NGA1-linker-mCherry* and *pCLV3:NGA2-linker-mCherry* (Figure 55A-F). Interestingly, we observed that about 35% of analysed plants displayed strong SAM fasciation, together with an overaccumulation of stem cells, demonstrating that *HEC* and *NGA* genes share similar function at the CZ (Figure 5; Figure 55B, E, G). In line with this result, the lists of HEC1 and NGA3 response genes identified by RNA-seq showed a significant overlap, suggesting that their function might also converge at the transcriptional level (Figure 55H). In contrast, 5 to 10% of the plants terminated shoot stem cell activity and formed a gynoecium-like structure (Figure 55C, F, G). As we never observed this phenotype in HEC gain-of-function experiments (Schuster et al., 2014), this result suggested that NGA factors may also carry independent functions from HEC factors.

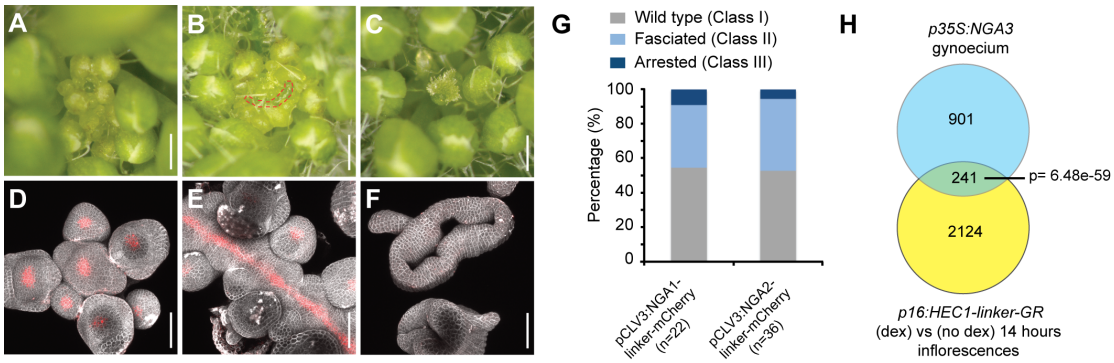

Figure 55: *NGA1* and *NGA2* and *HEC* genes share regulatory function in the SAM
(A-G) Wild type inflorescences (A-C) or shoot meristems (D-F) expressing *pCLV3:NGATHA1-linker-mCherry* and showing wild type-like (A, D), fasciated SAM (B, E) or gynoecium-like structure (C, F) phenotypes. Quantification of the phenotypic classes in T1 generation (G). **(H)** Venn diagram overlapping HEC1 and NGA3-response genes. Statistical test: hypergeometric test (H). Scale bars: 50*µ*m (D-F); 500*µ*m (A-C)

To test whether NGA and HEC also shared regulatory potential at the SAM periphery, we expressed *pCUC2:NGA1-linker-mCherry* (Figure 56). In contrast to HEC activity in this region, which delayed the fate transition from PZ to flower primordia (Figure 12), NGATHA factors did not interfere with this process. This demonstrated that HEC and NGA function diverged at the SAM periphery (Figure

56). Taken together, these data showed that NGA1 and NGA2 were relevant HEC1 direct target genes that could phenocopy HEC function specifically in the shoot stem cells.

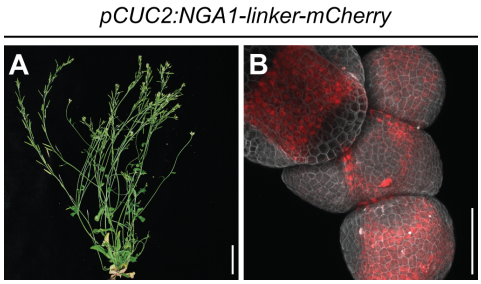

Figure 56: NGATHA and HEC functions diverge at the SAM periphery
(A-B) Wild-type inflorescence and shoot meristem expressing *pCUC2:NGA1-linker-mCherry*. Scale bar: 50*µ*m (B); 5cm (A)

IV.3.2.3.2 NGATHA can act independently from HEC

Having shown that *NGA* and *HEC* could share regulatory function in the stem cells, we next wanted to test whether these factors showed epistatic interactions.

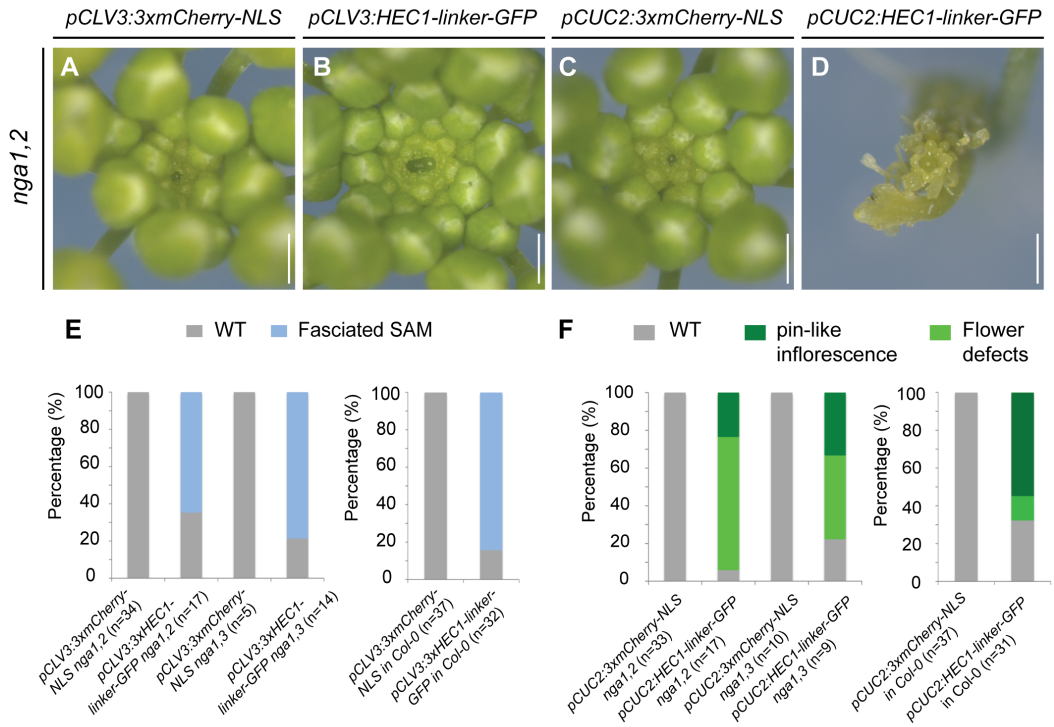

Figure 57: *NGA1* and *NGA2* do not mediate *HEC* functions in the SAM
(A-D) Phenotypic analysis of *nga1,2* inflorescences expressing *pCLV3:3xmCherry-NLS* (A), *pCLV3:HEC1-linker-GFP* (B), *pCUC2:3xmCherry-NLS* (C) or *pCUC2:HEC1-linker-GFP* (D) in T1 generation. **(E)** Phenotypic quantification of wild type, *nga1,2* and *nga1,3* inflorescences upon NGA or HEC gain-of-function in the CZ. **(F)** Phenotypic quantification of wild type, *nga1,2* and *nga1,3* inflorescences upon NGA or HEC gain-of-function in the PZ-BZ. Scale bar: 500*µ*m

To test this, we increased HEC1 levels specifically at the CZ and at the PZ/BZ by expressing *pCLV3:HEC1-linker-GFP* and *pCUC2:HEC1-linker-GFP* in *nga1,2* mutant background respectively. Interestingly, loss of *NGA1* and *NGA2* function did not interfere with HEC1 function neither at the CZ nor at the sites of primordia initiation, indicating that NGA1 and NGA2 were not required for HEC function at the SAM (Figure 57). To exclude that NGA could act upstream of HEC function or that HEC and NGA could act as protein complex, we conducted the reverse gain-of-function experiment by expressing *pCLV3:NGA1-linker-mCherry* in a HEC loss-of-function background (Figure 58A-B). Similarly, *HEC* genes were not required for NGA function within the stem cell region, indicating that HEC and NGA could act independently on stem cell activity (Figure 58A-B). Furthermore, combining HEC and NGA gain-of-function within the stem cells, did not lead to synergistic effects on stem cell activity as we observed with SPT, suggesting that HEC and NGA did not co-regulate SAM activity (Figure 58C). Together, these data demonstrated that although NGA were directly positively regulated by HEC1 and shared similar function in the CZ, they were not epistatic and could act independently from HEC function in the SAM.

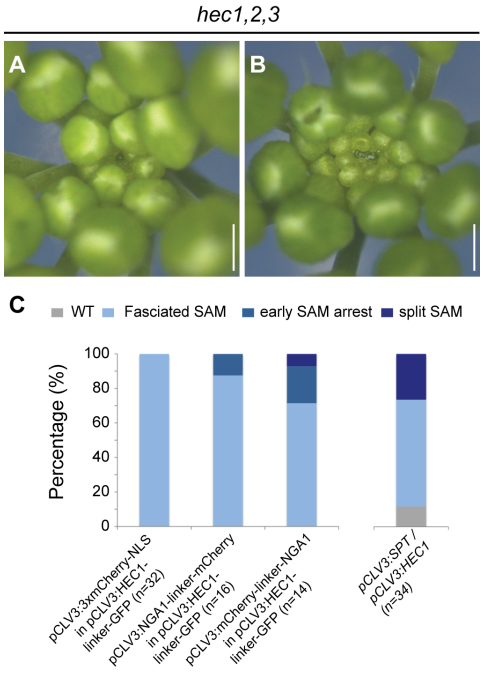

Figure 58: NGATHA and HEC can act independently
(A-B) *hec1,2,3* inflorescences expressing *pCLV3:mCherry-NLS* (A) or *pCLV3:NGA-linker-mCherry* (B). **(C)** Phenotypic quantification of *pCLV3:HEC1-linker-GFP* shoot meristems upon NGA gain-of-function in the CZ. Scale bar: 500 *µ*m

Given the contrasting phenotypes observed in *NGA* gain-of-function and their independent activity from HEC1 in the CZ, we next wanted to investigate whether these factors were required for SAM activity. We analyzed the meristem size of NGA loss-of-function mutant plants, from single to triple mutants (*nga1*; *nga1,2*; *nga1,3*

and *nga1,3,4*) (Figure 59A-C)(Trigueros et al., 2009). Surprisingly, we observed that all *nga* mutant displayed significantly larger SAM than wild type (Figure 59A-C) (Schuster et al., 2014). In contrast, *hec1,2,3* showed smaller shoot meristem, indicating that HEC and NGA might carry independent function in regulating SAM homeostasis. To confirm this observation, we next analysed cytokinin signalling in *nga1,3* and found that in contrast to *hec1,2,3*, *nga1,3* displayed a significantly larger cytokinin signalling domain, correlating with a larger SAM (Figure 18A-C, 59D-F).

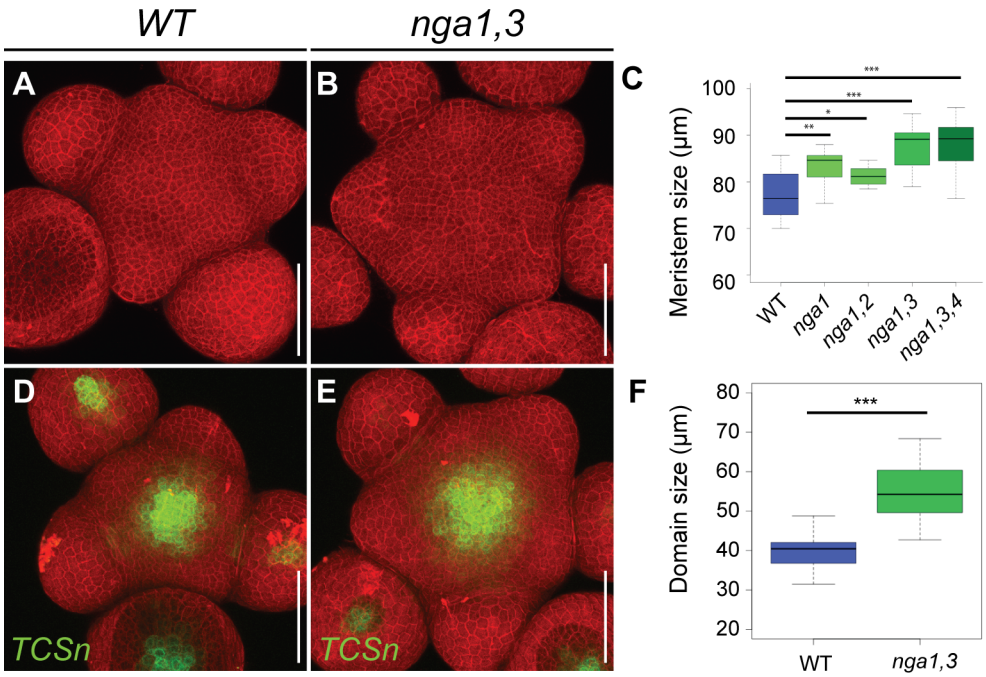

Figure 59: *NGA* genes antagonize cytokinin signalling at the SAM
(A-B) Wild type (A) and *nga1,3* (B) shoot meristems. **(C)** Quantification of the shoot meristem size in wild type and NGA loss-of-function plants. **(D-E)** Cytokinin response (*pTCSn:erGFP*) in wild type (D) and *nga1,3* (E) meristems **(F)** Quantification of cytokinin signalling domain size in wild type and *nga1,3* meristems. Scale bar: 50µm

Together these data revealed that NGA function was required and sufficient to modulate stem cell activity within the SAM and mostly acted independently from HEC genes. The convergence of HEC and NGA function to common regulatory nodes and similar target genes suggests that HEC and NGA factors are interacting to regulate similar processes in the shoot stem cells (Figure 60).

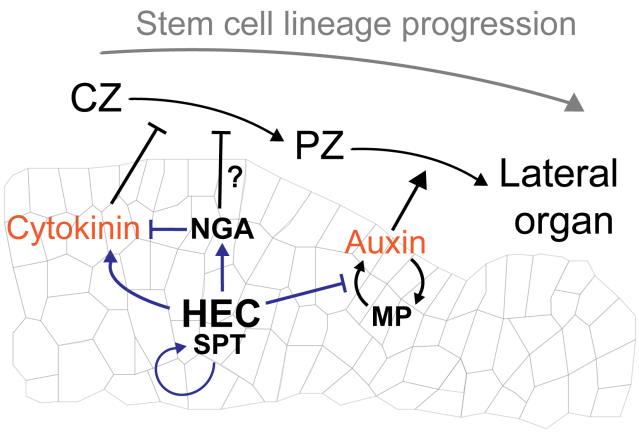

Figure 60: Theoretical model depicting HEC-NGA regulatory function at the SAM

V. Discussion

V.1 *HECATE* genes control plant cell fate transitions at the SAM

The successive cell fate decisions taking place at the shoot apical meristem are essential to shape the plant body plan. Although the concept of stem cell lineage progression has received a lot of attention in animal stem cells or in the plant stomatal lineage (Kumar et al., 2017; Simmons and Bergmann, 2016), our understanding of this process at the shoot apical meristem remained largely unexplored.

In this study, we used a multi-disciplinary approach combining reiterative experimental analysis with a computational approach and found that HEC function locally gates cellular fate transitions in distinct domains of the shoot meristem and thus modulates the timing of stem cell differentiation. Further, our present experimental strategy to analyse the SAM dynamics after domain-specific modulation of HEC activity underlines the importance to complement end-point genetic studies with high spatio-temporal analysis of gene function.

Our previous study using constitutive HEC-gain of function mutants suggested that HEC factors controlled cell proliferation independently of the WUS/CLV3 feedback circuitry. In contrast, we now reveal that these factors do not locally promote cell divisions but rather regulate this process non-cell autonomously. Additionally, we show that the expansion of the CZ and the shoot meristem are concomitant with an enhanced *WUS* domain activity and increased cytokinin responses. In contrast to our previous hypothesis, our study now supports that HEC1-driven SAM enlargement is mediated by an enhanced WUS and cytokinin signalling activity. The enhanced cytokinin responses and increase in the PZ cell proliferation also suggest that cells from the PZ respond to a cytokinin signal produced at the centre of the SAM, constituting a cell-to-cell communication system to adjust their mitotic behaviour.

In line with our previous study (Schuster et al., 2014), we observed a decrease in *WUS* expression at late time points after HEC induction, which was contrary to what we observed at early time points. Thus, we could now distinguish between early and late regulatory functions of *HEC* genes. The late repression of the core regulatory network arises likely as a result of a negative feedback mechanism. We have previously shown that HEC function positively regulates type-A ARRs expression, which in turn repress cytokinin signalling (Schuster et al., 2014). We hypothesise that the late increase in type-A ARRs levels could constitute this negative feedback loop, repressing cytokinin responses and *WUS* expression.

Although computational models in the SAM have been used to investigate auxin transport (de Reuille et al., 2006; Jönsson et al., 2006; Smith et al., 2006), cell division (Louveaux et al., 2016; Willis et al., 2016) or mechanical stresses (Bhatia et al., 2016; Hamant et al., 2008; Kierzkowski et al., 2012), few models have addressed the dynamics of stem cell differentiation (Mähönen et al., 2014).

Using a simplified 2D representation of the shoot meristem and by defining the model parameters from experimental measurements, we now bridge this gap and developed a model to investigate the dynamics of stem cell differentiation in the SAM. We used this model to simulate hypothetical regulatory scenarios driving HEC function and could quantitatively capture the dynamics of cell fate transitions and organ formation to deduct which regulatory scenarios would fit our *in vivo* observations. Furthermore, we could also assess quantitatively growth parameters that could not be measured experimentally. For example, this approach allowed us to compute that *hec1,2,3* display faster primordia initiation rate compared to wild type, together with a reduction in the time separating primordia initiation and separation. Taken together, the reiterative analysis of quantitative live cell imaging and computational model simulations allowed us to build a quantitative framework for the dynamics of stem cell differentiation in the SAM and to further understand the role of HEC factors during this process.

In contrast to other stem cell systems, the acquisition of cellular identities along shoot stem cell differentiation in the SAM depends on positional cues that cells receive within the tissue at a given time point, rather than being determined by their lineage (Reinhardt et al., 2003b; Reinhardt et al., 2003a). This situation is different in the hematopoietic stem cell system or in the intestine crypt, where intrinsic signals restrict daughter cell fate as they differentiate (reviewed in Clevers, 2013; Enver et al., 2009; Noah et al., 2011).

During differentiation, stem cells undergo a series of molecular transitions, including changes in chromatin structure and gene expression profiles. Recent technical advances in profiling single cells within stem cell compartments has opened an exciting field to further define the concept of cell identity and cell fate decision making (Macosko et al., 2015). Using molecular snapshots of single cells, differentiation trajectories can be inferred to identify transition states between cell types (reviewed in Kumar et al., 2017). Although CZ and PZ cells are marked by the activity of different reporters and display contrasting cell behaviour, the transition between those two domains remains poorly characterized at the molecular level. It will be

interesting in the future to use single cell genomics in the shoot apical meristem to further define the molecular process underlying shoot stem cell differentiation.

V.2 HEC function coordinates hormonal signals

Auxin and cytokinin are two key phytohormones controlling cell fate acquisition and cellular behaviour in various developmental contexts (reviewed in Schaller et al., 2015). Although they play key functions in instructing the spatial patterns and modulating cellular behaviour at the SAM, our understanding of the regulatory mechanisms balancing the response of those two pathways remained elusive. Here, we analysed hormonal reporter lines together with transcriptional profiles after modulation of HEC activity and revealed that HEC function indirectly promotes cytokinin signalling at the centre of the meristem, while dampening the auxin feedback system at the site of lateral organ initiation. Our data support the idea that the spatio-temporal responses to cytokinin and auxin shape the functional domains of the SAM and time stem cell differentiation. By adjusting this hormonal balance, we propose that HEC factors modulate the transition rate between CZ and PZ and further on to primordia, and ultimately control the dynamics of shoot stem cell lineage progression.

Similarly to the shoot meristem, the balance between auxin and cytokinin controls root stem cell differentiation. However in this context, auxin positions the stem cell niche whereas cytokinin triggers cell differentiation (Ioio et al., 2007; Ioio et al., 2008; Sabatini et al., 1999). Interestingly, ectopic HEC function in the root can shift the hormonal balance by promoting cytokinin while repressing auxin responses, leading to a faster root cell differentiation. These results demonstrate the potential of HEC factors to coordinate auxin and cytokinin responses in various developmental contexts.

Mechanistically, we showed that HEC factors dampen the auxin feedback system and physically interact with MP. During the initiation of flower primordia, auxin maxima are dynamically built by the coordination of auxin production, transport and signalling (reviewed in Weijers and Wagner, 2016). Auxin accumulation locally promotes MP expression, which in turn modulates auxin flow by redirecting PIN1 polarity towards the sites of MP accumulation (Bhatia et al., 2016). This positive feedback loop creates auxin sinks and inhibits the formation of auxin maxima in the surrounding tissues (de Reuille et al., 2006). In turn, inner tissues redirect auxin to form the vasculature and decreases the strength of the auxin sink, allowing the

establishment of new auxin maxima in other domains of the PZ (Bhatia et al., 2016; Reinhardt et al., 2003b). Importantly, flower primordia initiation is also associated with changes in chromatin accessibility as stable MP accumulation triggers epigenetic remodelling through the formation of a protein complex with the SWI-SNF ATPase BRM and SYD (Wu et al., 2015). Protein-protein interaction data together with the identical inflorescence phenotypes observed in *mp*, *brm syd*, and *pCUC2:HEC1* suggest that HEC factors, SPT, MP and BRM could physically interact and thereby form a functional protein complex at the sites of lateral organ initiation (Efroni et al., 2013; Hardtke and Berleth, 1998; Wu et al., 2015). Given the role of HEC factors in dampening auxin response dynamics, these results suggest that HEC function could modulate the pace of the auxin feedback dynamics by directly binding MP-BRM complex. Independently of their direct regulation of the MP-BRM complex activity, HEC function could locally control auxin levels or repress auxin transcriptional output. Thus, it will be crucial in the future to further dissect the regulatory mechanisms mediating HEC function on auxin homeostasis.

Although the key regulatory control of phyllotaxis by the auxin feedback system have largely been investigated, the molecular mechanisms timing the auxin regulatory loop have been underexplored. Correct patterns of cytokinin signalling controlled by AHP6 buffer the robustness of lateral organ initiation by controlling the temporal initiation of primordia (Besnard et al., 2014). However the mechanistic detailed of this regulation on the auxin feedback system still remains elusive.

Our results now suggest that the activity of the MP-BRM complex could pace the emergence of auxin maxima and in turn determine the rate of lateral organ formation. Future efforts to map the interaction domains between HEC, SPT, MP and BRM could provide key information to fine tune the activity of the protein complex. Along the same lines, modulating the stoichiometry of individual components could further reveal the dynamics of MP complex activity and open new avenues to engineer shoot architecture by controlling the rate of lateral organ initiation.

V.3 HECATE genes control organ patterning and hormonal responses at the gynoecium

Gynoecium patterning and fruit formation are essential for the reproductive success of plants. At the mechanistic level, transcriptional and hormonal signals are tightly coupled to regulate gynoecium patterning and specification. Previous studies have identified the key role of auxin during apical-basal gynoecium patterning and started

to unravel the key transcription factors modulating the signalling (Eklund et al., 2010; Girin et al., 2011; Gremski et al., 2007; Sorefan et al., 2009). However, the regulatory interactions mediating the communication between transcriptional inputs and auxin signalling pathway are still unclear. Here, we found that HEC factors directly regulate the patterns of PIN accumulation at the style of the gynoecium and in turn influence auxin distribution and responses. This regulation was specific to this tissue, as we did not observe changes in PIN1 accumulation patterns in the SAM, highlighting the domain-specific activity of HEC function during development.

PIN1 regulation is particularly crucial at stage 10 of gynoecium differentiation when the radialization of auxin signals instructs a switch from bilateral to radial symmetry at the developing style (Moubayidin and Østergaard, 2014). Interestingly, *INDEHISCENT* (*IND*), which is the closest homologous gene to the *HEC* clade, modulates PIN polar localization by positively regulating the protein kinase PINOID (PID) expression (Sorefan et al., 2009). Thus, the regulatory control of auxin homeostasis at the gynoecium involves homologous transcription factors that differentially regulate PIN transporter accumulation. While HEC proteins promote the expression of *PIN* genes, IND controls PIN sub-cellular localization, thereby constituting a two-layer control system on auxin flow directionality (Schuster et al., 2015; Sorefan et al., 2009).

Mechanistically, IND physically interacts with the auxin response factor ETT to regulate PID expression. The protein complex dissociates upon auxin sensing, constituting a parallel auxin sensing mechanism to the ubiquitin proteasome system required for proper style development (Gray et al., 2001; Simonini et al., 2016). Given the physical interaction between HEC and MP, the formation of IND-ETT complex suggests that HEC clade family members have a broad potential to associate with multiple ARFs in different developmental contexts.

In light of the regulatory control of auxin directionality by HEC and IND, HEC factors are tightly integrated in the auxin feedback system by forming a multilayer web of interactions with auxin signalling components. It would be interesting in the future to further test the potential of HEC and IND family members to form functional protein complexes with multiple ARFs in different developmental contexts including the gynoecium.

The previous identification of SPT as a putative HEC cofactor and their similar regulatory function in the gynoecium suggested that these factors may form a protein complex regulating specific aspects of gynoecium development (Gremski et al.,

2007). Nevertheless, their functional interaction in this context remained so far unexplored. We found that HEC and SPT factors synergistically control style specification. Interestingly, *spt* mutants displayed stronger defects in the style fusion than *hec1,2,3* and this phenotype was strongly enhanced in the *hec1,2,3,spt* quadruple mutant where both style and valves could not fuse. This synergistic interaction was reminiscent of the functional interaction between SPT and its cofactor ALC. Similarly to *hec* loss-of-function, *alc* single mutant does not display strong defects in style fusion, whereas *alc, spt* double mutants show enhanced defects (Groszmann et al., 2011). Furthermore, our protein-protein interaction screenings and functional tests showed that HEC factors physically and functionally interacted with ALC during style formation. Together, these results suggest that SPT has a key regulatory function in specifying style identity and that its activity can be modulated by HEC or ALC cofactors through the formation of protein complexes. In the shoot meristem, SPT is required to mediate HEC function in distinct domains of the SAM, whereas the function ALC diverges in this context. These results highlight the versatility of the HEC-SPT complex in controlling multiple developmental programs but also suggest that other cofactors may interact to spatially restrict HEC-SPT regulatory function.

Cytokinin signalling plays an important role in controlling cell proliferation at the carpel marginal meristem (CMM)(Marsch-Martínez et al., 2012). However, in contrast to other tissues, the interaction with auxin signalling in the gynoecium remained poorly characterized (Marsch-Martínez and de Folter, 2016). We found that HEC and SPT function buffer cytokinin signalling during style specification. In particular, *hec* and that *spt* loss-of-function were hypersensitive to cytokinin treatment and displayed tissue overproliferation at the style region. These results suggest that HEC and SPT function repress cytokinin responses, possibly by the positive regulation of type-A ARRs.

In contrast to these findings, a recent study shows that SPT directly positively regulates the expression of ARR1 to promote cytokinin signalling at the CMM. The authors show that *spt* mutants display weaker cytokinin responses at the CMM, and style fusion defects can be rescued by mild application of cytokinin (Reyes-Olalde et al., 2017). Although these results contradict our phenotypic analysis of *spt* mutants treated with cytokinin, this discrepancy could arise from indirect regulatory effect or from different strength of the pharmacological treatment. Furthermore, some of the regulatory interactions between SPT and cytokinin at the CMM may differ at the

developing style. It will thus be important in the future to further investigate these interactions at higher spatio-temporal resolution. Interestingly, this study also underlined the tight integration of auxin and cytokinin signals at the gynoecium. The authors showed that SPT and ARR1 bind at the promoter of the auxin biosynthesis gene *TAA1* and positively regulate its expression, forming a feed forward loop of regulation (Reyes-Olalde et al., 2017).

These results are in line with our findings that HEC function acts at the interface between auxin and cytokinin signalling pathways. Together with our analysis of the SAM, the characterization of HEC function in the gynoecium demonstrates that these factors coordinate hormonal balance in diverse developmental contexts. Collectively, these results also question the evolutionary trajectory of the interaction between HEC, auxin and cytokinin. Thus, it would be interesting in the future to investigate the regulatory function of *HEC* genes and their interaction with phytohormones in a range of plant species.

V.4 A network approach to investigating HEC1 functional versatility

The multiple developmental programs controlled by HEC factors under distinct cellular contexts demonstrated their important functional versatility. However, our molecular understanding of the mechanisms controlling this process remained elusive. To further characterize the molecular mechanisms driving HEC function, we used a systems approach by reconstructing HEC1-regulatory network. By integrating results from protein-protein interaction networks and genome-wide profiling data, we defined four core regulatory modules–including light signalling, gynoecium development, auxin signalling and a TCP transcription factor module–that may instruct HEC functional specificity.

To reconstruct HEC1 regulatory networks, we combined data from yeast system to identify HEC1 cofactors, from seedlings to record the genome-wide DNA-binding pattern and from inflorescences to detect HEC1 response genes. Although this strategy was largely tissue unspecific and the screenings were conducted in various developmental contexts, it allowed us to define multiple regulatory modules that were in line with known functions of *HEC* genes.

Our protein-protein interaction networks displayed a very high connectivity among transcription factors, suggesting that HEC1 interaction partners could define its functional specificity in controlling multiple transcriptional programs. Among putative cofactors, we found that PIF3 and PIF5 transcription factors physically interacted with

HEC1 (Figure 48). Interestingly, the physical interaction between HEC and PIF factors regulates photomorphogenesis (Zhu et al., 2016). In this context, HEC factors interfere with PIF transcriptional activity by inhibiting their binding to DNA. Interestingly, *in vitro* assays data show that HEC2 protein does not directly bind the G-box DNA motif, suggesting that HEC factors interact with DNA through the formation of a protein complex (Zhu et al., 2016). These results are in line with the full suppression of HEC gain-of function phenotypes observed in the *spt* mutant background (Figure 36, 37), and suggest that HEC factors could act as transcriptional coregulators by modulating the activity of multiple transcription factors. It will be crucial in the future to further refine HEC molecular function in different developmental contexts and to specifically test HEC1 DNA-binding capacity alone or in complex with key cofactors including SPT or MP.

Although our network reconstruction approach made use of fast, cost-effective and technically reliable methods, it also showed limitations. For example, many factors were not present in the yeast-two-hybrid transcription factor library, and the floral cDNA library mostly contained genes expressed at the inflorescence stage. Independently of the incomplete nature of these libraries, the overlap between our Y2H screening was low, as we detected only one factor in both screens. Surprisingly, we did not detect SPT and MP although we could confirm their physical and functional interaction with HEC factors *in vivo*. Along these lines, the results from our screenings differed substantially form large-scale *Arabidopsis* interactome data sets (Arabidopsis Interactome Mapping Consortium, 2011; Trigg et al., 2017). This suggests that while keeping its potential to identify key regulatory interactions, the yeast-two hybrid screening method display a high rate of false positive and thereby high variability depending on the experimental setup (Causier, 2004). Regarding both profiling methods, we used ubiquitously expressed tagged versions of HEC1, and therefore assessed the regulatory potential of the factor rather than its actual *in vivo* regulatory function. Furthermore, we profiled mixtures of tissues and cell types that might have masked HEC1 domain-specific regulations. Thus, the reconstruction of HEC1 regulatory networks could largely benefit from experimental improvements. In particular, the use of identical tissues or cell types to analyze the interactome, transcriptome and the DNA-binding profile would provide a better snapshot of HEC1 regulatory network at a specific developmental time and could be conducted using recently developed sorting methods (Moreno-Romero et al.; Reddy, 2014).

V.5 Functional characterization of HEC1 regulatory modules

In order to further investigate the molecular mechanisms driving HEC function we used the reconstructed regulatory modules as a springboard to start the functional characterization of specific factors. We used two complementary approaches: an unbiased method with the MIGS approach and a more targeted one based on information obtained from published studies.

V.5.1 MIGS approach

To identify new regulatory interactions independently of previously described gene function, we adapted the MIGS system to silence the expression of multiple transcription factors identified from the yeast-two-hybrid screenings (Felippes et al., 2012). Using *SPT* gene as a positive control, we confirmed the functionality of the MIGS method. However, in contrast to a full *SPT* loss-of-function, we observed that the reduction in *SPT* gene expression was only partial, suggesting that the silencing efficiency of the MIGS system was not complete. When analysing gynoecium development of the different MIGS lines, we did not identify functional interaction between *HEC* genes and its cofactors. In contrast, the deviations in silique densities along the stem of MIGS-silenced plants suggest that eight cofactors (SPT, PIF3, PIF5, GAI, PAR1, bHLH112, P1R3 and bHLH146) may play a role in SAM activity. It will be important in the future to further characterize these factors. Alternatively to the MIGS strategy, the substantial development of CRISPR-CAS9 based molecular tools makes it a method of choice to rapidly target or mutate multiple genomic loci (Čermák et al., 2017). This could for example be used to simultaneously target multiple HEC cofactors, circumventing the low efficiency of the gene knock down observed with MIGS and overcoming the potential functional redundancy of the cofactors.

V.5.2 Characterization of ALC and DELLA function in the meristem

Previous analyses of the gynoecium have identified the role ALC-DELLAs during valve margin specification (Arnaud et al., 2010; Groszmann et al., 2011). Interestingly, we found that HEC1 forms a highly connective protein-protein interaction network with SPT, ALC, RGA and GAI, suggesting that the formation of multiple or larger complexes with these factors may mediate various regulatory functions. To investigate this idea, we tested whether DELLA proteins could modulate HEC activity in the SAM or in the gynoecium. Although DELLA loss-of-function mutants did not modulate HEC function in the stem cells, we found that

gibberellic acid treatment partially rescued the gynoecium size in HEC loss-of-function mutants. These results indicate that HEC factors and DELLAs may functionally interact only in the context of the gynoecium. Given the role of DELLA proteins in promoting floral initiation, it would also be interesting to further investigate their interaction in this developmental context (Yamaguchi et al., 2014). In light of the role of HEC factors in balancing auxin and cytokinin responses, their interaction with GA signalling suggest that they may constitute a regulatory hub in integrating inputs from multiple hormonal pathways.

V.5.3 Characterization of NGATHA function in the meristem

By carefully analysing HEC1 regulatory module controlling gynoecium development, we identified *NGA1* and *NGA2* as direct target genes. Interestingly, previous studies have shown that *NGA* genes are co-expressed with *HEC* genes and share similar function to promote style fusion (Alvarez et al., 2009; Trigueros et al., 2009). We found that NGA factors shared regulatory function with HEC in the stem cells to promote CZ and SAM expansion, however they were not mediating HEC activity in this context and could also give rise to fully terminated and differentiated shoot meristems, which we never observed in HEC gain-of-function experiments. These results suggest that NGA function can initiate distinct developmental programs depending on their expression level. Surprisingly, NGA loss-of-function also gave rise to larger meristems with enhanced cytokinin signalling, indicating that both NGA gain and loss-of-function could promote SAM enlargement.

Although these results are not sufficient to delineate a clear mechanism for NGA activity in the SAM, multiple processes could influence the outcome of these experiments and would need to be further investigated. Given the multiple regulatory feedback loops of communication within the SAM, it would be crucial to better understand the dynamics of their activity. Furthermore, *NGATHA* genes may have distinct functions within different domains of the SAM, which could lead to counter-intuitive results when comparing domain-specific gain-of-function with constitutive loss-of-function mutants. Thus, it will be important to further understand their spatial activity. Finally the expression level of these factors could trigger different developmental programs by controlling distinct target genes. Thus, further resolving their transcriptional target genes and comparing them with HEC transcriptional network could identify a set of convergent target genes.

V.6 Hypothetical mechanisms encoding HEC functional versatility

The analysis of HEC1 regulatory network led us to identify functional relevant players interacting or mediating HEC function. Although SPT is a key cofactor in some developmental contexts, it does not instruct HEC1 domain-specific activity. Furthermore, the functional analysis of ALC, DELLA proteins and NGA did not resolve the mechanistic basis for HEC1 functional versatility. We hypothesized that this process could be encoded by the formation of multiple protein complexes, however alternative scenarios could also explain HEC domain-specific activity; namely protein dosage; differential chromatin accessibility leading to differential cellular responsiveness or domain-specific post-translational modification.

First, the dosage of HEC expression level could trigger different cellular responses. In line with this idea, PLETHORA transcription factors accumulate in the root apical meristem in a gradient like fashion, and control stem cells at high protein level, mitotic activity at medium level and cell differentiation at low accumulation level (Galinha et al., 2007). Mechanistically, this suggests that changes in protein concentration could dictate the establishment of distinct regulatory programs, similarly to the concept of morphogenes (Briscoe and Small, 2015). Alternatively, differential accessibility of HEC1 to genomic regions could specify its regulatory potential. Previous studies have demonstrated that chromatin structure undergoes important remodelling processes during stem cell differentiation (Xie et al., 2013). This suggests that chromatin accessibility in distinct cellular domains of the SAM or gynoecium may be different, restricting the range of target genes that HEC can regulate in these specific cellular contexts. The putative interaction between HEC factors, BRM and SWI3C further suggest that HEC function could in turn actively regulate chromatin accessibility (Figure 48). Finally, HEC proteins could be post-translationally modified by factors in specific spatial domains, modulating their regulatory function. Taken together, it will be important in the future to investigate these alternative regulatory scenarios and to reveal whether they participate in encoding HEC functional versatility.

V.7 Conclusion

By using a multi-disciplinary approach integrating results from quantitative live-cell imaging, computational modelling, interaction screenings, genome-wide profiling and genetic analyses, this study revealed that HEC function controls the timing of stem cell differentiation in the SAM and patterns the gynoecium during differentiation. We

found that both functions were associated with the modulation of the balance between auxin and cytokinin signalling pathways. Furthermore, we could reconstruct HEC1-regulatory networks and identify specific regulatory modules potentially mediating HEC functional versatility. This also proved to be a powerful data mining strategy, as we identified *NGATHA* genes as novel regulators of shoot meristem activity. Together, we provide a molecular framework for HEC function during plant development.

VI. References

Alvarez, J. and Smyth, D. R. (1999). CRABS CLAW and SPATULA, two Arabidopsis genes that control carpel development in parallel with AGAMOUS. *Development* **126**, 2377–2386.

Alvarez, J. P. (2006). Endogenous and Synthetic MicroRNAs Stimulate Simultaneous, Efficient, and Localized Regulation of Multiple Targets in Diverse Species. *The Plant Cell* **18**, 1134–1151.

Alvarez, J. P., Goldshmidt, A., Efroni, I., Bowman, J. L. and Eshed, Y. (2009). The NGATHA distal organ development genes are essential for style specification in Arabidopsis. *The Plant cell* **21**, 1373–1393.

Anders, S., Pyl, P. T. and Huber, W. (2015). HTSeq--a Python framework to work with high-throughput sequencing data. *Bioinformatics* **31**, 166–169.

Arabidopsis Interactome Mapping Consortium (2011). Evidence for network evolution in an Arabidopsis interactome map. *Science* **333**, 601–607.

Arnaud, N., Girin, T., Sorefan, K., Fuentes, S., Wood, T. A., Lawrenson, T., Sablowski, R. and Ostergaard, L. (2010). Gibberellins control fruit patterning in Arabidopsis thaliana. *Genes & Development* **24**, 2127–2132.

Bailey, T. L., Boden, M., Buske, F. A., Frith, M., Grant, C. E., Clementi, L., Ren, J., Li, W. W. and Noble, W. S. (2009). MEME SUITE: tools for motif discovery and searching. *Nucleic Acids Research* **37**, W202–W208.

Band, L. R., Ubeda-Tomás, S., Dyson, R. J., Middleton, A. M., Hodgman, T. C., Owen, M. R., Jensen, O. E., Bennett, M. J. and King, J. R. (2012). Growth-induced hormone dilution can explain the dynamics of plant root cell elongation. *Proceedings of the National Academy of Sciences* **109**, 7577–7582.

Barbez, E., Kubeš, M., Rolčík, J., Béziat, C., Pěnčík, A., Wang, B., Rosquete, M. R., Zhu, J., Dobrev, P. I., Lee, Y., et al. (2012). A novel putative auxin carrier family regulates intracellular auxin homeostasis in plants. *Nature* **485**, 119–122.

Barbier de Reuille, P., Routier-Kierzkowska, A.-L., Kierzkowski, D., Bassel, G. W., Schüpbach, T., Tauriello, G., Bajpai, N., Strauss, S., Weber, A., Kiss, A., et al. (2015). MorphoGraphX: A platform for quantifying morphogenesis in 4D. *eLife* **4**, 05864.

Benjamins, R. and Scheres, B. (2008). Auxin: the looping star in plant development. *Annu. Rev. Plant Biol.* **59**, 443–465.

Berthold, M. R., Cebron, N., Dill, F., Gabriel, T. R., Kötter, T., Meinl, T., Ohl, P., Sieb, C., Thiel, K. and Wiswedel, B. (2008). KNIME: The Konstanz Information Miner. In *Studies in Classification, Data Analysis, and Knowledge Organization*, pp. 319–326. Berlin, Heidelberg: Springer Berlin Heidelberg.

Besnard, F., Refahi, Y., Morin, V., Marteaux, B., Brunoud, G., Chambrier, P., Rozier, F., Mirabet, V., Legrand, J., Lainé, S., et al. (2014). Cytokinin signalling inhibitory fields provide robustness to phyllotaxis. *Nature* **505**, 417–421.

Betsuyaku, S., Takahashi, F., Kinoshita, A., Miwa, H., Shinozaki, K., Fukuda, H. and Sawa, S. (2011). Mitogen-activated protein kinase regulated by the CLAVATA receptors contributes to shoot apical meristem homeostasis. *Plant and Cell Physiology* **52**, 14–29.

Bhargava, A., Clabaugh, I., To, J. P., Maxwell, B. B., Chiang, Y.-H., Schaller, G. E., Loraine, A. and Kieber, J. J. (2013). Identification of cytokinin-responsive genes using microarray meta-analysis and RNA-Seq in Arabidopsis. *Plant Physiology* **162**, 272–294.

Bhatia, N., Bozorg, B., Larsson, A., Ohno, C., Jönsson, H. and Heisler, M. G. (2016). Auxin Acts through MONOPTEROS to Regulate Plant Cell Polarity and Pattern Phyllotaxis. *Current Biology.* **26**, 3202–3208.

Bleckmann, A., Weidtkamp-Peters, S., Seidel, C. A. M. and Simon, R. (2009). Stem Cell Signaling in Arabidopsis Requires CRN to Localize CLV2 to the Plasma Membrane. *Plant Physiology* **152**, 166–176.

Bommert, P., Je, B. I., Goldshmidt, A. and Jackson, D. (2013). The maize Gα gene COMPACT PLANT2 functions in CLAVATA signalling to control shoot meristem size. *Nature* **502**, 555–558.

Brand, U., Fletcher, J. C., Hobe, M., Meyerowitz, E. M. and Simon, R. (2000). Dependence of stem cell fate in Arabidopsis on a feedback loop regulated by CLV3 activity. *Science* **289**, 617–619.

Briscoe, J. and Small, S. (2015). Morphogen rules: design principles of gradient-mediated embryo patterning. *Development* **142**, 3996–4009.

Byrne, M. E., Barley, R., Curtis, M., Arroyo, J. M., Dunham, M., Hudson, A. and Martienssen, R. A. (2000). Asymmetric leaves1 mediates leaf patterning and stem cell function in Arabidopsis. *Nature* **408**, 967–971.

Byrne, M. E., Simorowski, J. and Martienssen, R. A. (2002). ASYMMETRIC LEAVES1 reveals knox gene redundancy in Arabidopsis. *Development* **129**, 1957–1965.

Calderon-Villalobos, L. I. A., Lee, S., De Oliveira, C., Ivetac, A., Brandt, W., Armitage, L., Sheard, L. B., Tan, X., Parry, G., Mao, H., et al. (2012). A combinatorial TIR1/AFB-Aux/IAA co-receptor system for differential sensing of auxin. *Nat Chem Biol* **8**, 477–485.

Castrillo, G., Turck, F., Leveugle, M., Lecharny, A., Carbonero, P., Coupland, G., Paz-Ares, J. and Oñate-Sánchez, L. (2011). Speeding Cis-Trans Regulation Discovery by Phylogenomic Analyses Coupled with Screenings of an Arrayed Library of Arabidopsis Transcription Factors. *PLoS ONE* **6**, e21524.

Causier, B. (2004). Studying the interactome with the yeast two-hybrid system and mass spectrometry. *Mass Spectrom. Rev.* **23**, 350–367.

Cheng, Y., Dai, X. and Zhao, Y. (2006). Auxin biosynthesis by the YUCCA flavin monooxygenases controls the formation of floral organs and vascular tissues in Arabidopsis. *Genes & Development* **20**, 1790–1799.

Chickarmane, V. S., Gordon, S. P., Tarr, P. T., Heisler, M. G. and Meyerowitz, E. M. (2012). Cytokinin signaling as a positional cue for patterning the apical-basal axis of the growing Arabidopsis shoot meristem. *Proceedings of the National Academy of Sciences* **109**, 4002–4007.

Clark, S. E., Williams, R. W. and Meyerowitz, E. M. (1997). The CLAVATA1 gene encodes a putative receptor kinase that controls shoot and floral meristem size in Arabidopsis. *Cell* **89**, 575–585.

Clevers, H. (2013). The intestinal crypt, a prototype stem cell compartment. *Cell* **154**, 274–284.

Clough, S. J. and Bent, A. F. (1998). Floral dip: a simplified method for Agrobacterium-mediated transformation of Arabidopsis thaliana. *Plant J.* **16**, 735–743.

Coen, E. S. and Meyerowitz, E. M. (1991). The war of the whorls: genetic interactions controlling flower development. *Nature* **353**, 31–37.

Čermák, T., Curtin, S. J., Gil-Humanes, J., Čegan, R., Kono, T. J. Y., Konečná, E., Belanto, J. J., Starker, C. G., Mathre, J. W., Greenstein, R. L., et al. (2017). A Multipurpose Toolkit to Enable Advanced Genome Engineering in Plants. *The Plant cell* **29**, 1196–1217.

Daum, G., Medzihradszky, A., Suzaki, T. and Lohmann, J. U. (2014). A mechanistic framework for noncell autonomous stem cell induction in Arabidopsis. *Proceedings of the National Academy of Sciences* **111**, 14619–14624.

Davière, J.-M., Wild, M., Regnault, T., Baumberger, N., Eisler, H., Genschik, P. and Achard, P. (2014). Class I TCP-DELLA interactions in inflorescence shoot apex determine plant height. *Current Biology.* **24**, 1923–1928.

de Lucas, M., Davière, J.-M., Rodríguez-Falcón, M., Pontin, M., Iglesias-Pedraz, J. M., Lorrain, S., Fankhauser, C., Blázquez, M. A., Titarenko, E. and Prat, S. (2008). A molecular framework for light and gibberellin control of cell elongation. *Nature* **451**, 480–484.

de Reuille, P. B., Bohn-Courseau, I., Ljung, K., Morin, H., Carraro, N., Godin, C. and Traas, J. (2006). Computer simulations reveal properties of the cell-cell signaling network at the shoot apex in Arabidopsis. *Proceeedings of the National Academy of Sciences* **103**, 1627–1632.

Denay, G., Chahtane, H., Tichtinsky, G. and Parcy, F. (2017). A flower is born: an update on Arabidopsis floral meristem formation. *Current Opinion in Plant Biology* **35**, 15–22.

Depuydt, S. and Hardtke, C. S. (2011). Hormone Signalling Crosstalk in Plant Growth Regulation. *Current Biology* **21**, R365–R373.

Dharmasiri, N., Dharmasiri, S., Weijers, D., Lechner, E., Yamada, M., Hobbie, L., Ehrismann, J. S., Jürgens, G. and Estelle, M. (2005). Plant Development Is Regulated by a Family of Auxin Receptor F Box Proteins. *Developmental Cell* **9**, 109–119.

Du, Z., Zhou, X., Ling, Y., Zhang, Z. and Su, Z. (2010). agriGO: a GO analysis toolkit for the agricultural community. *Nucleic Acids Research* **38**, W64–W70.

Efroni, I., Han, S.-K., Kim, H. J., Wu, M.-F., Steiner, E., Birnbaum, K. D., Hong, J. C., Eshed, Y. and Wagner, D. (2013). Regulation of Leaf Maturation by Chromatin-Mediated Modulation of Cytokinin Responses. *Developmental Cell* **24**, 438–445.

Eklund, D. M., Ståldal, V., Valsecchi, I., Cierlik, I., Eriksson, C., Hiratsu, K., Ohme-Takagi, M., Sundström, J. F., Thelander, M., Ezcurra, I., et al. (2010). The Arabidopsis thaliana STYLISH1 protein acts as a transcriptional activator regulating auxin biosynthesis. *The Plant cell* **22**, 349–363.

Enver, T., Pera, M., Peterson, C. and Andrews, P. W. (2009). Stem Cell States, Fates, and the Rules of Attraction. *Cell Stem Cell* **4**, 387–397.

Felippes, F. F. de, Wang, J.-W. and Weigel, D. (2012). MIGS: miRNA-induced gene silencing. *Plant J.* **70**, 541–547.

Feng, S., Martinez, C., Gusmaroli, G., Wang, Y., Zhou, J., Wang, F., Chen, L., Yu, L., Iglesias-Pedraz, J. M., Kircher, S., et al. (2008). Coordinated regulation of Arabidopsis thaliana development by light and gibberellins. *Nature* **451**, 475–479.

Feng, X. and Dickinson, H. G. (2010). Tapetal cell fate, lineage and proliferation in the Arabidopsis anther. *Development* **137**, 2409–2416.

Friml, J., Benková, E., Blilou, I., Wiśniewska, J., Hamann, T., Ljung, K., Woody, S., Sandberg, G., Scheres, B., Jürgens, G., et al. (2002a). AtPIN4 mediates sink-driven auxin gradients and root patterning in Arabidopsis. *Cell* **108**, 661–673.

Friml, J., Vieten, A., Sauer, M., Weijers, D., Schwarz, H., Hamann, T., Offringa, R. and Jürgens, G. (2003). Efflux-dependent auxin gradients establish the apical-basal axis of Arabidopsis. *Nature* **426**, 147–153.

Friml, J., Wiśniewska, J., Benková, E., Mendgen, K. and Palme, K. (2002b). Lateral relocation of auxin efflux regulator PIN3 mediates tropism in Arabidopsis. *Nature* **415**, 806–809.

Fuentes, S., Ljung, K., Sorefan, K., Alvey, E., Harberd, N. P. and Østergaard, L. (2012). Fruit growth in Arabidopsis occurs via DELLA-dependent and DELLA-independent gibberellin responses. *The Plant cell* **24**, 3982–3996.

Gaillochet, C. and Lohmann, J. U. (2015). The never-ending story: from pluripotency to plant developmental plasticity. *Development* **142**, 2237–2249.

Gaillochet, C., Daum, G. and Lohmann, J. U. (2015). O Cell, Where Art Thou? The mechanisms of shoot meristem patterning. *Current Opinion in Plant Biology* **23**, 91–97.

Galinha, C., Hofhuis, H., Luijten, M., Willemsen, V., Blilou, I., Heidstra, R. and Scheres, B. (2007). PLETHORA proteins as dose-dependent master regulators of Arabidopsis root development. *Nature* **449**, 1053–1057.

Geisler, M., Blakeslee, J. J., Bouchard, R., Lee, O. R., Vincenzetti, V., Bandyopadhyay, A., Titapiwatanakun, B., Peer, W. A., Bailly, A., Richards, E. L., et al. (2005). Cellular efflux of auxin catalyzed by the Arabidopsis MDR/PGP transporter AtPGP1. *Plant J.* **44**, 179–194.

Gendrel, A.-V., Lippman, Z., Martienssen, R. and Colot, V. (2005). Profiling histone modification patterns in plants using genomic tiling microarrays. *Nat. Methods* **2**, 213–218.

Gietz, R. D. and Schiestl, R. H. (2007). High-efficiency yeast transformation using the LiAc/SS carrier DNA/PEG method. *Nat Protoc* **2**, 31–34.

Girin, T., Paicu, T., Stephenson, P., Fuentes, S., Korner, E., O'Brien, M., Sorefan, K., Wood, T. A., Balanza, V., Ferrandiz, C., et al. (2011). INDEHISCENT and SPATULA Interact to Specify Carpel and Valve Margin Tissue and Thus Promote Seed Dispersal in Arabidopsis. *The Plant cell* **23**, 3641–3653.

Girin, T., Sorefan, K. and Østergaard, L. (2009). Meristematic sculpting in fruit development. *Journal of Experimental Botany* **60**, 1493–1502.

Gordon, S. P., Chickarmane, V. S., Ohno, C. and Meyerowitz, E. M. (2009). Multiple feedback loops through cytokinin signaling control stem cell number within the Arabidopsis shoot meristem. *Proceedings of the National Academy of Sciences* **106**, 16529–16534.

Gray, W. M., Kepinski, S., Rouse, D., Leyser, O. and Estelle, M. (2001). Auxin regulates SCF(TIR1)-dependent degradation of AUX/IAA proteins. *Nature* **414**, 271–276.

Gremski, K., Ditta, G. and Yanofsky, M. F. (2007). The HECATE genes regulate female reproductive tract development in Arabidopsis thaliana. *Development* **134**, 3593–3601.

Grieneisen, V. A., Xu, J., Marée, A. F. M., Hogeweg, P. and Scheres, B. (2007). Auxin transport is sufficient to generate a maximum and gradient guiding root growth. *Nature* **449**, 1008–1013.

Groszmann, M., Bylstra, Y., Lampugnani, E. R. and Smyth, D. R. (2010). Regulation of tissue-specific expression of SPATULA, a bHLH gene involved in carpel development, seedling germination, and lateral organ growth in Arabidopsis. *Journal of Experimental Botany* **61**, 1495–1508.

Groszmann, M., Paicu, T., Alvarez, J. P., Swain, S. M. and Smyth, D. R. (2011). SPATULA and ALCATRAZ, are partially redundant, functionally diverging bHLH genes required for Arabidopsis gynoecium and fruit development. *Plant J.* **68**, 816–829.

Hamant, O., Heisler, M. G., Jonsson, H., Krupinski, P., Uyttewaal, M., Bokov, P., Corson, F., Sahlin, P., Boudaoud, A., Meyerowitz, E. M., et al. (2008). Developmental Patterning by Mechanical Signals in Arabidopsis. *Science* **322**, 1650–1655.

Hardtke, C. S. and Berleth, T. (1998). The Arabidopsis gene MONOPTEROS encodes a transcription factor mediating embryo axis formation and vascular development. *The EMBO Journal* **17**, 1405–1411.

Heinz, S., Benner, C., Spann, N., Bertolino, E., Lin, Y. C., Laslo, P., Cheng, J. X., Murre, C., Singh, H. and Glass, C. K. (2010). Simple Combinations of Lineage-Determining Transcription Factors Prime cis-Regulatory Elements Required for Macrophage and B Cell Identities. *Molecular Cell* **38**, 576–589.

Heisler, M. G., Atkinson, A., Bylstra, Y. H., Walsh, R. and Smyth, D. R. (2001). SPATULA, a gene that controls development of carpel margin tissues in Arabidopsis, encodes a bHLH protein. *Development* **128**, 1089–1098.

Heisler, M. G., Ohno, C., Das, P., Sieber, P., Reddy, G. V., Long, J. A. and Meyerowitz, E. M. (2005). Patterns of auxin transport and gene expression during primordium development revealed by live imaging of the Arabidopsis inflorescence meristem. *Current Biology* **15**, 1899–1911.

Hoffman, C. S. and Winston, F. (1987). A ten-minute DNA preparation from yeast efficiently releases autonomous plasmids for transformation of Escherichia coli. *Gene* **57**, 267–272.

Hwang, I. and Sheen, J. (2001). Two-component circuitry in Arabidopsis cytokinin signal transduction. *Nature* **413**, 383–389.

Hwang, I., Sheen, J. and Müller, B. (2012). Cytokinin Signaling Networks. *Annu. Rev. Plant Biol.* **63**, 353–380.

Ichihashi, Y., Horiguchi, G., Gleissberg, S. and Tsukaya, H. (2010). The bHLH transcription factor SPATULA controls final leaf size in Arabidopsis thaliana. *Plant and Cell Physiology* **51**, 252–261.

Ioio, Dello, R., Linhares, F. S., Scacchi, E., Casamitjana-Martinez, E., Heidstra, R., Costantino, P. and Sabatini, S. (2007). Cytokinins Determine Arabidopsis Root-Meristem Size by Controlling Cell Differentiation. *Current Biology* **17**, 678–682.

Ioio, Dello, R., Nakamura, K., Moubayidin, L., Perilli, S., Taniguchi, M., Morita, M. T., Aoyama, T., Costantino, P. and Sabatini, S. (2008). A genetic framework for the control of cell division and differentiation in the root meristem. *Science* **322**, 1380–1384.

Ishida, T., Tabata, R., Yamada, M., Aida, M., Mitsumasu, K., Fujiwara, M., Yamaguchi, K., Shigenobu, S., Higuchi, M., Tsuji, H., et al. (2014). Heterotrimeric G proteins control stem cell proliferation through CLAVATA signaling in Arabidopsis. *EMBO Reports*.

Jasinski, S., Piazza, P., Craft, J., Hay, A., Woolley, L., Rieu, I., Phillips, A., Hedden, P. and Tsiantis, M. (2005). KNOX Action in Arabidopsis Is Mediated by Coordinate Regulation of Cytokinin and Gibberellin Activities. *Current Biology* **15**, 1560–1565.

Je, B. I., Gruel, J., Lee, Y. K., Bommert, P., Arevalo, E. D., Eveland, A. L., Wu, Q., Goldshmidt, A., Meeley, R., Bartlett, M., et al. (2016). Signaling from maize organ primordia via FASCIATED EAR3 regulates stem cell proliferation and yield traits. *Nat Genet* **48**, 785–791.

José Ripoll, J., Bailey, L. J., Mai, Q.-A., Wu, S. L., Hon, C. T., Chapman, E. J., Ditta, G. S., Estelle, M. and Yanofsky, M. F. (2015). microRNA regulation of fruit growth. *Nature Plants* **1**, 15036.

José Ripoll, J., Ferrándiz, C., Martínez-Laborda, A. and Vera, A. (2006). PEPPER, a novel K-homology domain gene, regulates vegetative and gynoecium development in Arabidopsis. *Developmental Biology* **289**, 346–359.

Jönsson, H., Heisler, M. G., Shapiro, B. E., Meyerowitz, E. M. and Mjolsness, E. (2006). An auxin-driven polarized transport model for phyllotaxis. *Proceeedings of the National Academy of Sciences* **103**, 1633–1638.

Kasili, R., Walker, J. D., Simmons, L. A., Zhou, J., De Veylder, L. and Larkin, J. C. (2010). SIAMESE cooperates with the CDH1-like protein CCS52A1 to establish endoreplication in Arabidopsis thaliana trichomes. *Genetics* **185**, 257–268.

Kaufmann, K., Wellmer, F., Muino, J. M., Ferrier, T., Wuest, S. E., Kumar, V., Serrano-Mislata, A., Madueno, F., Krajewski, P., Meyerowitz, E. M., et al. (2010). Orchestration of Floral Initiation by APETALA1. *Science* **328**, 85–89.

Khanna, R., Huq, E., Kikis, E. A., Al-Sady, B., Lanzatella, C. and Quail, P. H. (2004). A novel molecular recognition motif necessary for targeting photoactivated phytochrome signaling to specific basic helix-loop-helix transcription factors. *The Plant cell* **16**, 3033–3044.

Kierzkowski, D., Nakayama, N., Routier-Kierzkowska, A.-L., Weber, A., Bayer, E., Schorderet, M., Reinhardt, D., Kuhlemeier, C. and Smith, R. S. (2012). Elastic domains regulate growth and organogenesis in the plant shoot apical meristem. *Science* **335**, 1096–1099.

Kim, D., Pertea, G., Trapnell, C., Pimentel, H., Kelley, R. and Salzberg, S. L. (2013). TopHat2: accurate alignment of transcriptomes in the presence of insertions, deletions and gene fusions. *Genome Biol.* **14**, R36.

Kubota, A., Ito, S., Shim, J. S., Johnson, R. S., Song, Y. H., Breton, G., Goralogia, G. S., Kwon, M. S., Laboy Cintrón, D., Koyama, T., et al. (2017). TCP4-dependent induction of CONSTANS transcription requires GIGANTEA in photoperiodic flowering in Arabidopsis. *PLoS Genet* **13**, e1006856.

Kuhlemeier, C. (2007). Phyllotaxis. *Trends in Plant Science* **12**, 143–150.

Kumar, P., Tan, Y. and Cahan, P. (2017). Understanding development and stem cells using single cell-based analyses of gene expression. *Development* **144**, 17–32.

Kuroha, T., Tokunaga, H., Kojima, M., Ueda, N., Ishida, T., Nagawa, S., Fukuda, H., Sugimoto, K. and Sakakibara, H. (2009). Functional analyses of LONELY GUY cytokinin-activating enzymes reveal the importance of the direct activation pathway in Arabidopsis. *The Plant cell* **21**, 3152–3169.

Kuusk, S., Sohlberg, J. J., Long, J. A., Fridborg, I. and Sundberg, E. (2002). STY1 and STY2 promote the formation of apical tissues during Arabidopsis gynoecium development. *Development* **129**, 4707–4717.

Lampropoulos, A., Sutikovic, Z., Wenzl, C., Maegele, I., Lohmann, J. U. and Forner, J. (2013). GreenGate---a novel, versatile, and efficient cloning system for plant transgenesis. *PLoS ONE* **8**, e83043.

Landrein, B., Refahi, Y., Besnard, F., Hervieux, N., Mirabet, V., Boudaoud, A., Vernoux, T. and Hamant, O. (2015). Meristem size contributes to the robustness of phyllotaxis in Arabidopsis. *Journal of Experimental Botany* **66**, 1317–1324.

Langmead, B. and Salzberg, S. L. (2012). Fast gapped-read alignment with Bowtie 2. *Nat. Methods* **9**, 357–359.

Larsson, E., Roberts, C. J., Claes, A. R., Franks, R. G. and Sundberg, E. (2014). Polar auxin transport is essential for medial versus lateral tissue specification and vascular-mediated valve outgrowth in Arabidopsis gynoecia. *Plant Physiology* **166**, 1998–2012.

Lau, O. S., Davies, K. A., Chang, J., Adrian, J., Rowe, M. H., Ballenger, C. E. and Bergmann, D. C. (2014). Direct roles of SPEECHLESS in the specification of stomatal self-renewing cells. *Science* **345**, 1605–1609.

Lau, S., De Smet, I., Kolb, M., Meinhardt, H. and Jürgens, G. (2011). Auxin triggers a genetic switch. *Nat Cell Biol* **13**, 611–615.

Laux, T., Mayer, K. F., Berger, J. and Jurgens, G. (1995). The WUSCHEL gene is required for shoot and floral meristem integrity in Arabidopsis. *Development* **122**, 87–96.

Leibfried, A., To, J. P. C., Busch, W., Stehling, S., Kehle, A., Demar, M., Kieber, J. J. and Lohmann, J. U. (2005). WUSCHEL controls meristem function by direct regulation of cytokinin-inducible response regulators. *Nature* **438**, 1172–1175.

Li, H., Handsaker, B., Wysoker, A., Fennell, T., Ruan, J., Homer, N., Marth, G., Abecasis, G., Durbin, R.1000 Genome Project Data Processing Subgroup (2009). The Sequence Alignment/Map format and SAMtools. *Bioinformatics* **25**, 2078–2079.

Li, S., Yamada, M., Han, X., Ohler, U. and Benfey, P. N. (2016). High-Resolution Expression Map of the Arabidopsis Root Reveals Alternative Splicing and lincRNA Regulation. *Developmental Cell* **39**, 508–522.

Liao, C.-Y., Smet, W., Brunoud, G., Yoshida, S., Vernoux, T. and Weijers, D. (2015). Reporters for sensitive and quantitative measurement of auxin response. *Nat. Methods* **12**, 207-210.

Liscum, E. and Briggs, W. R. (1995). Mutations in the NPH1 locus of Arabidopsis disrupt the perception of phototropic stimuli. *The Plant cell* **7**, 473–485.

Lohmann, J. U., Hong, R. L., Hobe, M., Busch, M. A., Parcy, F., Simon, R. and Weigel, D. (2001). A molecular link between stem cell regulation and floral patterning in Arabidopsis. *Cell* **105**, 793–803.

Louveaux, M., Julien, J.-D., Mirabet, V., Boudaoud, A. and Hamant, O. (2016). Cell division plane orientation based on tensile stress in Arabidopsis thaliana. *Proceedings of the National Academy of Sciences* **113**, E4294–303.

Lucero, L. E., Uberti-Manassero, N. G., Arce, A. L., Colombatti, F., Alemano, S. G. and Gonzalez, D. H. (2015). TCP15 modulates cytokinin and auxin responses during gynoecium development in Arabidopsis. *Plant J.* **84**, 267–282.

Macosko, E. Z., Basu, A., Satija, R., Nemesh, J., Shekhar, K., Goldman, M., Tirosh, I., Bialas, A. R., Kamitaki, N., Martersteck, E. M., et al. (2015). Highly Parallel Genome-wide Expression Profiling of Individual Cells Using Nanoliter Droplets. *Cell* **161**, 1202–1214.

Marsch-Martínez, N. and de Folter, S. (2016). Hormonal control of the development of the gynoecium. *Current Opinion in Plant Biology* **29**, 104–114.

Marsch-Martínez, N., Ramos-Cruz, D., Irepan Reyes-Olalde, J., Lozano-Sotomayor, P., Zúñiga-Mayo, V. M. and de Folter, S. (2012). The role of cytokinin during Arabidopsis gynoecia and fruit morphogenesis and patterning. *Plant J.* **72**, 222–234.

Martínez-Fernández, I., Sanchís, S., Marini, N., Balanzá, V., Ballester, P., Navarrete-Gómez, M., Oliveira, A. C., Colombo, L. and Ferrándiz, C. (2014). The effect of NGATHA altered activity on auxin signaling pathways within the Arabidopsis gynoecium. *Front Plant Sci* **5**, 210.

Mayer, K. F., Schoof, H., Haecker, A., Lenhard, M., Jurgens, G. and Laux, T. (1998). Role of WUSCHEL in regulating stem cell fate in the Arabidopsis shoot meristem. *Cell* **95**, 805–815.

Mähönen, A. P., Bishopp, A., Higuchi, M., Nieminen, K. M., Kinoshita, K., Törmäkangas, K., Ikeda, Y., Oka, A., Kakimoto, T. and Helariutta, Y. (2006). Cytokinin signaling and its inhibitor AHP6 regulate cell fate during vascular development. *Science* **311**, 94–98.

Mähönen, A. P., Tusscher, ten, K., Siligato, R., Smetana, O., Díaz-Triviño, S., Salojärvi, J., Wachsman, G., Prasad, K., Heidstra, R. and Scheres, B. (2014). PLETHORA gradient formation mechanism separates auxin responses. *Nature* **515**, 125–129.

Medzihradszky, A., Schneitz, K. and Lohmann, J. U. (2014). Detection of mRNA Expression Patterns by Nonradioactive In Situ Hybridization on Histological Sections of Floral Tissue. In *Flower Development: Methods and Protocols* (eds. Riechmann, J. L. and Wellmer, F., pp. 275–293. New York, NY: Springer New York.

Merelo, P., Xie, Y., Brand, L., Ott, F., Weigel, D., Bowman, J. L., Heisler, M. G. and Wenkel, S. (2013). Genome-Wide Identification of KANADI1 Target Genes. *PLoS ONE* **8**, e77341.

Mering, von, C. (2004). STRING: known and predicted protein-protein associations, integrated and transferred across organisms. *Nucleic Acids Research* **33**, D433–D437.

Michniewicz, M., Zago, M. K., Abas, L., Weijers, D., Schweighofer, A., Meskiene, I., Heisler, M. G., Ohno, C., Zhang, J., Huang, F., et al. (2007). Antagonistic Regulation of PIN Phosphorylation by PP2A and PINOID Directs Auxin Flux. *Cell* **130**, 1044–1056.

Miyawaki, K., Matsumoto-Kitano, M. and Kakimoto, T. (2004). Expression of cytokinin biosynthetic isopentenyltransferase genes in Arabidopsis: tissue specificity and regulation by auxin, cytokinin, and nitrate. *Plant J.* **37**, 128–138.

Miyawaki, K., Tarkowski, P., Matsumoto-Kitano, M., Kato, T., Sato, S., Tarkowska, D., Tabata, S., Sandberg, G. and Kakimoto, T. (2006). Roles of Arabidopsis ATP/ADP isopentenyltransferases and tRNA isopentenyltransferases in cytokinin biosynthesis. *Proc. Natl. Acad. Sci. U.S.A.* **103**, 16598–16603.

Moreno-Romero, J., Santos-Gonzalez, J., Hennig, L. and Köhler, C. Applying the INTACT method to purify endosperm nuclei and to generate parental-specific epigenome profiles. *Nat. Protocols* **12**, 238–254.

Moubayidin, L. and Østergaard, L. (2014). Dynamic Control of Auxin Distribution Imposes a Bilateral-to-Radial Symmetry Switch during Gynoecium Development. *Current Biology* **24**, 2743–2748.

Moyroud, E., Minguet, E. G., Ott, F., Yant, L., Posé, D., Monniaux, M., Blanchet, S., Bastien, O., Thevenon, E., Weigel, D., et al. (2011). Prediction of regulatory interactions from genome sequences using a biophysical model for the Arabidopsis LEAFY transcription factor. *The Plant cell* **23**, 1293–1306.

Murase, K., Hirano, Y., Sun, T.-P. and Hakoshima, T. (2008). Gibberellin-induced DELLA recognition by the gibberellin receptor GID1. *Nature* **456**, 459–463.

Nemhauser, J. L., Feldman, L. J. and Zambryski, P. C. (2000). Auxin and ETTIN in Arabidopsis gynoecium morphogenesis. *Development* **127**, 3877–3888.

Nimchuk, Z. L., Zhou, Y., Tarr, P. T., Peterson, B. A. and Meyerowitz, E. M. (2015). Plant stem cell maintenance by transcriptional cross-regulation of related receptor kinases. *Development* **142**, 1043–1049.

Noah, T. K., Donahue, B. and Shroyer, N. F. (2011). Intestinal development and differentiation. *Experimental Cell Research* **317**, 2702–2710.

Ogawa, M., Shinohara, H., Sakagami, Y. and Matsubayashi, Y. (2008). Arabidopsis CLV3 Peptide Directly Binds CLV1 Ectodomain. *Science* **319**, 294–294.

Oliva, M., Farcot, E. and Vernoux, T. (2013). Plant hormone signaling during development: insights from computational models. *Current Opinion in Plant Biology* **16**, 19–24.

Østergaard, L. (2009). Don't "leaf" now. The making of a fruit. *Current Opinion in Plant Biology* **12**, 36–41.

Perales, M., Rodriguez, K., Snipes, S., Yadav, R. K., Diaz-Mendoza, M. and Reddy, G. V. (2016). Threshold-dependent transcriptional discrimination underlies stem cell homeostasis. *Proceedings of the National Academy of Sciences* **113**, E6298–E6306.

Péret, B., Swarup, K., Ferguson, A., Seth, M., Yang, Y., Dhondt, S., James, N., Casimiro, I., Perry, P., Syed, A., et al. (2012). AUX/LAX genes encode a family of auxin influx transporters that perform distinct functions during Arabidopsis development. *The Plant cell* **24**, 2874–2885.

Pfeiffer, A., Janocha, D., Dong, Y., Medzihradszky, A., Schöne, S., Daum, G., Suzaki, T., Forner, J., Langenecker, T., Rempel, E., et al. (2016). Integration of light and metabolic signals for stem cell activation at the shoot apical meristem. *eLife* **5**. e17023

Pfeiffer, A., Shi, H., Tepperman, J. M., Zhang, Y. and Quail, P. H. (2014). Combinatorial complexity in a transcriptionally centered signaling hub in Arabidopsis. *Molecular Plant* **7**, 1598–1618.

Pires, H. R., Monfared, M. M., Shemyakina, E. A. and Fletcher, J. C. (2014). ULTRAPETALA trxG genes interact with KANADI transcription factor genes to regulate Arabidopsis gynoecium patterning. *The Plant cell* **26**, 4345–4361.

Quinlan, A. R. and Hall, I. M. (2010). BEDTools: a flexible suite of utilities for comparing genomic features. *Bioinformatics* **26**, 841–842.

Rajani, S. and Sundaresan, V. (2001). The Arabidopsis myc/bHLH gene ALCATRAZ enables cell separation in fruit dehiscence. *Current Biology* **11**, 1914–1922.

Reddy, G. V. (2014). Fluorescence Activated Cell Sorting of Shoot Apical Meristem Cell Types. In *Flower Development: Methods and Protocols* (eds. Riechmann, J. L. and Wellmer, F., pp. 315–321. New York, NY: Springer New York.

Reddy, G. V., Heisler, M. G., Ehrhardt, D. W. and Meyerowitz, E. M. (2004). Real-time lineage analysis reveals oriented cell divisions associated with morphogenesis at the shoot apex of Arabidopsis thaliana. *Development* **131**, 4225–4237.

Reinhardt, D., Frenz, M., Mandel, T. and Kuhlemeier, C. (2003a). Microsurgical and laser ablation analysis of interactions between the zones and layers of the tomato shoot apical meristem. *Development* **130**, 4073–4083.

Reinhardt, D., Pesce, E.-R., Stieger, P., Mandel, T., Baltensperger, K., Bennett, M., Traas, J., Friml, J. and Kuhlemeier, C. (2003b). Regulation of phyllotaxis by polar auxin transport. *Nature* **426**, 255–260.

Reyes-Olalde, J. I., Zúñiga-Mayo, V. M., Serwatowska, J., Chávez Montes, R. A., Lozano-Sotomayor, P., Herrera-Ubaldo, H., Gonzalez-Aguilera, K. L., Ballester, P., Ripoll, J. J., Ezquer, I., et al. (2017). The bHLH transcription factor SPATULA enables cytokinin signaling, and both activate auxin biosynthesis and transport genes at the medial domain of the gynoecium. *PLoS Genet* **13**, e1006726.

Riefler, M., Novak, O., Strnad, M. and Schmülling, T. (2006). Arabidopsis cytokinin receptor mutants reveal functions in shoot growth, leaf senescence, seed size, germination, root development, and cytokinin metabolism. *The Plant cell* **18**, 40–54.

Robinson, J. T., Thorvaldsdóttir, H., Winckler, W., Guttman, M., Lander, E. S., Getz, G. and Mesirov, J. P. (2011). Integrative genomics viewer. *Nat Biotechnol* **29**, 24–26.

Robinson, M. D., McCarthy, D. J. and Smyth, G. K. (2009). edgeR: a Bioconductor package for differential expression analysis of digital gene expression data. *Bioinformatics* **26**, 139–140.

Rodriguez, K., Perales, M., Snipes, S., Yadav, R. K., Diaz-Mendoza, M. and Reddy, G. V. (2016). DNA-dependent homodimerization, sub-cellular partitioning, and protein destabilization control WUSCHEL levels and spatial patterning. *Proceedings of the National Academy of Sciences* **113**, E6307–E6315.

Roeder, A. H. K. and Yanofsky, M. F. (2006). Fruit development in Arabidopsis. *Arabidopsis Book* **4**, e0075.

Rojo, E., Sharma, V. K., Kovaleva, V., Raikhel, N. V. and Fletcher, J. C. (2002). CLV3 is localized to the extracellular space, where it activates the Arabidopsis CLAVATA stem cell signaling pathway. *The Plant cell* **14**, 969–977.

Sabatini, S., Beis, D., Wolkenfelt, H., Murfett, J., Guilfoyle, T., Malamy, J., Benfey, P., Leyser, O., Bechtold, N., Weisbeek, P., et al. (1999). An auxin-dependent distal organizer of pattern and polarity in the Arabidopsis root. *Cell* **99**, 463–472.

Schaller, G. E., Bishopp, A. and Kieber, J. J. (2015). The yin-yang of hormones: cytokinin and auxin interactions in plant development. *The Plant cell* **27**, 44–63.

Scheres, B. and van der Putten, W. H. (2017). The plant perceptron connects environment to development. *Nature* **543**, 337–345.

Schindelin, J., Arganda-Carreras, I., Frise, E., Kaynig, V., Longair, M., Pietzsch, T., Preibisch, S., Rueden, C., Saalfeld, S., Schmid, B., et al. (2012). Fiji: an open-source platform for biological-image analysis. *Nat. Methods* **9**, 676–682.

Schmid, M., Davison, T. S., Henz, S. R., Pape, U. J., Demar, M., Vingron, M., Schölkopf, B., Weigel, D. and Lohmann, J. U. (2005). A gene expression map of Arabidopsis thaliana development. *Nat Genet* **37**, 501–506.

Schoof, H., Lenhard, M., Haecker, A., Mayer, K. F., Jurgens, G. and Laux, T. (2000). The stem cell population of Arabidopsis shoot meristems in maintained by a regulatory loop between the CLAVATA and WUSCHEL genes. *Cell* **100**, 635–644.

Schuster, C., Gaillochet, C. and Lohmann, J. U. (2015). Arabidopsis HECATE genes function in phytohormone control during gynoecium development. *Development* **142**, 3343–3350.

Schuster, C., Gaillochet, C., Medzihradszky, A., Busch, W., Daum, G., Krebs, M., Kehle, A. and Lohmann, J. U. (2014). A Regulatory Framework for Shoot Stem Cell Control Integrating Metabolic, Transcriptional, and Phytohormone Signals. *Developmental Cell* **28**, 438–449.

Shan, X., Yan, J. and Xie, D. (2012). Comparison of phytohormone signaling mechanisms. *Current Opinion in Plant Biology* **15**, 84–91.

Shimada, A., Ueguchi-Tanaka, M., Nakatsu, T., Nakajima, M., Naoe, Y., Ohmiya, H., Kato, H. and Matsuoka, M. (2008). Structural basis for gibberellin recognition by its receptor GID1. *Nature* **456**, 520–523.

Shinohara, H. and Matsubayashi, Y. (2015). Reevaluation of the CLV3-receptor interaction in the shoot apical meristem: dissection of the CLV3 signaling pathway from a direct ligand-binding point of view. *Plant J.* **82**, 328–336.

Silverstone, A. L., Jung, H. S., Dill, A., Kawaide, H., Kamiya, Y. and Sun, T. P. (2001). Repressing a repressor: gibberellin-induced rapid reduction of the RGA protein in Arabidopsis. *The Plant cell* **13**, 1555–1566.

Simmons, A. R. and Bergmann, D. C. (2016). Transcriptional control of cell fate in the stomatal lineage. *Current Opinion in Plant Biology* **29**, 1–8.

Simonini, S., Deb, J., Moubayidin, L., Stephenson, P., Valluru, M., Freire-Rios, A., Sorefan, K., Weijers, D., Friml, J. and Østergaard, L. (2016). A noncanonical auxin-sensing mechanism is required for organ morphogenesis in Arabidopsis. *Genes & Development* **30**, 2286–2296.

Smith, H. (2000). Phytochromes and light signal perception by plants--an emerging synthesis. *Nature* **407**, 585–591.

Smith, R. S., Guyomarc'h, S., Mandel, T., Reinhardt, D., Kuhlemeier, C. and Prusinkiewicz, P. (2006). A plausible model of phyllotaxis. *Proceeedings of the National Academy of Sciences* **103**, 1301–1306.

Sorefan, K., Girin, T., Liljegren, S. J., Ljung, K., Robles, P., Galván-Ampudia, C. S., Offringa, R., Friml, J., Yanofsky, M. F. and Østergaard, L. (2009). A regulated auxin minimum is required for seed dispersal in Arabidopsis. *Nature* **459**, 583–586.

Stepanova, A. N., Robertson-Hoyt, J., Yun, J., Benavente, L. M., Xie, D.-Y., Dolezal, K., Schlereth, A., Jürgens, G. and Alonso, J. M. (2008). TAA1-Mediated Auxin Biosynthesis Is Essential for Hormone Crosstalk and Plant Development. *Cell* **133**, 177–191.

Sun, B., Looi, L. S., Guo, S., He, Z., Gan, E. S., Huang, J., Xu, Y., Wee, W. Y. and Ito, T. (2014). Timing Mechanism Dependent on Cell Division Is Invoked by Polycomb Eviction in Plant Stem Cells. *Science* **343**, 1248559.

Sun, B., Xu, Y., Ng, K.-H. and Ito, T. (2009). A timing mechanism for stem cell maintenance and differentiation in the Arabidopsis floral meristem. *Genes & Development* **23**, 1791–1804.

Sun, T.-P. (2010). Gibberellin-GID1-DELLA: a pivotal regulatory module for plant growth and development. *Plant Physiology* **154**, 567–570.

Sundberg, E. and Østergaard, L. (2009). Distinct and dynamic auxin activities during reproductive development. *Cold Spring Harbor Perspectives in Biology* **1**, a001628.

Szklarczyk, D., Franceschini, A., Wyder, S., Forslund, K., Heller, D., Huerta-Cepas, J., Simonovic, M., Roth, A., Santos, A., Tsafou, K. P., et al. (2015). STRING v10: protein-protein interaction networks, integrated over the tree of life. *Nucleic Acids Research* **43**, D447–D452.

Tal, I., Zhang, Y., Jørgensen, M. E., Pisanty, O., Barbosa, I. C. R., Zourelidou, M., Regnault, T., Crocoll, C., Olsen, C. E., Weinstain, R., et al. (2016). The Arabidopsis NPF3 protein is a GA transporter. *Nature Communications* **7**, 11486.

Toledo-Ortiz, G., Huq, E. and Quail, P. H. (2003). The Arabidopsis basic/helix-loop-helix transcription factor family. *The Plant cell* **15**, 1749–1770.

Trigg, S. A., Garza, R. M., MacWilliams, A., Nery, J. R., Bartlett, A., Castanon, R., Goubil, A., Feeney, J., O'Malley, R., Huang, S.-S. C., et al. (2017). CrY2H-seq: a massively multiplexed assay for deep-coverage interactome mapping. *Nat. Methods* **14**, 819–825.

Trigueros, M., Navarrete-Gómez, M., Sato, S., Christensen, S. K., Pelaz, S., Weigel, D., Yanofsky, M. F. and Ferrándiz, C. (2009). The NGATHA genes direct style development in the Arabidopsis gynoecium. *The Plant cell* **21**, 1394–1409.

Uchida, N., Shimada, M. and Tasaka, M. (2013). ERECTA-Family Receptor Kinases Regulate Stem Cell Homeostasis via Buffering its Cytokinin Responsiveness in the Shoot Apical Meristem. *Plant and Cell Physiology* **54**, 343–351.

Vandenbussche, M., Horstman, A., Zethof, J., Koes, R., Rijpkema, A. S. and Gerats, T. (2009). Differential recruitment of WOX transcription factors for lateral development and organ fusion in Petunia and Arabidopsis. *The Plant cell* **21**, 2269–2283.

Vercruyssen, L., Verkest, A., Gonzalez, N., Heyndrickx, K. S., Eeckhout, D., Han, S.-K., Jégu, T., Archacki, R., Van Leene, J., Andriankaja, M., et al. (2014). ANGUSTIFOLIA3 binds to SWI/SNF chromatin remodeling complexes to regulate transcription during Arabidopsis leaf development. *The Plant cell* **26**, 210–229.

Vernoux, T., Brunoud, G., Farcot, E., Morin, V., Van den Daele, H., Legrand, J., Oliva, M., Das, P., Larrieu, A., Wells, D., et al. (2011). The auxin signalling network translates dynamic input into robust patterning at the shoot apex. *Molecular Systems Biology* **7**, 508.

Voß, U., Bishopp, A., Farcot, E. and Bennett, M. J. (2014). Modelling hormonal response and development. *Trends in Plant Science* **19**, 311–319.

Vriet, C., Lemmens, K., Vandepoele, K., Reuzeau, C. and Russinova, E. (2015). Evolutionary trails of plant steroid genes. *Trends in Plant Science* **20**, 301–308.

Weigel, D., Alvarez, J., Smyth, D. R., Yanofsky, M. F. and Meyerowitz, E. M. (1992). LEAFY controls floral meristem identity in Arabidopsis. *Cell* **69**, 843–859.

Weijers, D. and Wagner, D. (2016). Transcriptional Responses to the Auxin Hormone. *Annu. Rev. Plant Biol.* **67**, 539–574.

Weller, B., Zourelidou, M., Frank, L., Barbosa, I. C. R., Fastner, A., Richter, S., Jürgens, G., Hammes, U. Z. and Schwechheimer, C. (2017). Dynamic PIN-FORMED auxin efflux carrier phosphorylation at the plasma membrane controls auxin efflux-dependent growth. *Proceedings of the National Academy of Sciences* **114**, E887–E896.

Werner, T., Motyka, V., Laucou, V., Smets, R., Van Onckelen, H. and Schmülling, T. (2003). Cytokinin-deficient transgenic Arabidopsis plants show multiple developmental alterations indicating opposite functions of cytokinins in the regulation of shoot and root meristem activity. *The Plant cell* **15**, 2532–2550.

Willis, L., Refahi, Y., Wightman, R., Landrein, B., Teles, J., Huang, K. C., Meyerowitz, E. M. and Jönsson, H. (2016). Cell size and growth regulation in the Arabidopsis thaliana apical stem cell niche. *Proceedings of the National Academy of Sciences* **113**, E8238–E8246.

Winter, C. M., Austin, R. S., Blanvillain-Baufumé, S., Reback, M. A., Monniaux, M., Wu, M.-F., Sang, Y., Yamaguchi, A., Yamaguchi, N., Parker, J. E., et al. (2011). LEAFY target genes reveal floral regulatory logic, cis motifs, and a link to biotic stimulus response. *Developmental Cell* **20**, 430–443.

Wu, M.-F., Yamaguchi, N., Xiao, J., Bargmann, B., Estelle, M., Sang, Y. and Wagner, D. (2015). Auxin-regulated chromatin switch directs acquisition of flower primordium founder fate. *eLife* **4**, e09269.

Xie, W., Schultz, M. D., Lister, R., Hou, Z., Rajagopal, N., Ray, P., Whitaker, J. W., Tian, S., Hawkins, R. D., Leung, D., et al. (2013). Epigenomic analysis of multilineage differentiation of human embryonic stem cells. *Cell* **153**, 1134–1148.

Yadav, R. K., Perales, M., Gruel, J., Girke, T., Jönsson, H. and Reddy, G. V. (2011). WUSCHEL protein movement mediates stem cell homeostasis in the Arabidopsis shoot apex. *Genes & Development* **25**, 2025–2030.

Yadav, R. K., Perales, M., Gruel, J., Ohno, C., Heisler, M., Girke, T., Jönsson, H. and Reddy, G. V. (2013). Plant stem cell maintenance involves direct transcriptional repression of differentiation program. *Molecular Systems Biology* **9**, 654.

Yadav, R. K., Tavakkoli, M. and Reddy, G. V. (2010). WUSCHEL mediates stem cell homeostasis by regulating stem cell number and patterns of cell division and differentiation of stem cell progenitors. *Development* **137**, 3581–3589.

Yamaguchi, N., Winter, C. M., Wu, M. F., Kanno, Y., Yamaguchi, A., Seo, M. and Wagner, D. (2014). Gibberellin Acts Positively Then Negatively to Control Onset of Flower Formation in Arabidopsis. *Science* **344**, 638–641.

Yamaguchi, N., Wu, M.-F., Winter, C. M., Berns, M. C., Nole-Wilson, S., Yamaguchi, A., Coupland, G., Krizek, B. A. and Wagner, D. (2013). A molecular framework for auxin-mediated initiation of flower primordia. *Developmental Cell* **24**, 271–282.

Yanai, O., Shani, E., Dolezal, K., Tarkowski, P., Sablowski, R., Sandberg, G., Samach, A. and Ori, N. (2005). Arabidopsis KNOXI Proteins Activate Cytokinin Biosynthesis. *Current Biology* **15**, 1566–1571.

Yang, Y., Hammes, U. Z., Taylor, C. G., Schachtman, D. P. and Nielsen, E. (2006). High-Affinity Auxin Transport by the AUX1 Influx Carrier Protein. *Current Biology* **16**, 1123–1127.

Zhang, W., Zhang, T., Wu, Y. and Jiang, J. (2012). Genome-Wide Identification of Regulatory DNA Elements and Protein-Binding Footprints Using Signatures of Open Chromatin in Arabidopsis. *The Plant cell* **24**, 2719–2731.

Zhang, Y., Liu, T., Meyer, C. A., Eeckhoute, J., Johnson, D. S., Bernstein, B. E., Nussbaum, C., Myers, R. M., Brown, M., Li, W., et al. (2008). Model-based Analysis of ChIP-Seq (MACS). *Genome Biol.* **9**, R137.

Zhao, Y. (2010). Auxin Biosynthesis and Its Role in Plant Development. *Annu. Rev. Plant Biol.* **61**, 49–64.

Zhao, Z., Andersen, S. U., Ljung, K., Dolezal, K., Miotk, A., Schultheiss, S. J. and Lohmann, J. U. (2010). Hormonal control of the shoot stem-cell niche. *Nature* **465**, 1089–1092.

Zhou, P., Song, M., Yang, Q., Su, L., Hou, P., Guo, L., Zheng, X., Xi, Y., Meng, F., Xiao, Y., et al. (2014). Both PHYTOCHROME RAPIDLY REGULATED1 (PAR1) and PAR2 Promote Seedling Photomorphogenesis in Multiple Light Signaling Pathways. *Plant Physiology* **164**, 841–852.

Zhu, L., Xin, R., Bu, Q., Shen, H., Dang, J. and Huq, E. (2016). A Negative Feedback Loop between PHYTOCHROME INTERACTING FACTORs and HECATE Proteins Fine-Tunes Photomorphogenesis in Arabidopsis. *The Plant cell* **28**, 855–874.

Zürcher, E., Liu, J., di Donato, M., Geisler, M. and Müller, B. (2016). Plant development regulated by cytokinin sinks. *Science* **353**, 1027–1030.

Zürcher, E., Tavor-Deslex, D., Lituiev, D., Enkerli, K., Tarr, P. T. and Müller, B. (2013). A robust and sensitive synthetic sensor to monitor the transcriptional output of the cytokinin signaling network in planta. *Plant Physiology* **161**, 1066–1075.

Publications

Research articles

Schuster, C., **Gaillochet, C.,** Medzihradszky, A., Busch, W., Daum, G., Krebs, M., Kehle, A. and Lohmann, J. U. (2014). A Regulatory Framework for Shoot Stem Cell Control Integrating Metabolic, Transcriptional, and Phytohormone Signals. *Developmental Cell* 28, 438–449.

Schuster, C.*, **Gaillochet, C**.* and Lohmann, J. U. (2015). Arabidopsis HECATE genes function in phytohormone control during gynoecium development. Development 142, 3343–3350 * equal contribution

Gaillochet, C., Stiehl, T.*, Wenzl, C.*, Ripoll, JJ., Bailey-Steinitz, L. J., Li, L., Pfeiffer, A., Miotk, A., Hakenjos J., Forner, J., Yanofsky, M. F., Marciniak-Czochra, A. and Lohmann, J. U. Control of plant cell fate transitions by transcriptional and hormonal signals. *Under review, eLIFE* * equal contribution

Gaillochet, C., Van der Froukje, W., Jamge, S., Angenent, G., Immink, R., Lohmann J. U. Specificity of HECATE function through local regulatory modules. *Under preparation*

Reviews

Gaillochet, C. and Lohmann, J. U**.** (2015). The never-ending story: from pluripotency to plant developmental plasticity. *Development* 142, 2237–2249.

Gaillochet, C.*, Daum, G.* and Lohmann, J. U**.** (2015). O Cell, Where Art Thou? The mechanisms of shoot meristem patterning. *Current Opinion in Plant Biology* 23, 91–97 * equal contribution

Acknowledgements

First and foremost, I would like to thank Jan Lohmann for giving me the opportunity to work on this project, for his supervision and support both on the scientific and personal level. I am also grateful to Karin Schumacher, Jochen Wittbrodt, and Marcus Heisler for their supervision and guidance during annual TAC meetings and to Lazaro Centanin for being part of my PhD thesis defense committee.

I did my first steps in this lab as a master student under the supervision of Christoph Schuster. I am very grateful to him for the time he spent discussing and guiding me during my first experiments with the shoot apical meristem.

The presented work results from multiple fruitful scientific collaborations and thus, I would like to thank Thomas Stiehl and Ana Marciniack-Czochkra for implementing the computational model; Christian Wenzl for developing and helping me with the image analysis pipeline; David Ibberson for conducting next-generation sequencing; Wal van der Froukje and Richard Immink for conducting the transcription factor library Yeast-Two-Hybrid screening. I would also like to thank every members of Jan Lohmann´s group from whom I learned a lot, but especially to Anne, Jana and Denis for critically reading my thesis. Many thanks to Katja for the great technical support in the plant growth chambers, which was invaluable over these years of intense gardening! Greetings to all the nice people from other groups at the COS, it was a great place to be.

Finally, I would like to thank my family for supporting and encouraging me throughout my doctoral work.

Appendix

Gene	AGI	CYC-DEX FC	DEX_3h FC	DEX_14h FC
ARF2	AT5G62000	0.96	1.01	1.02
ARF3	AT2G33860	0.89	0.91	0.80
ARF4	AT5G60450	1.12	1.12	1.05
ARF5	AT1G19850	0.84	1.03	**0.62**
ARF6	AT1G30330	0.98	1.12	1.04
ARF7	AT5G20730	1.18	0.99	1.26
ARF8	AT5G37020	0.95	0.94	0.88
ARF9	AT4G23980	0.85	0.95	0.85
ARF10	AT2G28350	0.65	0.94	0.96
ARF11	AT2G46530	**1.48**	**1.39**	1.56
ARF18	AT3G61830	**1.43**	1.24	1.27
ARF19	AT1G19220	**0.60**	1.25	1.00
IAA8	AT2G22670	1.07	1.01	0.93
IAA9	AT5G65670	0.89	0.97	0.83
IAA12	AT1G04550	0.95	1.02	1.04
IAA13	AT2G33310	1.37	**2.02**	0.96
IAA16	AT3G04730	0.90	0.88	0.93
IAA18	AT1G51950	0.88	0.77	1.05
IAA20	AT2G46990	1.60	0.80	1.42
IAA26	AT3G16500	0.94	0.98	1.07
IAA27	AT4G29080	0.78	0.94	0.57

Supplementary table 1:
Transcriptional response of canonical auxin and cytokinin signalling factors after *p16:HEC1-linker-GR* induction with dexamethasome (DEX) with or without cycloheximide (CYC). Statistical test: Fischer´s exact test (EdgeR), blue: $p<0.05$, green: $p<0.01$, red: $p<0.001$

AGI	Gene	Identication	bHLH TF	Network cluster
AT5G67060	HEC1	Bait	+	+
AT3G54990	SMZ	TF library screen		
AT1G09530	PIF3	TF library screen	+	+
AT2G22750	bHLH18	TF library screen	+	
AT3G59060	PIF5	TF library screen	+	+
AT2G31210	bHLH91	TF library screen	+	
AT2G17870	CSP3	TF library screen		
AT2G21060	CSP4	TF library screen		
AT1G53230	TCP3	TF library screen		
AT3G15030	TCP4	TF library screen		
AT3G45150	TCP16	TF library screen		
AT1G35560	TCP23	TF library screen		
AT5G51910	TCP19	TF library screen		+
AT3G07650	COL9	TF library screen		
AT2G01570	RGA	TF library screen		+
AT1G14920	GAI	TF library screen		+
AT1G59640	BIG PETAL	TF library screen	+	+
AT3G47620	TCP14	TF library screen		+
AT1G69690	TCP15	TF library screen		+
AT1G61660	bHLH112	TF library screen	+	
AT4G30180	bHLH146	TF + floral library screen	+	
AT5G08141	bZIP75	TF library screen		+
AT5G62610	bHLH79	TF library screen	+	
AT1G10120	bHLH (CIB4)	TF library screen	+	
AT5G06080	LBD33	TF library screen		
AT5G67110	ALCATRAZ	Floral library	+	+
AT3G04760	PPR-like protein	Floral library		
AT3G29370	P1R3	Floral library	+	
AT2G42870	PAR1	Floral library	+	+
AT4G17950	AHL13	Floral library		+
AT3G20550	DDL	Floral library		+
AT4G02060	PROLIFERA	Floral library		+
AT4G36930	SPATULA	Published		+
AT1G19850	MONOPTEROS	Published		+
AT2G21230	bZIP30	Published		+
AT2G46020	BRAHMA	Efroni & al, 2011		+
AT1G21700	SWI3C	Efroni & al, 2011		+
AT2G33610	SWI3B	Efroni & al, 2011		+

Supplementary table 2:
List of putative HEC1 cofactors identified from yeast-two-hybrid screenings. bHLH transcription factors and genes clustering in the Arabidopsis interactome (Arabidopsis Interactome Mapping Consortium, 2011) are marked by a blue and red cross respectively.

Primers	Sequence (5´to 3´)	Purpose
A04749	gaa caG AAT TCG GTC TCa acc tag atg gat cag cat ttc c	CUC2 promoter
A04780	gaa caG GAT CCG GTC TCt tgt tta aga aga aag atc taa agc	CUC2 promoter
A01602	gac tGG ATC Caa caa tgg tga gca agg gcg ag	FluorescentTimer
A01603	gct tGA ATT Cgg ccg ctg cag caa tct tgt aca gct cgt cca tg	FluorescentTimer
A01261	att gGG TAC Cgt taa gtg atc ttg acc gtc	KNOLLE promoter
A01262	tag tGG ATC Cct ttt tca cct gaa agt caa caa ttt tac aag	KNOLLE promoter
A02299	CGG CAG GAT CCA ACA ATG GAT TCT GAC ATA ATG	HEC1-linker-GFP
A02300	TTG CCT CTA Gat GCg Gca CTt GCG ATC GC	HEC1-linker-GFP
A02301	GGC AAT CTA GAA TGG TGA GCA AGG GCG AG	HEC1-linker-GFP
A02302	GGT TCC TCG AGT CAC CAT GGT ACG TAG AGC TCC TTG TAC AGC TCG TCC AT	HEC1-linker-GFP
A01862	TGA CCG GAT CCA ACA ATG GAT TCT GAC ATA ATG	HEC1-linker-GR
A01863	GGT CAG CGG CCG CTC TAA GAA TCT GTG CAT T	HEC1-linker-GR
oJJR858	CTATTTACAATTGTCGACATGATGGCTTCATTGTCTTGTG	ARF5 in SPYCE/SPYNE
oJJR859	TTTCGAACCCGGGGTACCTGAAACAGAAGTCTTAAGATCG	ARF5 in SPYCE/SPYNE
oJJR340B	CTATTTACAATTGTCGACATGGATTCTGACATAATGAACATG	HEC1 in SPYCE/SPYNE
oJJR341B	TTTCGAACCCGGGGTACCTCTAAGAATCTGTGCATTGCCC	HEC1 in SPYCE/SPYNE
oJJR342B	CTATTTACAATTGTCGACATGGATAACTCCGACATTCTAATGAAC	HEC2 in SPYCE/SPYNE
oJJR343B	TTTCGAACCCGGGGTACCTCTAAGAATCTGTGCATTTCC	HEC2 in SPYCE/SPYNE
oJJR344B	CTATTTACAATTGTCGACATGAATAATTATAATATGAACCCATCTC	HEC2 in SPYCE/SPYNE
oJJR345B	TTTCGAACCCGGGGTACCGATTAATTCTCCTACTCCTCTTC	HEC2 in SPYCE/SPYNE
oLJB175	CTATTTACAATTGTCGACATGCGTGGTGTGTCAGAAT	IAA12 in SPYCE/SPYNE
oLJB176	TTTCGAACCCGGGGTACCAACAGGGTTGTTTCTTTGT	IAA12 in SPYCE/SPYNE
oLJB173	AACGGCGACTGGCTGGAATTCATGCGTGGTGTGTCAGAAT	IAA12/BDL pGILDA
oLJB174	TTGGCTGCAGGTCGACTCGAGCTAAACAGGGTTGTTTCTT	IAA12/BDL pGILDA
oLJB215	AACGGCGACTGGCTGGAATTCATGGATTCTGACATAATGA	HEC1 pGILDA
oLJB216	TTGGCTGCAGGTCGACTCGAGTCATCTAAGAATCTGTGC	HEC1 pGILDA
oLJB217	AACGGCGACTGGCTGGAATTCATGGATAACTCCGACATT	HEC2 pGILDA
oLJB218	TTGGCTGCAGGTCGACTCGAGTCATCTAAGAATCTGTGCA	HEC2 pGILDA
oLJB219	AACGGCGACTGGCTGGAATTCATGAATAATTATAATATGA	HEC3 pGILDA
oLJB220	TTGGCTGCAGGTCGACTCGAGCTAGATTAATTCTCCTACT	HEC3 pGILDA
oJJR860	GATTATGCCTCTCCCGAATTCATGATGGCTTCATTGTCTTGTG	ARF5 pB42AD
oJJR861	AGAAGTCCAAAGCTTCTCGAGTGAAACAGAAGTCTTAAGATCG	ARF5 pB42AD
A00444	gag cct tac aac gct act ctg tct gtc	qRT-PCR_TUB
A00445	aca cca gac ata gta gca gaa atc aag	qRT-PCR_TUB
A06637	GTA AAG GCT CAT CAT GGC AGA	qRT-PCR_MP
A06638	TCA ATT GAT CTC CCG ACT GAC	qRT-PCR_MP
A06643	GGT GGG TTA ACT CAT CCA AGG	qRT-PCR_SPT
A06644	TTT TAG GTC AGG TTG TCC ATC A	qRT-PCR_SPT
A02190	ATG ATA TCA CAG AGA GAA GA	SPT_cloning_pGemT
A02191	TCA AGT AAT TCG ATC TTT TA	SPT_cloning_pGemT
A02255	GAG GGA AAG GTC CAA AGT GAC	SPT_Genotyping
A02256	CGT GTC GGA GAT TTC TCT GAG	SPT_Genotyping
A02308	GGG GAC AAG TTT gta caa aAA AGC AGG Cta aca ATG ATA TCA CAG AGA GAA GA	SPT_cloning_Gateway
A02309	GGG GAC CAC TTT gta caa gAA AGC TGG GTT CAA GTA ATT CGA TCT TTT A	SPT_cloning_Gateway

A02330	GGC AAG AAT TCA TGG ATT CTG ACA TAA TG	HEC1_cloning_GBKT7
A02331	GGC AAC TGC AGT CAT CTA AGA ATC TGT GC	HEC1_cloning_GBKT7
A02346	GGC AAC TCG AGT CAT CTA AGA ATC TGT GC	HEC1_cloning_GBKT7
A02332	GGC AAG AAT TCA TGA TAT CAC AGA GAG AA	SPT_cloning_GADT7
A02333	GGC AAG GAT CCT CAA GTA ATT CGA TCT TT	SPT_cloning_GADT7
A02357	GGG CAG TCG ACA ACA ATG ATA TCA CAG AGA GAA	SPT-linker-mCherry_cloning
A02358	GTG CCG CGG CCG CAG TAA TTC GAT CTT TTA G	SPT-linker-mCherry_cloning
A02359	GGG CAG TCG ACA ACA atg gtg agc aag ggc gag	mCherry-linker-SPT_cloning
A02360	TTG CCG GTA CCt Gca GCg GCc GCc Gat CC	mCherry-linker-SPT_cloning
A02361	GGG CAG GTA CCA TGA TAT CACA GAG AGA A	mCherry-linker-SPT_cloning
A02362	TTG CCC CCG GGT CAA GTA ATT CGA TCT TT	mCherry-linker-SPT_cloning
A02783	CTA TTC GAT GAT GAA GAT ACC CCA CCA AAC CC	sequencing_GADT7_constructs
A02673	ATG GGT GAT TCT GAC GTC	ALC_cloning_pGemT
A02674	TCA AAG CAG AGT GGC TGT	ALC_cloning_pGemT
A02675	GGG GAC AAG TTT gta caa aAA AGC AGG CTA ACA ATG GGT GAT TCT GAC GTC	ALC_cloning_Gateway
A02676	GGG GAC CAC TTT gta caa gAA AGC TGG GTT CAA AGC AGA GTG GCT GT	ALC_cloning_Gateway
A02693	GGG CAG AAT TCA TGG GTG ATT CTG ACG TC	ALC_cloning_pGADT7
A02694	GGG CAG GAT CCT CAA AGC AGA GTG GCT GT	ALC_cloning_pGADT7
A02854	TTC ATA ATT TCA TCC CCT CCT C	alc_genotyping
A02855	TGG ACT TGA AGT TGA AGC TGC	alc_genotyping
A03660	gaacaGGTCTCaggctcaacaATGCCTCTGTTTGAGCTT	AT1G09530_PIF3_F
A03661	gaacaGGTCTCtctgaCGACGATCCACAAAACTG	AT1G09530_PIF3_R
A03662	gaacaGGTCTCaggctcaacaATGAAGAGAGATCATCAT	AT1G14920_GAI_F
A03663	gaacaGGTCTCtctgaATTGGTGGAGAGTTTCCA	AT1G14920_GAI_R
A03664	gaacaGGTCTCaggctcaacaATGGATCCGAGTGGGATG	AT1G59640_BIG_PETAL_F
A03665	gaacaGGTCTCtctgaAGAAAACAAAACAGATTT	AT1G59640_BIG_PETAL_R
A03666	gaacaGGTCTCaggctcaacaATGGCGGAGGAGTTTAAA	AT1G61660_bHLH112_F
A03667	gaacaGGTCTCtctgaCCTGAAATTGTTGCCCCC	AT1G61660_bHLH112_R
A03668	gaacaGGTCTCaggctcaacaATGAAGAGAGATCATCAC	AT2G01570_RGA_F
A03669	gaacaGGTCTCtctgaGTACGCCGCCGTCGAGAG	AT2G01570_RGA_R
A03670	gaacaGGTCTCaggctcaacaATGAACTCACTCGTCGGA	AT2G22750_bHLH18_F
A03671	gaacaGGTCTCtctgaAGTGAGCTTTGATAAGCC	AT2G22750_bHLH18_R
A03672	gaacaGGTCTCaggctcaacaATGTATGAGGAAAGTTCA	AT2G31210_bHLH91_F
A03673	gaacaGGTCTCtctgaTTAATAGTTACTGTTGGG	AT2G31210_bHLH91_R
A03674	gaacaGGTCTCaggctcaacaATGGAAGAAACTCTAGCC	AT2G42870_PAR1_F
A03675	gaacaGGTCTCtctgaACCTCCGAACTTCATGTC	AT2G42870_PAR1_R
A03676	gaacaGGTCTCaggctcaacaATGGGTTACATGTGTGAC	AT3G07650_COL9_F
A03677	gaacaGGTCTCtctgaATAACTTCTGGTTGGGGT	AT3G07650_COL9_R
A03678	gaacaGGTCTCaggctcaacaATGAGAACCTTAAAGACT	AT3G29370_P1R3_F
A03679	gaacaGGTCTCtctgaTAAAACAACATCTTTCTT	AT3G29370_P1R3_R
A03680	gaacaGGTCTCaggctcaacaATGCAAAAGCCAACATCA	AT3G47620_TCP14_F
A03681	gaacaGGTCTCtctgaATCTTGCTGATCCTCCTC	AT3G47620_TCP14_R
A03682	gaacaGGTCTCaggctcaacaATGGAACAAGTGTTTGCT	AT3G59060_PIF5_F
A03683	gaacaGGTCTCtctgaGCCTATTTTACCCATATG	AT3G59060_PIF5_R
A03684	gaacaGGTCTCaggctcaacaATGGATTCCAGAGAGATC	AT4G17950_AHL13_F
A03685	gaacaGGTCTCtctgaTTGAGGACTGTTGCCAGG	AT4G17950_AHL13_R
A03686	gaacaGGTCTCaggctcaacaATGGAGAGGCAAATCATA	AT4G30180_bHLH146_F
A03687	gaacaGGTCTCtctgaAGTACTATCTTGAACAAT	AT4G30180_bHLH146_R
A03688	gaacaGGTCTCaggctcaacaATGGCAAGTCATGGATCA	AT5G06080_LBD33_F
A03689	gaacaGGTCTCtctgaGTAATAATAATCCATGTT	AT5G06080_LBD33_R

A03690	gaacaGGTCTCaggctcaacaATGTTCCAACAAAACTTA	AT5G08141_bZIP75_F
A03691	gaacaGGTCTCtctgaAGATGGTTGATACGAAGA	AT5G08141_bZIP75_R
A03692	gaacaGGTCTCaggctcaacaATGGGTGATTCTGACGTC	AT5G67110_ALCATRAZ_F
A03693	gaacaGGTCTCtctgaAAGCAGAGTGGCTGTGGA	AT5G67110_ALCATRAZ_R
A03694	GCAGCAGGTCTCGAAACCTTCTTCCCTTCCGTTTCC	ALCATRAZ_Eco31I_F1
A03695	GGAAACGGAAGGGAAGAAGGTTTCGAGACCTGCTGC	ALCATRAZ_Eco31I_R1
A03696	GCAGCAGGTCTCGACATTAGAGCAAGACCTGAAC	ALCATRAZ_Eco31I_F2
A03697	TGCTGCGGTCTCAATGTCTCATTGATCCTTGTATGAGT	ALCATRAZ_Eco31I_R2
A03698	gaacaGGTCTCaggctcaacaATGGACCCTCCACTAGTG	AT5G62610_bHLH79_F
A03699	gaacaGGTCTCtctgaTGTGGTTCGGTTAAAGTT	AT5G62610_bHLH79_R
A03700	GCAGCAGGTCTCGGCCTCCGTTTAGCTGTTAACTCC	bHLH79_Eco31I_F1
A03701	TGCTGCGGTCTCGAGGCCAGAGCGAACGGCGTCGTT	bHLH79_Eco31I_R1
A03702	GCAGCAGGTCTCGAGGCCTGAAGGCGAAACAAGTTC	bHLH79_Eco31I_F2
A03703	TGCTGCGGTCTCGGCCTCATCGAACCATCTCCATTT	bHLH79_Eco31I_R2
A03704	gaacaGGTCTCaggctcaacaATGACTCCGTTATCCTCT	AT3G04760_PPR_F
A03705	gaacaGGTCTCtctgaATAACCAAATGTCTGAGA	AT3G04760_PPR_R
A03706	GCAGCAGGTCTCGAAACCATGGTACGCAAAGGTTAC	PPR_Eco31I_F1
A03707	TGCTGCGGTCTCGGTTTCGAGTAAGTGTAGAGATTC	PPR_Eco31I_R1
A03708	gaacaGGTCTCaggctcaacaATGTTGGATCTTAACCTA	AT3G54990_SMZ_F
A03709	gaacaGGTCTCtctgaTGGATCAAAACAATTGGA	AT3G54990_SMZ_R
A03710	GCAGCAGGTCTCGATCTCGTAGCTCCCAATATCGTG	SMZ_Eco31I_F1
A03711	TGCTGCGGTCTCGAGATCTTGGTCCTCTTCTGCTCT	SMZ_Eco31I_R1
A03712	GCAGCAGGTCTCGGCCTCGATGCAGACATCAATTTC	SMZ_Eco31I_F2
A03713	TGCTGCGGTCTCGAGGCCACGGAATTTGATAGCAGC	SMZ_Eco31I_R2
A00118	GCT ATC CAC AGG TTA GAT AAA GGA G	HSF1_F_ChIP
A00119	GAG AAA GAT TGT GTG AGA ATG AAA	HSF1_R_ChIP
A04999	acg cct cta ctt taa ttt tcc cat t	PIN1_1_F_ChIP
A05000	tag aag aaa gaa cag agc gag aaa c	PIN1_1_R_ChIP
A05006	cat cca tca ccc ata acc ata agt c	PIN1_2_F_ChIP
A05007	aca act gcg act ttg tgt aat att g	PIN1_2_R_ChIP
A05010	gca ccc atc aac cac cat ttt	PIN1_3_F_ChIP
A05011	agt gtg tgt gat gta att ttg att ga	PIN1_3_R_ChIP
A05012	gga agc atg att ctc tct gtt ttc t	PIN1_4_F_ChIP
A05013	ctt tct gct gtg aag cca gtt tt	PIN1_4_R_ChIP
A05015	cgt aag gtc ata gtt gca gat gtt a	PIN1_5_F_ChIP
A05017	aaa agc tct caa tac tct gtc tgg g	PIN1_5_R_ChIP
A05020	gac aat gta tat gtg gac tcg tct c	PIN3_1_F_ChIP
A05021	gtc tct tat ttc tca ctt acc aca ca	PIN3_1_R_ChIP
A05022	aga aag ata cag caa cac taa gtc a	PIN3_2_F_ChIP
A05023	ttt agt aca gag cca aag ttt cac a	PIN3_2_R_ChIP
A05026	aaa agc aaa gat tag ggg aca gaa g	PIN3_3_F_ChIP
A05027	ctt aag aag aag gtc tac atg tgg c	PIN3_3_R_ChIP
A05029	CTA TCT GAT GCT GGT CTT GGA ATG	PIN3_4_F_ChIP
A05031	gct tca aaa cta aaa ttt cga gag g	PIN3_4_R_ChIP
A05032	tcg tca cgg aat cag aaa cat tta t	PIN3_5_F_ChIP
A05033	taa tat atc acc gag aca atc ccc t	PIN3_5_R_ChIP
A06039	CTC TGT AAT ACG ACT CAC TAT AGG GCG ATG ATG ACA GAT TTA TCT	NGA1_T7_in situ
A06040	CTC Tct att tag gtg aca cta tag aaT TGA TCC AAA TCA AAA GA	NGA1_SP6_in situ
A06041	CTC TGT AAT ACG ACT CAC TAT AGG GCG ATG AAT CAA GAA GAT AAA	NGA2_T7_in situ
A06042	CTC Tct att tag gtg aca cta tag aaC CTA TCC AAA TCA AAA GA	NGA2_SP6_in situ

A05299	cca cat gag gtt aaa ggg cc	MIGS genotyping
A05300	TAG TGG TTC CTG CGT CTG AG	MIGS genotyping
A05301	AAC CTT GTT ACA TCC CGG AAC	MIGS genotyping
A05302	ACC TCC GAA CTT CAT GTC TTC T	MIGS genotyping
A05303	AGA GGG GTT AAA GGC GGT AC	MIGS genotyping
A05304	TTC TCC TCC CTC TTC CGT CT	MIGS genotyping
A05305	AAT GAC TCG GTC CGA CTG TT	MIGS genotyping
A05306	ACT CAT CTG TCT CGT TGC CA	MIGS genotyping
A05321	AGT CTG CAC TTC ATA TGA GC	MIGS genotyping
A05319	ATG AAG AGA GAT CAT CAC C	RGA_cloning
A05320	GTA CGC CGC CGT CGA GAG TTT C	RGA_cloning
A05367	GTT GAT AGA CAT TTT CAA TGA	rga-24_genotyping
A05368	GGT CAT CAG TAG AGA CTA A	rga-24_genotyping
A05369	GGT GAT TTT CAC GGT GGT TG	rga-24_genotyping
A05370	TCG GTA CGG GAT TTT CGC AT	gai-t6_genotyping
A05371	CTA GAT CCG ACA TTG AAG GA	gai-t6_genotyping
A05372	AGC ATC AAG ATC AGC TAA AG	gai-t6_genotyping
A05469	gaa caG GTC TCa ggc tca aca ATG ATG ACA GAT TTA TCT	NGA1_cloning
A05470	gaa caG GTC TCt ctg aTT GAT CCA AAT CAA AAG ACA	NGA1_cloning
A05471	gaa caG GTC TCa ggc tca aca ATG AAT CAA GAA GAT AAA GA	NGA2_cloning
A05472	gaa caG GTC TCt ctg aCC TAT CCA AAT CAA AAG ACA	NGA2_cloning
A05553	AGC AGC AGC AGC AGC CAT ATT TAG	nga1_genotyping
A05554	AAC GTC ATC ATC ACA GTG GTG GTG G	nga1_genotyping
A05555	AAC GTC CGC AAT GTG TTA TTA AGT TGT C	nga1_genotyping
A05556	CGA CAA AGT AGT AAC ACC AAG	nga2_genotyping
A05557	CCA ACC ATA GAA ACT CTG CC	nga2_genotyping
A05558	CCA ACG GCT CTG ATC CAA CAA TG	nga3_genotyping
A05559	ACC GTC GAC AAC TAA ACA TAT ACA TAC	nga3_genotyping
A05560	GAG CGT CGG TCC CCA CAC TTC TAT AC	nga3_genotyping
A05561	CCT CTC GAG TGA TAC TTT TGA TGA ATA TCT CAA C	nga4_genotyping
A05562	GGA GGA TCC TCT TCA AAG CTC TAA AGA TTT CCC	nga4_genotyping
A00132	TAG AAG GGA GAG AAT AAG CGA G	hec1_genotyping
A00133	AAT GAA CAC AAG CCT GAT AGC	hec1_genotyping
A00134	ACC ACA ACA ACA CTT ACC CTT TTC	hec1_genotyping
A00135	ATA TTG ACC ATC ATA CTC ATT GC	hec1_genotyping
A00136	CTC ACA AAA CCT TAA CTA GAT GTC TGA	hec2_genotyping
A00754	ATG CTT TCT GAA TCC AAC ACC C	hec2_genotyping
A00138	ccg aca ctc ttt aat taa ctg aca ctc	hec2_genotyping
A00139	TCT TTA TTT TTT CTC CGA ACC A	hec3_genotyping
A00140	AAG CCG TAT CCA TTT TAG TGC C	hec3_genotyping
A00141	GTT CAC GTA GTG GGC CAT C	hec3_genotyping

Supplementary table 3:
List of primers used in this study

Supplemental information (uploaded on the attached CD):

Detailed description of the computational model (written by Dr. Thomas Stiehl)

Complete list of genes detected in RNA-seq and ChIP-seq experiments